Indian and Northern Affairs Canada
Affaires indiennes et du Nord Canada

Exploration and Geological Services Division, Yukon Region

BULLETIN 2

GEOLOGY AND GENESIS OF THE MOUNT SKUKUM EPITHERMAL GOLD - SILVER DEPOSITS, SOUTHWESTERN YUKON TERRITORY (NTS 105D 3, 6)

B.W.D. McDonald

1990

Canada

103-05907/

EXPLORATION AND GEOLOGICAL SERVICES DIVISION

YUKON REGION

BULLETIN 2

GEOLOGY AND GENESIS OF THE MOUNT SKUKUM EPITHERMAL GOLD - SILVER DEPOSITS, SOUTHWESTERN YUKON TERRITORY (NTS 105D 3, 6)

B.W.D. MCDONALD

1990

Minister of Supply and Services Canada 1990
Available in Canada through
authorized bookstore agents and other bookstores

or by mail from

Canadian Government Publishing Center
Supply and Services Canada
Ottawa, Canada K1A 0S9

and primarily from

Exploration and Geological Services
Indian and Northern Affairs Canada
200 Range Road, Whitehorse
Yukon, Canada, Y1A 3V1

QS - Y073 - 000 - EF - A1
Cat. No. R72 - 217/1990E

ISBN 0 - 660 - 13749 - 6

Price subject to change without notice

Cover
View south to Mt. Skukum from the upper adit of the Mt. Skukum Mine

Editor
J.G. Abbott

Author's address
Homestake Mineral Development Company
1000-700 West Pender Street
Vancouver, B.C., V6C 1G8

PREFACE

The Mt. Skukum gold-silver epithermal deposits, the first lode gold mine in the Yukon, are recent discoveries in an area where exploration first began in 1893. Their recent discovery resulted from both the use of modern geochemical exploration techniques and predictive metallogeny using the relatively new epithermal mineral deposit model.. This report refines that model for southern Yukon and northern British Columbia and and provides valuable data that will aid exploration for similar deposits.

S. Morison
Chief Geologist

CONTENTS

1 Abstract

2 Introduction
2 Climate and Physiography
2 Previous Work and Exploration History
2 Scope
4 Acknowledgements

4 Regional Geology

4 Geology of the Mt. Skukum Caldera Complex

7 Geology of Main Cirque
9 Formation 2
11 Formation 3
14 Formation 4
15 Igneous Intrusive Rocks
16 Whole Rock Geochemistry of Igneous Rocks in Main Cirque
16 Classification
16 Discussion
17 Structure
19 Summary

21 Mineralization
21 The Main Cirque Zone
25 Ore Petrology
31 Distribution of Gold in the Main Cirque Ore Zone
33 Interpretation

33 Alteration
33 Supergene Alteration
34 Hypogene Alteration
37 Discussion

37 Fluid Inclusions
37 Data Collection
41 Homogenization Data
41 Freezing Data
41 Pressure Correction
41 Interpretation

46 Stable Isotope Composition of Hydrothermal Minerals, Fluids, and Surrounding Host Rocks
47 Oxygen Isotopes
47 Isotopic Composition of Hydrothermal Fluids
48 Water to Rock Ratio
48 Geothermometry
48 Discussion
50 Carbon Isotopes
51 Data
51 Conclusions

51 Deposit Model

54 Summary and Conclusions

55 References

59 Appendix A - Geochemical data for igneous rocks at Mt. Skukum

59 Appendix B - Location of drill core samples

60 Appendix C - Potassium argon data

61 Appendix D - Calibration data for the Chaixmea fluid inclusion stage

63 Appendix E - Homogenization and freezing data for fluid inclusions

65 Appendix F - Oxygen isotope methods and results

Figures

3 1. Location map of the Mt. Skukum area.

5 2. Regional geology of the Mt. Skukum Caldera Complex surrounding area (after Wheeler, 1961 and Pride, 1985).

7 3. Generalized geology map of the Mt. Skukum Caldera Complex (after Pride, 1985).

8 4. Stratigraphy in the western portion of the Mt. Skukum Caldera Complex. The Mt. Skukum gold deposits occur in Formation 3.

9 5. Photograph of well bedded epiclastic units typical of the upper portion of Formation 2.

10 6. Photograph showing a typical section of Formation 3 as seen in a cliff exposure near Main Cirque.

12 7. Geologic map of Main Cirque.

13 8. Geologic cross section of Main Cirque. Section is based on field observation and the geologic map (Figure 3).

14 9. Photograph of rhyolite ash tuff of Formation 2 showing concentrically layered accretionary lapilli..

16 10. Photograph of a hand specimen of densely-welded felsic tuff of Formation 4 showing elongate essential fragments and associated fiammé.

17 11. AFM plot after Irvine and Baragar illustrating the calc-alkaline nature of igneous rocks at Mt. Skukum.

18 12. Plot of Na_2O+K_2O and SiO_2 after LeBas (1986) illustrating the distribution of lithologies at Mt. Skukum, Yukon Territory using this geochemical classification scheme.

18 13. Geochemical classification plot after Winchester and Floyd, 1977 showing the positions of igneous rocks from Main Cirque.

20 14. Photograph of Main Cirque looking due south showing the fault scarps forming the east and west walls of the cirque and the step-like topography produced by down dropped blocks.

22 15. Series of four schematic cartoons (a to d) illustrating the possible sequence of events forming the excellent ground preparation which led to formation of epithermal vein mineralization.

24 16. Photograph of quartz-carbonate vein-breccia showing open-space filling textures in a drusy, quartz-lined cavity from the Main Cirque Ore Zone.

25 17. Photograph of a quartz-carbonate vein showing the distribution and abundance of wall rock fragments in the Main Cirque Ore Zone.

26 18. Photograph of brecciated quartz-carbonate vein material re-cemented by a later phase of quartz-carbonate which illustrates the similarity of appearance and later composition between early brecciated vein fragments and later matrix in the Main Cirque Zone.

26 19. Photograph of a specimen of high grade ore showing wall rock fragments in relatively coarse-grained quartz and lamellar carbonate.

27 20. Photomicrograph of quartz-carbonate vein material showing the lamellar morphology of calcite crystals in the Main Cirque Zone. Magnification is 45 times.

27 21. Photomicrograph of quartz-carbonate vein material from the Main Cirque Zone.

28 22. Photomicrograph showing clusters of tightly packed bladed calcite crystals occuring in randomly oriented bundles distributed thoughout the vein material from the Main Cirque Zone.

28 23. Photomicrograph of quartz-carbonate vein material showing exfoliation textures.

29 24. Photograph showing prominent blades of equant, fine-grained quartz pseudomorphing calcite on weathered surfaces of quartz-carbonate vein from the Main Cirque Zone.

29 25. Photomicrograph showing brecciated vein material re-cemented in a chaotic matrix of quartz-carbonate-sericite vein material.

30 26. Photomicrograph showing a typical occurrence of fine-grained euhedral adularia grains intergrown with quartz in a brecciated specimen of quartz-carbonate material which was re-cemented by matrix material containing abundant adularia.

31 27. Contour diagram showing distribution of gold values in the Main Cirque Zone (Figure 3).

32 28. Isopach diagram illustrating vein thickness in the Main Cirque Ore Zone .

32 29. Contour diagram of grade times thickness outlining zones of maximum vein width and gold grade.

35 30. Schematic illustration showing gradation between veins and zones of vein breccia and the distribution of hypogene alteration around quartz-carbonate veins and vein breccia in Main Cirque.

36 31. Photograph of intense argillic alteration in rock of the Alunite Cap Zone, Mt. Skukum .

39 32. Fluid inclusion homogenization data from the Main Cirque Zone.

39 33. Fluid inclusion homogenization data obtained from individual samples of vein material from the Main Cirque Zone.

34 34. Eutectic melting temperatures by distribution of inclusion types in vein material from the Main Cirque Zone.

40 35. Final melting temperatures of fluid inclusions by distribution of inclusion types in vein material from the Main Cirque Zone.

42 36. Frequency distribution of volume percent gas in fluid inclusions from the Main Cirque Zone.

43 37. Homogenization temperature versus L:V ratio for primary fluid inclusions from the Main Cirque Zone.

43 38. Distribution of the last melting temperature of primary fluid inclusions from veins in the Main Cirque Zone.

44 39. Distribution of the homogenization temperature of primary fluid inclusions from veins in the Main Cirque Zone.

44 40. Primary fluid inclusion data for temperature of last melt versus homogenization temperature from veins in the Main Cirque Zone.

46 41 Phase equilibria in the lower temperature part of the system H_2O-CO_2 showing the limitations of CO_2 content in depositional fluids at Mt. Skukum, Yukon Territory (after Roedder, 1984).

49 42. $d^{18}O$ versus dD values showing fields for magmatic and metamorphic water and the possible range of depositional fluid composition at Mt. Skukum.

50 43. North America with contours of dD values in meteoric surface waters (from Taylor, 1979).

52 44. Spatial relationships among known mineralized zones in the Main Cirque.

Tables

11 1. Average visually estimated mineralogical modes of igneous rocks present in Main Cirque.

17 2. Average major element geochemistry of the three igneous rock compositions found in Main Cirque.

34 3. Hypogene alteration facies and zones in Main Cirque.

41 4. Summary of homogenization temperature (T_h) data from fluid inclusions in vein samples from the Main Cirque Zone.

41 5. Summary of freezing data from fluid inclusions in vein samples from the Main Cirque Zone.

47 6. Oxygen isotope composition of hydrothermal fluids at Mt. Skukum, Yukon Territory. Calculations are from data in Appendix E and equations 1, 2, and 3 in text.

48 7. Water to rock mass ratio calculations for Mt. Skukum, Yukon Territory. Calculations are from data in Table 7 and equation 4 in text.

48 8. Calculated isotopic temperature of deposition from mineral pairs from the Main Cirque Zone. Calculations use data from Appendix E and equation 5 in text.

51 9. Carbon isotope composition of hydrothermal minerals at Mt. Skukum.

GEOLOGY AND GENESIS OF THE MOUNT SKUKUM EPITHERMAL GOLD - SILVER DEPOSITS, SOUTHWESTERN YUKON TERRITORY

ABSTRACT

The Eocene Mt. Skukum gold - silver epithermal deposits are 65 km southwest of Whitehorse in the Yukon Territory. Veins are in nearly flat-lying Eocene andesitic volcanic rocks of the Mt. Skukum Caldera Complex, part of the Sloko Volcanic Province, which unconformably overlies the Mesozoic Coast Plutonic Complex and Paleozoic to Precambrian metamorphic rocks.

Significant veins are contained in a regional halo of propylitic alteration centered on a graben in the southwestern corner of the Mt. Skukum Caldera Complex. Zones of steeply-dipping quartz-carbonate-sericite veins are associated with major faults and rhyolite dykes which bound blocks in the graben.

Electrum and native silver form fine grains which average 15 to 20 microns and locally exceed 1 mm across, in veins containing only trace amounts of sulphides. Fluid inclusions indicate that vein minerals were deposited from fluids averaging 313°C with an average salinity of 0.7 weight percent NaCl equivalent. Primary inclusions show that depositional fluids existed under two pressure régimes; one close to hydrostatic, the other approaching lithostatic. Both indicate deposition about 470 m below paleosurface.

Oxygen and carbon isotope composition of minerals in the deposit and surrounding wall rocks indicate that depositional fluids were meteoric. Large depletions in O^{18} content of andesitic rocks in the deposit area indicate a minimum water : rock mass ratio of 0.81:1.

Precious metals at the Mt. Skukum deposit were emplaced at relatively low temperature, near surface, by a meteoric water dominated hydrothermal system driven by heat from associated rhyolite dykes. Gold and silver were leached from andesitic and rhyolitic stocks and volcanic rocks as well as metamorphic and granitic basement, and precipitated with quartz and carbonate in permeable conduits such as fault zones, and breccia bodies.

RÉSUMÉ

Les gisements épithermaux d'or-argent du mont Skukum de l'Éocène sont situés à 65 km au sud-ouest de Whitehorse (Yukon). Les filons se trouvent dans des roches volcaniques andésitiques Éocènes quasi horizontales du Complexe de Mt. Skukum Caldera dans la province volcanique de Sloko. Ce complex repose en discordance sur le Complex putonique côtier mésozique et sur des roches métamorphiques du Paléozoioque au Précambrien.

Des filons importants logent dans un eauréole régionale d'altération propylitique centrée sur un graben dans le coin sud-ouest du Complexe de Mt. Skukum Caldera. Des zones de filons très inclinés de quartz-carbonate-séricite sont associées à des failles importantes et des dykes de rhyolite qui limitent des blocs dans le graben.

L'or argentifère et l'argent natif forment des grains fins de 15 à 20 microns en taille moyenne dépassant par endroits 1mm transverselement dans des filons ne contenant que des quantités traces de sulfures. Des inclusions fluides indquent que les minéraux déposees provenaient de fluides dont la température a élèvait en moyenne à 313°C et dont la salinité moyenne équivalait à 0,7 de pourcentage en poids de NaCl. Les inclusions primaires rélèvant que deux régimes de pression différénts s'exerçaient sur les fluides de depot: l'un proche de la pression hydrostatique, l'autre de la pression lithostatique. Les deux indiquent un dépôt à une paléoprofondeur de 470 m.

La composition en oxygène et carbone isotopiques des mineraux du gisement et des roches encaissantes indiquent des fluides de dépôt météoriques. D'importants appauvrissements en 018 dans les roches andésitiques du gisement indiquent un rapport minimal eau-massif rocheux de 0,81-1.

Les métaux précieux dans le gissement du mont Skukum ont été mis en place à une température relativement faible, près de la surface, par un système hydrothermal surtout composé d'eau météorique dirigé par la chaleur dégagé par des dykes de rhyolite associés. L'or et l'argent ont été lessivés de stocks andésitiques et rhyolitiques et de roches volcaniques sinsi que du socle métamorphique et granitique et ont précipité avec du quartz et des carbonates dans des conduits perméables comme des zones de failles et des massifs bréchiques.

INTRODUCTION

The Mt Skukum deposit, centered near latitude 60° 12' north and longitude 135° 28' west (NTS:105D SW), is approximately 65 km southwest of Whitehorse, Yukon Territory (Figure 1), in the Wheaton River valley. The opening of the Mt. Skukum Mine in March, 1986 is a landmark in the history of mineral production in Yukon Territory. This was the first mine to open in Yukon since Faro in 1969, and the first hard-rock gold mine in the territory to see substantial production despite the long and rich placer gold mining history. Although mining operations on the Mt. Skukum property ceased in August of 1988 the project had operated profitably for over two years producing almost 80,000 oz of gold. In the process, gold mining operations at Mt. Skukum have helped stimulate intensive and successful exploration of the Wheaton Valley district. Exploration efforts are ongoing on the Mt. Skukum property and tremendous potential remains for discovery of additional ore on the large property surrounding the mine site.

This report is intended as a descriptive guide to the mineralization and the nature of the Main Cirque Zone which was one of several large gold bearing epithermal veins in the Main Cirque area of the property and the only vein which was mined. The report also serves to describe the geology which surrounds the deposit and suggest a scenario under which epithermal mineralization may have come to be emplaced where it is.

Climate and Physiography

Climate is typical of uplands in the southern Yukon with harsh winters and cool but pleasant summers enhanced by long periods of daylight lasting up to 20 hours in June (Wheeler, 1961). Weather is, at times, unpredictable. Calm sunny mornings can quickly change to windy, rainy, and even snowy afternoons. Rare blizzards in the middle of summer have lasted several days.

The Mt. Skukum area is characterized by jagged peaks with a relief of 1,400 m between the top of Mt. Skukum at about 2,400 m, and the floor of the adjacent Wheaton River valley at 1,000 m. Continental glaciers covered the area to an elevation of about 2,000 m leaving peaks such as Mt. Skukum rising above the ice as nunataks (Wheeler, 1961). Alpine glaciers still cover north-facing slopes at higher elevations. One such glacier occurs in Main Cirque on the north foot of Mt. Skukum.

Previous Work and Exploration History

Exploration of the Wheaton River District, including the Mt. Skukum area, began when precious metal and antimony veins were discovered in 1893. Small scale mining began at several locations, but resulted in only limited production. The first geologic investigation of the area was undertaken in 1906 by D.D. Cairnes who mapped the district at a scale of 1 inch to 1 mile and studied deposits in the area (Cairnes, 1912, 1916). In 1940, H.S. Bostock examined antimony occurrences in the Wheaton River District as part of a study of strategic minerals (Bostock, 1941). Pride (née Smith) has described much of the geology of the Mt. Skukum Volcanic Complex as part of a Ph.D. study (Smith, 1982, 1983; Pride, 1985, 1987) and more recently A. Doherty and others mapped the Mt. Skukum region at 1:50,000 scale (Doherty et. al., 1988). Despite the prolonged period of geologic interest in the district, no record exists of staking in Main Cirque prior to 1981.

In 1980, prospecting, mapping, and extensive stream sediment geochemistry conducted by Agip Canada Ltd. of Calgary, indicated anomalous concentrations of gold and arsenic in sediment from Butte Creek (Figure 1). In all, nine samples from the headwaters of Butte Creek contained values in excess of 85 ppb Au and as high as 630 ppb Au and 192 ppm As against a background of 5 ppb Au. In May 1981, 48 claims were staked to cover this anomaly and several brightly coloured gossanous zones in Main Cirque (Doherty et. al., 1981; McDonald et al., 1986). Exploration drilling and prospecting over a four year period led to the discovery of the Main Cirque Zone. Mine production began in 1986 at a rate of 300 tonnes per day and continued until August, 1988 when problems with uneven grade distribution and dilution due to structural irregularities led to a temporary shut down of mining operations. Exploration on the property continues.

Scope

This field and laboratory study of the Mt. Skukum deposit investigated the nature of mineralized veins and their relationship to surrounding rocks of the Mt. Skukum Volcanic Complex. The objectives were to: (1) map the deposit and surrounding volcanic rocks, (2) determine the mineralogical and chemical character of host rocks, (3) determine the nature and precious metal mineralogy of veins, (4) determine the character and distribution of hydrothermal alteration, and (5) define the depth of formation and hydrothermal environment of deposition of gold and silver bearing veins using fluid inclusions and stable isotope chemistry.

Most of the field work for this study was conducted during the summers of 1984 and 1985 while the writer was employed by the Geological Services Division of the Department of Indian and Northern Affairs. During this time the area surrounding the Main Cirque Zone was mapped at a scale of 1:1,000 and later incorporated into a map of the Main Cirque at a scale of 1:5,000. Over 6,000 m of core was also logged and sampled.

Observation and study has continued through 1986, 1987 and 1988 while the writer was employed by Mt. Skukum Gold Mining Corp. first as Exploration Geologist, then as

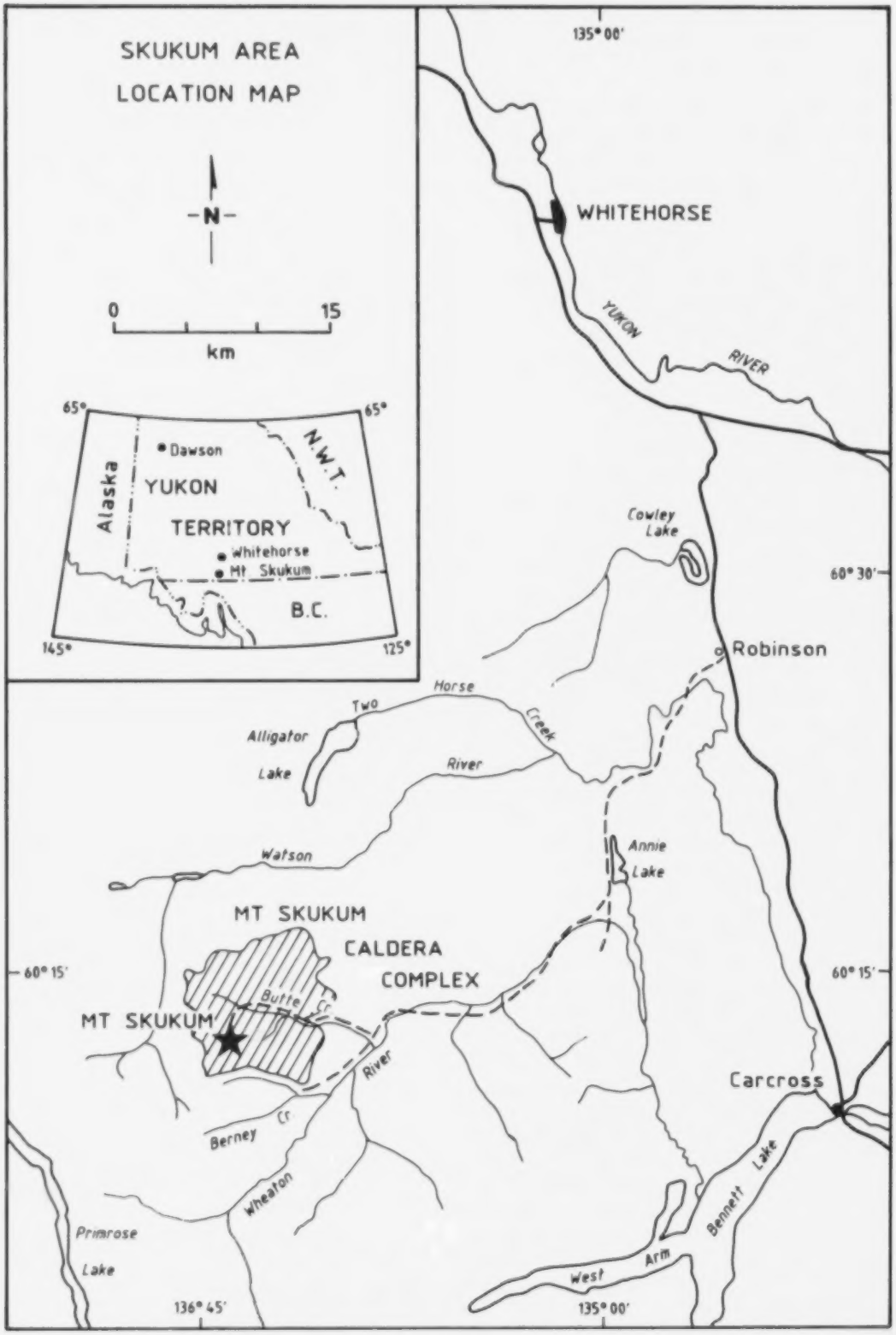

Figure 1 *Location map of the Mt. Skukum area.*

Mine Geologist, and currently as Senior Project Geologist.

Acknowledgements

The author is indebted to C.I. Godwin for his guidance, encouragement and support throughout this project. I also wish to thank A.J. Sinclair, S. Horsky, and J. Knight, and others among the friends and colleagues at U.B.C. who provided helpful suggestions, assistance and encouragement throughout the course of this research. Many thanks are also due to J.A. Morin of the Exploration and Geological Services Division of the Department of Indian and Northern Affairs, Yukon for initiating this project and funding fieldwork and much of the analytical work. The author is also indebted to G. Abbott for his detailed editorial assistance in preparation for publication. Assistance in the form of field accommodation and many useful discussions were generously provided by geologists R.A. Doherty, and E.B. Stewart of Agip Canada Ltd., as well as R. Basnett and R. Somerville of Total-Erickson Ltd. I would also like to express my appreciation to K. Muehlenbachs of The University of Alberta for undertaking oxygen isotope analyses used in this project.

REGIONAL GEOLOGY

The Mt. Skukum Caldera Complex (Figure 2) comprises an early Eocene (53.2 ± 1.8 Ma.; Appendix C) continental volcanic complex. It lies approximately 27 km north-northwest of the Bennett Lake Caldera Complex (Figure 2) described by Lambert (1974). These volcanic complexes represent the northern extent of the Sloko Volcanic Province which extends southeastward from south-central Yukon into northern British Columbia. This belt of volcanic centers lies along the northeast margin of the Coast Plutonic Complex and is characterized by intermediate to felsic volcanic rocks. Rocks of the Sloko Volcanic Province unconformably overlie Jurassic to Precambrian metasedimentary and Cretaceous granitic and volcanic rocks (Figure 2) (Souther, 1967) and are characteristically preserved as erosional remnants in down-faulted blocks. Mt. Nansen and Carmacks volcanic rocks, until recently considered correlative with the Skukum Group (Templeman-Kluit, 1981), are now thought to represent older, separate suites (Templeman-Kluit, pers. comm., 1987).

Rocks of Skukum Group in Yukon Territory comprise the Mt. Skukum Caldera Complex and the Bennett Lake Caldera Complex. The Mt. Skukum Caldera Complex (Figure 2) is comprised predominantly of andesitic flow and pyroclastic rocks whereas the Bennett Lake Caldera Complex has a relatively higher proportion of felsic volcanic rocks and is partially surrounded by a well-defined felsic ring dyke (Lambert, 1974). Based on lithogeochemical, structural, and lithological evidence, Smith (1982 and 1983) has interpreted the complexes to represent two distinct volcanic centers rather than two erosional remnants of the same volcanic system.

Late stage, high-level porphyritic rhyolite stocks occur sporadically throughout the Mt. Skukum Caldera Complex and the region surrounding it (Figure 2). In the Bennett Lake Caldera Complex, similar intrusive centers form two nested, arcuate series of ring fracture intrusions. No consistently elongate or arcuate stocks are apparent in or surrounding the Mt. Skukum Caldera Complex; however, those occurring well outside the complex surround it in an elliptical arrangement which vaguely follows the outline of the complex and may reflect an elliptical zone of weakness associated with collapse that facilitated emplacement of this unit. Swarms of similar rhyolite dykes identified by Doherty and Hart (1988) northeast of the caldera are oriented parallel to a northeast - southwest regional structural grain. These dyke swarms and stocks may represent late intrusions analogous to formation of ring dykes associated with final subsidence of the Mt. Skukum Caldera (McDonald and Godwin, 1986; McDonald, 1987; Doherty and Hart, 1988). These peripheral rhyolite stocks have been dated at 53 ± 1.1 Ma using rubidium-strontium geochronometry (Pride and Clark, 1985).

GEOLOGY OF THE MT. SKUKUM CALDERA COMPLEX

The Mt. Skukum Caldera Complex (Figure 3) forms a sub-rounded, fault-bounded remnant of andesite, dacite and rhyolite flows, pyroclastic rocks, intrusives and episediments 20 km long and 11 km wide. The volcanic complex is divided into two parts by two north-south trending faults (Figure 3) which down-drop the eastern block as much as 300 m relative to the western block (Pride, 1986). The eastern block consists mainly of felsic pyroclastic rocks interlayered with brecciated, flow-banded and spherulitic rhyolite lava flows. These felsic units are particularly thick in the northeastern and southeastern parts of the complex where prominent large-scale arcuate fracture systems visible from the air, large slump blocks, vent facies pyroclastic rocks, and other features indicate centers of volcanism and associated margins of nested caldera subsidence. The western block of the Mt. Skukum Caldera Complex is characterized by andesites, at least 850 m thick, which host the Mt. Skukum deposit. The andesites unconformably overlie basement on a highly irregular surface which results from paleotopography and post-depositional block faulting. Pride (1986) divided rocks of the Mt. Skukum Caldera Complex into five formations. These stratigraphic divisions have been generally maintained, but, in this study, the writer interprets Pride's Formation 5 as part of Formation 3, leaving Pride's Formation 4 as the uppermost stratigraphic horizon (Figure 4).

Formation 1, the oldest of the Mt. Skukum Caldera Complex, is distributed in rare, isolated exposures around the peripherys of the complex and is locally exposed central to the complex in areas where deep erosion penetrates volcanic units to basement (Figure 3). This formation unconformably overlies basement (Figure 4), is 5 to 100 m thick, and consists of coarse, alluvial material dominated by basement fragments (Pride, 1986). Basal conglomerate composed of boulder to cobble sized clasts of basement granitic rocks is overlain by channelled, interlayered siltstone, sandstone, and debris flow material in

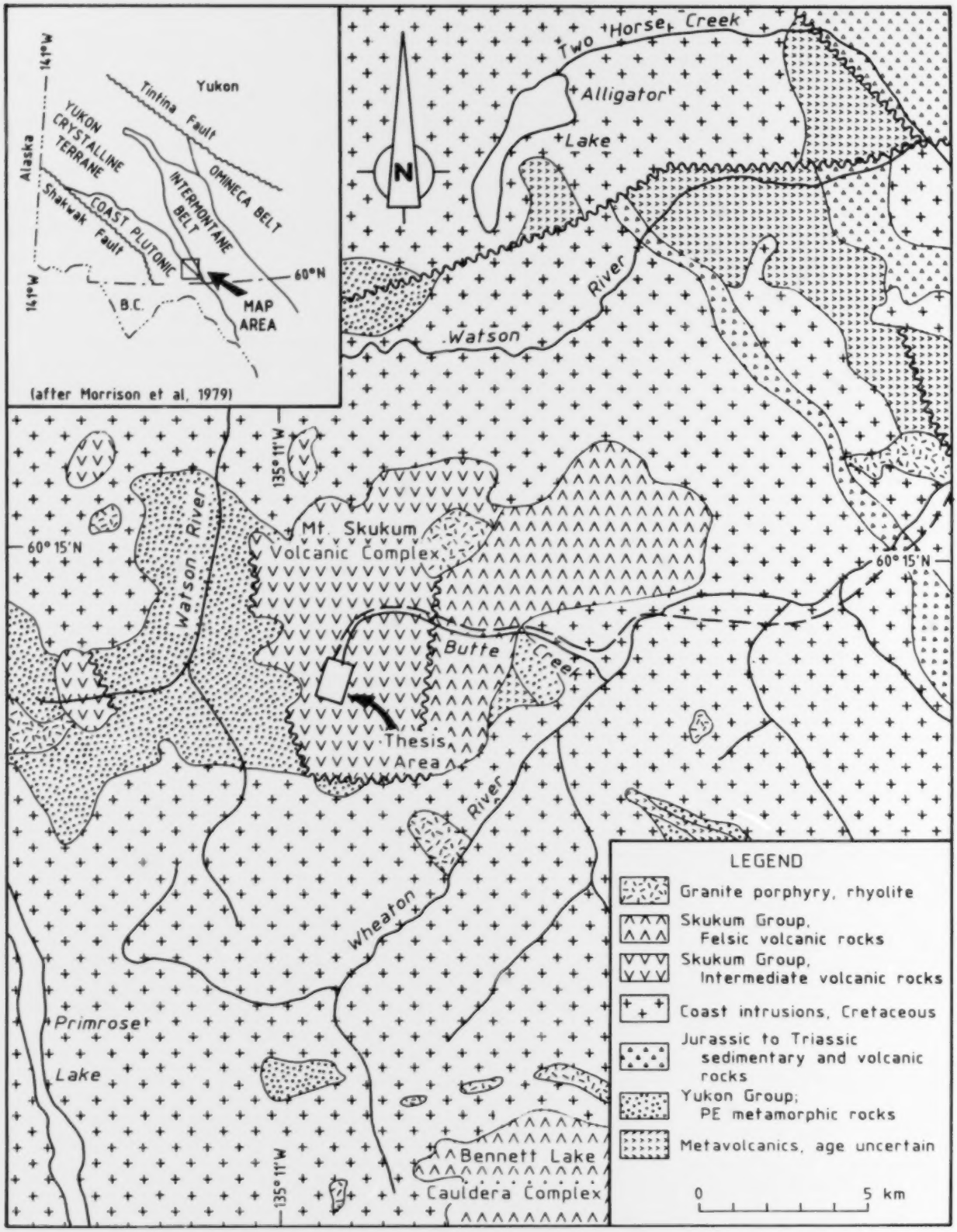

Figure 2 *Regional geology of the Mt. Skukum Caldera Complex and surrounding area (after Wheeler, 1961 and Pride, 1985)*

which the proportion of volcanic fragments increases up-section. Deposition coincided with tectonic disruption during incipient stages of volcanism and emplacement of magma at depth.

Formation 2 occurs throughout the western block of the Mt. Skukum Caldera Complex. It forms a discontinuous unit around the western margin of the complex and in central areas of the complex where deep erosion exposes underlying basement (Figure 3). Formation 2 includes up to 300 m of interbedded pyroclastic rocks and derived epiclastic rocks, both of which contain abundant basement material and lie unconformably on basement and conformably over Formation 1 (Figure 4) from which it is distinguished by the presence of primary volcanic rocks and a greater diversity in clast composition and types (Pride, 1986; Smith, 1984). Pyroclastic units grade upward from lower pale brown to green rhyolite containing basement fragments, to upper olive-green and maroon andesitic ashfall and lapilli tuffs containing abundant fragments of lower felsic volcanic material but fewer basement fragments. Epiclastic interbeds are invariably similar in composition to the surrounding volcanic rocks (Figure 5) and include well bedded, fine to coarse grained siltstone and sandstone as well as debris flows which become less predominant up-section. Formation 2 represents more proximal and widespread volcanism than Formation 1. The gradual decrease in accessory basement fragments and debris flow deposits up-section reflects a broad accumulation of volcanic detritus which slowly covered basement, leveling topography, and was concluded by comparatively well sorted and well bedded epiclastic rocks and andesitic tuffs which may locally be water-lain. The upward gradation from rhyolite to andesite in Formation 2 reflects a magmatic evolution typical of compositionally stratified terrestrial volcanoes (Fischer and Schmenke, 1984). Lambert (1974) describes a similar upward gradation from felsic to intermediate volcanism in the Bennett Lake Caldera Complex.

Formation 3 underlies most of the western block of the Mt. Skukum Caldera Complex and conformably overlies Formation 2 . It reaches 700 m in thickness and consists of gently dipping porphyritic andesite flows interbedded with andesitic ash and lapilli tuff, and epiclastic rocks. Porphyritic andesite flows are less abundant and display distinct changes in phenocryst type, size, and abundance in the lower parts of the section and become more abundant and texturally monotonous at higher stratigraphic levels. Individual porphyritic andesite flows range from 2 to 10 m thick, are laterally continuous, and can be traced for more than 1 km (Figure 6). Flows are massive, locally columnar jointed, and commonly have vesicular tops and brecciated flow bottoms. In the highest stratigraphic levels of Formation 3 the proportion of andesitic pyroclastic and epiclastic rocks increases (Figure 4), but porphyritic andesite flows remain dominant. Interbedded andesite flows and fragmental rocks are capped by a thick section of monolithic andesite breccia comprised of poorly sorted, sub-rounded to angular fragments of boulder to pebble sized andesite clasts in a matrix of sand-sized andesite grains (Pride, 1986). These breccias are about 320 m thick, generally poorly bedded, and locally intruded by pod-like columnar jointed andesite sills and dykes. Formation 3 represents proximal and vent facies volcanic rocks deposited on the upper part of a strata-volcano with the thick accumulation of monolithic andesite breccia representing a vent facies mantle of exploded debris scattered down-slope from the vent and locally intruded by sills and feeder dykes of andesitic flow rocks.

Pride (1986) incorporated the monolithic andesite breccia and a portion of the underlying porphyritic andesite flows into a distinct formation (Formation 5) separating lower porphyritic andesite flows and Formation 4 felsic volcanic rocks. Pride's division between porphyritic andesite of Formation 3 and porphyritic andesite of Formation 5 was determined by a slight increase in MgO content in andesites of Formation 5. This author feels that such a geochemical distinction does not form a useful basis for categorization in this case. Although the significance of a monolithic andesite breccia deposited as a final mantle of eruptive activity may warrant recognition, including an upper portion of porphyritic andesite flow rocks on the basis of lithogeochemistry alone is not practical. Andesites of Pride's Formation 3 and 5 are seen in the field to grade into each other without intervening lithologies or textural distinction making field identification impossible without chemical analysis. In addition, an increase in mafic mineral components up-section in any terrestrial volcanic sequence may be expected, and is observed elsewhere in the Mt. Skukum Caldera Complex, the Bennett Lake Caldera Complex (Lambert, 1974) as well as other localities (Fischer and Schmenke, 1984). Thus, the increase in MgO in porphyritic andesites up-section may be expected as the natural sequence of eruptive products from a compositionally stratified magma chamber. All porphyritic andesites and derived monolithic breccia in the south western part of the Mt. Skukum Caldera Complex are considered here to be part of Formation 3. Pride's Formation 4 is retained as the youngest lithological division within the Mt. Skukum Caldera Complex.

Formation 4 comprises the uppermost stratigraphic sequence in the Mt. Skukum Caldera Complex. In the western block, this formation occurs as several irregularly shaped, isolated bodies (Figure 3) that consist mainly of brecciated, flow-banded and spherulitic rhyolite flows and pyroclastic rocks which lie unconformably over Formation 3 (Figure 4). In the eastern block Formation 4 occurs in greater thicknesses and appears to fill at least one nested cauldron subsidence structure in the northeast corner of the volcanic complex. These rocks appear to have been emplaced from small, discrete vent areas on the eastern flank of the older andesitic strata volcano some time after its extinction. Some time after deposition of Formation 4 the entire volcanic complex underwent differential collapse particularly along its southern and western borders. Differential collapse caused the area of felsic volcanics in the east to be down-dropped at least 300 m more than andesitic volcanics in the west. This differential collapse led to preservation of Formation 4 in the east leaving only small erosional remnants

at high elevation in the western side of the complex.

Early Eocene radiometric ages were obtained from two samples of porphyritic andesite from the Main Cirque using whole rock K-Ar methods (Appendix C). Unaltered porphyritic andesite gave an age of 53.2 ± 1.8 Ma; propylitically altered porphyritic andesite gave an age of 50.7 ± 1.8 Ma.

Potassium-argon ages correspond with K-Ar whole rock ages of 52 and 51 Ma (Morrison et al., 1979) from rhyolite porphyry ring-dyke material and associated ashflow tuff from the Bennett Lake Caldera Complex. Pride and Clarke (1985) obtained Rb-Sr dates of 53.3 ± 1.1 Ma from high level rhyolite intrusions associated with the Mt. Skukum Caldera Complex.

The difference of 2.5 Ma in apparent ages between altered and unaltered porphyritic andesite might reflect re-equilibration of the altered sample with hydrothermal fluids responsible for vein formation at Main Cirque. Although these ages overlap if worst case errors are considered, the data indicates veins may have formed 2.5 Ma after deposition of volcanic rocks. Long delays between the time of formation of host rocks and the time of mineral emplacement in epithermal systems are common, particularly in adularia-sericite type deposits where ore deposition generally post-dates rock deposition by more than 1 Ma (Hayba et al., 1985).

GEOLOGY OF MAIN CIRQUE

Economic gold deposits at Mt. Skukum are in the southwestern part of the Mt. Skukum Caldera Complex, in Main Cirque, which forms the headwaters of Butte Creek (Figure 3). Sub-parallel, steeply-dipping, vein-fault systems trending between N10°W and N45°E contain three major mineralized zones in Main Cirque; the Lake Zone, Brandy Zone, and Main Cirque Zone, as well as several others outside the cirque perimeter. The three main zones have been extensively explored through diamond drilling and drifting. The ore-bearing portion of the Main Cirque Zone has been mined out while the remaining two underwent limited production before being temporarily abandoned. Geology discussed below is based on detailed mapping at scales of

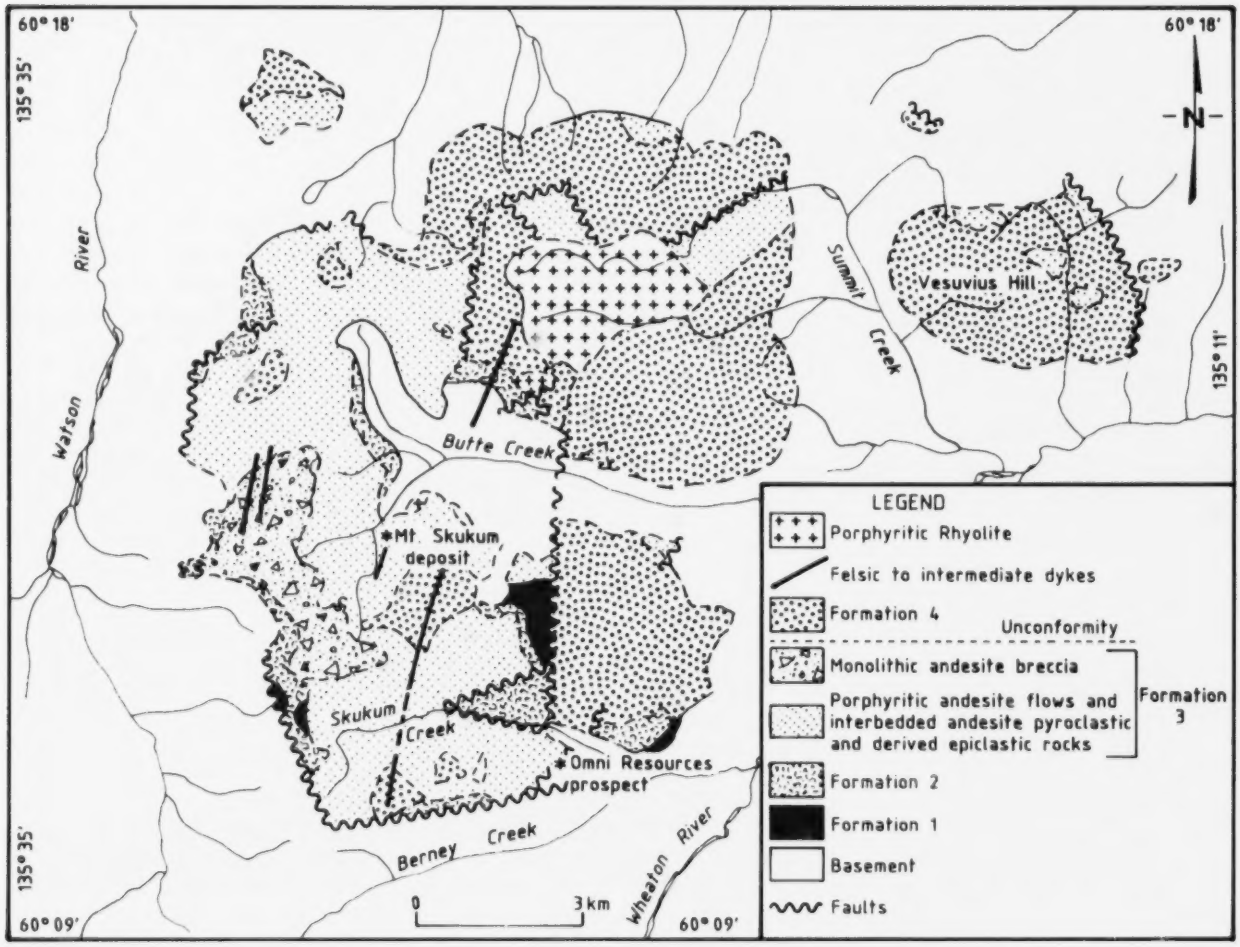

Figure 3. Generalized geology map of the Mt. Skukum Caldera Complex (after Pride,1985)

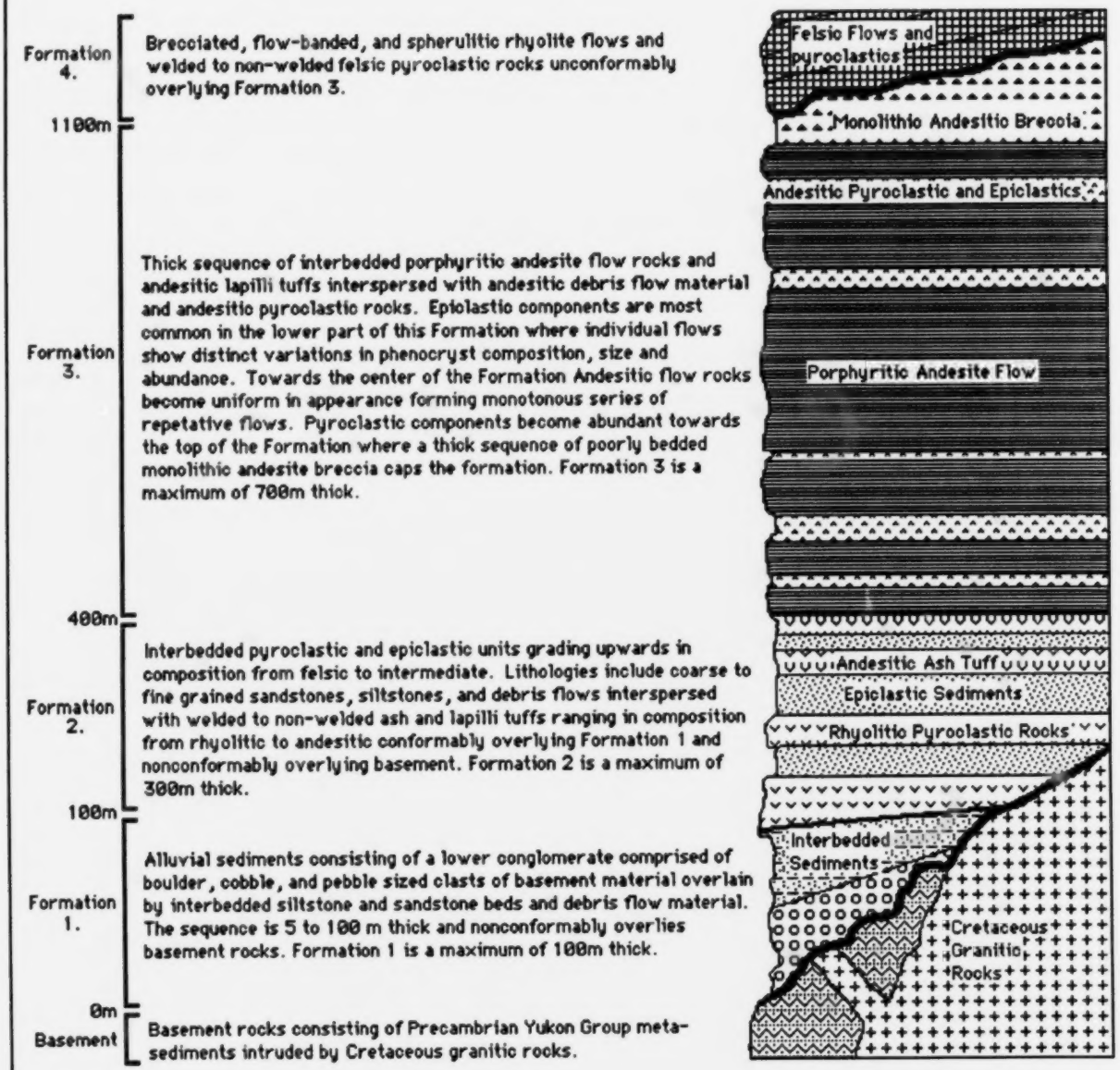
Formation 4.
Brecciated, flow-banded, and spherulitic rhyolite flows and welded to non-welded felsic pyroclastic rocks unconformably overlying Formation 3.
1100m
Formation 3.
Thick sequence of interbedded porphyritic andesite flow rocks and andesitic lapilli tuffs interspersed with andesitic debris flow material and andesitic pyroclastic rocks. Epiclastic components are most common in the lower part of this Formation where individual flows show distinct variations in phenocryst composition, size and abundance. Towards the center of the Formation Andesitic flow rocks become uniform in appearance forming monotonous series of repetative flows. Pyroclastic components become abundant towards the top of the Formation where a thick sequence of poorly bedded monolithic andesite breccia caps the formation. Formation 3 is a maximum of 700m thick.
400m
Formation 2.
Interbedded pyroclastic and epiclastic units grading upwards in composition from felsic to intermediate. Lithologies include coarse to fine grained sandstones, siltstones, and debris flows interspersed with welded to non-welded ash and lapilli tuffs ranging in composition from rhyolitic to andesitic conformably overlying Formation 1 and nonconformably overlying basement. Formation 2 is a maximum of 300m thick.
100m
Formation 1.
Alluvial sediments consisting of a lower conglomerate comprised of boulder, cobble, and pebble sized clasts of basement material overlain by interbedded siltstone and sandstone beds and debris flow material. The sequence is 5 to 100 m thick and nonconformably overlies basement rocks. Formation 1 is a maximum of 100m thick.
0m
Basement
Basement rocks consisting of Precambrian Yukon Group meta-sediments intruded by Cretaceous granitic rocks.
Felsic Flows and pyroclastics
Monolithic Andesitic Breccia
Andesitic Pyroclastic and Epiclastics
Porphyritic Andesite Flow
Andesitic Ash Tuff
Epiclastic Sediments
Rhyolitic Pyroclastic Rocks
Interbedded Sediments
Cretaceous Granitic Rocks

Figure 4 *Stratigraphy in the western portion of the Mt. Skukum Caldera Complex. The Mt. Skukum gold deposits occur in Formation 3*

1:1,000 and 1:5,000; and on detailed logs from over 20,000 m of drill core.

Formations 2, 3, and 4 (Figures 7 and 8) underlie the Main Cirque with andesite flows of Formation 3 predominant. The andesites, which host the gold-bearing veins, are cross-cut by steeply dipping felsic to intermediate dykes, and pebble dykes. These dykes are concentrated in and around zones of structural weakness between fault-bounded, down-dropped blocks which form a collapse feature centered in Main Cirque. Nine mappable units (Figures 7 and 8) have been recognized based on field observation, as well as hand specimen and thin section examination. Each unit encompasses one or more related lithologies including interbedded pyroclastic and epiclastic rocks of Formation 2; interbedded andesite flow rocks and epiclastic rocks of lower Formation 3, monotonous, repetitive andesite flow rocks of middle Formation 3; interbedded andesitic pyroclastic and porphyritic andesite flow rocks of upper Formation 3; and flow-banded rhyolite, felsic megabreccia, and densely-welded felsic tuff of Formation 4. All volcanic units are gently dipping — rarely inclined more than 12°.

Three varieties of igneous rocks occur in Main Cirque; andesite, rhyolite, and dacite. Pyroclastic and epiclastic rocks present in Main Cirque are composed of cognate, essential, and accessory clasts (Fisher and Schmencke, 1984) derived mainly from igneous rocks of these compositions. Table 2 shows the average mineralogical mode for each of the igneous rock compositions in Main Cirque. These and derived volcanic and epiclastic rocks which comprise Formations 2, 3, and 4 in Main Cirque, are described below in order of stratigraphic age from oldest to youngest.

Formation 2:

Formation 2 is restricted to the extreme north-central portion of Figure 7. This formation, in Main Cirque, comprises a bedded sequence of felsic to intermediate pyroclastic and derived epiclastic rocks which form thin individual beds normally about 0.5 m thick and not more than 6.5 m thick (Figure 5). Six lithologies, gradational with respect to grain size and composition, are recognized (in order from oldest to youngest): rhyolite lapilli tuff, rhyolite ash tuff, debris flow/ lahar rocks, volcaniclastic sedimentary rocks, andesitic lapilli tuff, and andesitic ash tuff.

Rhyolite lapilli tuff is relatively uncommon and occurs

Figure 5 *Photograph of well bedded epiclastic units typical of the upper portion of Formation 2. As pictured here, epiclastic unit in the upper portion of this formation are mainly derived from volcanics of andesitic composition.*

mainly in the lower part of Formation 2 as thin beds which, in the Main Cirque, do not exceed 1 m in thickness. Heterolithic fragments, primarily rhyolitic, comprise up to 15 percent basement fragments including pelitic schist, quartzite, and marble. Essential and cognate rhyolite fragments comprise up to 45 percent of the rock and commonly display some degree of welding as indicated by the alignment of collapsed, devitrified pumice fragments which can comprise up to 30 percent of the rock. Matrix material is typically composed of an aphanitic pale-green volcanic ash.

Rhyolite ash tuff is common throughout the lower portion of Formation 2 as pale-green, extremely fine-grained beds, less than 81 cm thick. These rocks are composed of minute shards of partially devitrified volcanic glass containing 2 mm sized essential and cognate rhyolite fragments, minor basement fragments, rare quartz "eyes", and fragmental feldspar crystals. These fragments locally comprise up to 85 percent of the rock but usually constitute less than 10 percent of the rock by volume. Essential fragments are abundant and commonly occur as elongate, collapsed pumice clasts drawn out parallel to bedding and wrapped around cognate fragments to produce a mildly welded texture. Accretionary and armoured lapilli up to 7 mm across are common and comprise up to 30 percent of the rock (Figure 9).

Debris flow/lahar occurs only in the lower part of Formation 2 interbedded with rhyolitic pyroclastic and minor finer grained epiclastic rocks. Beds are commonly 2.5 m thick but locally up to 6.5 m thick, and massive. In hand specimen, these rocks contain an average of 60 percent sub-rounded fragments that are commonly 1 cm across but locally exceed 26 cm across and are enclosed in a matrix of finer grained, poorly sorted material of the same composition. Clasts grade up-section from coarse to fine and from predominantly basement composition in the lower part to predominantly rhyolite in the upper part of the formation. In the lower part of the formation, beds of debris flow/lahar contain clasts averaging 4 cm across comprised of up to 70 percent basement clasts with minor rhyolite and rare andesite clasts. In the upper part of the formation clasts do not exceed 2 cm across and are comprised of 50 percent rhyolite volcanics, 40 percent basement rocks, and 10 percent andesite volcanics. Individual beds commonly display crude reverse grading with coarsest fragments near the

Figure 6 *Photograph showing a typical section of Formation 3 as seen in a cliff exposure near Main Cirque. Repetitive, laterally extensive flows of porphyritic andesite are visible as pale and dark coloured bands running across the cliff. Pale bands represent relatively highly altered zones of interflow breccia, dark bands represent relatively unaltered bands which correspond to massive, unfractured flow centers. The eastern wall of Main Cirque and the reddish-brown gossan of the Alunite Cap Zone is seen in the background.*

top and finer fragments near the bottom. Debris flow/lahaar rocks were deposited as mud and rock slides and are the products of slope instability.

Volcaniclastic sedimentary rocks are most common in the middle and upper portions of Formation 2. Typically, well-defined beds (Figure 5) consist of layers of differing grain size ranging from coarse sand to silt. Clasts vary from rhyolite to andesite with minor basement fragments that become less common in beds higher in the stratigraphy. Hand specimens display a fine laminar bedding characteristically consisting of interbedded sandstone and siltstone layers ranging from 0.5 to 2 cm thick and contain sub-rounded clasts which rarely exceed 4 mm across. Beds range from poorly to well-sorted, and display either reverse or normal grading. Clasts commonly display weathered rinds with compositions and textures similar to enclosing volcanic units .

Andesite ash tuff is common throughout the upper portion of Formation 2. It occurs as massive olive-green to maroon beds ranging from 0.5 to 2.1 m thick. Maroon beds predominate and consist primarily of ash-sized fragments ranging in size from minute to 1 mm across. Lapilli-sized fragments of cognate and essential porphyritic andesite rarely exceed 5 mm across, and can comprise up to 3 percent of the rock enclosed in a matrix of finer cognate and essential grains. Accretionary and armoured lapilli are characteristic. They range from 1.5 to 3 mm across and typically comprise 1 percent, but locally up to 90 percent of the rock. These lapilli are typically ovoid with long axes oriented parallel to bedding and display concentric layers of fine ash particles with an intense hematitic colouration in the outermost layer. Essential fragments are devitrified and commonly highly vesicular with chlorite replacing the andesitic glass and forming rosettes that fill many of the vesicles. Maroon beds occur only in the uppermost part of Formation 2 and form an excellent marker horizon in several exposures in the western part of the Mt. Skukum Volcanic Complex.

Andesitic lapilli tuff is uncommon; found only in the upper portion of Formation 2 where it forms beds ranging in thickness from 10 cm to 2.5 m. A prominent thick bed, which is particularly coarse-grained, forms the cap of Formation 2. Beds are massive, dark grey-green to maroon, and locally display fiammé textures and a weakly welded appearance through the presence of elongate, compressed pumice fragments aligned parallel to bedding. Angular to sub-rounded fragments comprise up to 75 percent of the rock. The other 25% consists of a matrix of ash-sized particles. Fragments are entirely andesite and comprise up to 70 percent devitrified essential fragments and minor cognate fragments altered mainly to chlorite. Fragments are up to 4 cm across but typically between 4 mm and 1 cm. The bed capping Formation 2 is an exception in that it is relatively coarse-grained, approaching a volcanic breccia, and consists primarily of cognate fragments of grey-green andesite with a bi-modal size distribution of 1 and 20 cm across in a matrix of ash-sized maroon andesite particles.

Table 1. *Average visually estimated mineralogical modes of igneous rocks present in Main Cirque, Mt. Skukum, Yukon Territory.*

	Porphyritic Andesite	Andesite Dykes	Dacite	Rhyolite
Whole Rock Mode				
Phenocrysts	15	2	2	26
Groundmass	85	98	98	74
Mineralogical Mode				
Primary Minerals:				
Plagioclase	62	53	41	32
K-Feldspar	-	-	14	25
Quartz	-	-	15	33
Pyroxene	3	Tr	-	-
Apatite	Tr	Tr	-	Tr
Opaques	2	2	-	-
Secondary Minerals:				
Chlorite	13	25	15	3
Epidote	13	-	10	1
Sericite	3	10	-	4
Calcite	2	6	-	2
Leucoxene	-	-	5	-
Pyrite	-	-	Tr	Tr
Quartz	2	4	-	-
Hematite	Tr	-	-	-
Zircon	-	-	-	Tr

Tr = Trace amount

Formation 3:

Formation 3 comprises a widespread sequence of andesite flows intercalated with andesitic pyroclastic and epiclastic rocks. Formation 3 conformably overlies Formation 2 and is unconformably overlain by Formation 4. Formation 3 includes; porphyritic andesite flows, andesitic debris flows, volcaniclastic sandstone, and andesite tuff. These rocks form three sub-units (Figure 7) that reflect textural differences in andesite flows and different associations between lithologies. The lower portion of Formation 3 includes thin, maroon andesite flows displaying variable phenocryst size (from 0.5 to 3 mm) and composition. These flows are intercalated with andesitic debris flows containing a relatively high proportion of felsic clasts. The central portion of Formation 3 is characterized by thick, monotonous porphyritic andesite flows, sparsely interbedded with volcaniclastic sediments and rare pyroclastic rocks. The upper portion of Formation 3 is typified by abundant andesitic pyroclastic rocks interbedded with porphyritic andesite flows.

Porphyritic andesite flow rocks form an integral part of Formation 3 and comprise the major rock type in Main Cirque (Figure 7). The unit forms narrow, extensive, gently dipping

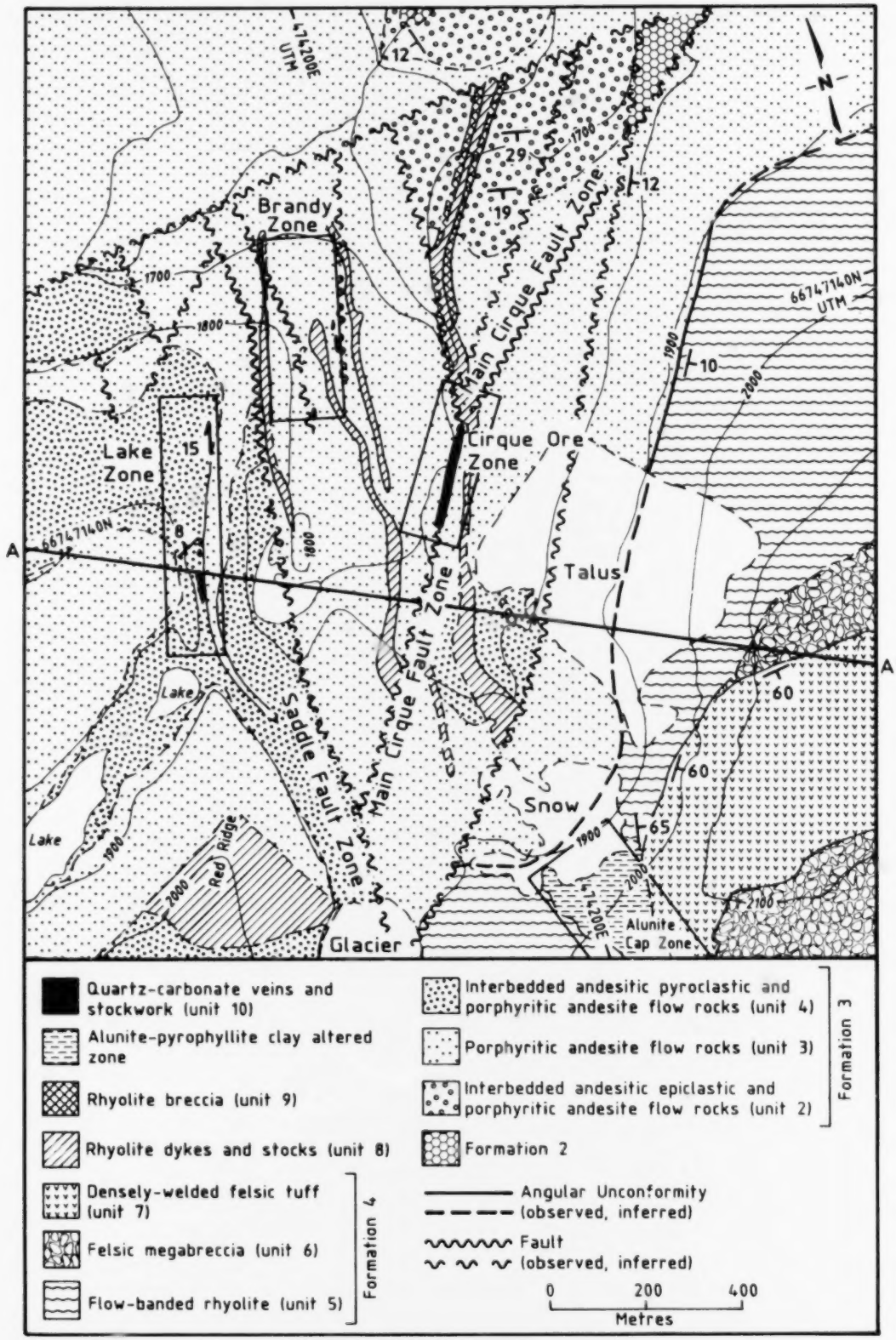

Figure 7 *Geologic map of Main Cirque*

flows (Figure 6) which may be separated from one another by debris flows and pyroclastic rocks, or form a series of flows marked only by brecciated flow tops and bottoms. Fresh surfaces are typically dark grey-green, but range from a dark greenish-black to dark maroon. Darkest coloured rocks tend to be least affected by alteration, are uncommon, and usually occur far from veins in competent central zones of individual flows away from the fractured flow tops and bottoms. Paler grey-green rocks are invariably propylitically to phyllically altered with abundant chlorite, sericite and minor silicification. Dark maroon rocks occur only in the lower part of the formation. Andesite flows contain 15 to 30 percent plagioclase phenocrysts ranging from 2 to 5 mm across and up to 10 percent pyroxene phenocrysts averaging 1 to 2 mm across. Phenocryst size and composition remains relatively constant throughout the central and upper parts of the formation, but vary in the lower part of the formation. Plagioclase phenocrysts may be randomly oriented or display a trachytic alignment. They show oscillatory zonation and range in composition from An_{30} to An_{48}, with an average of about An_{42}. In the freshest samples, plagioclase is nearly free of alteration; however, more commonly, grains are variably saussuritized, sericitized, and silicified. Augite phenocrysts, ubiquitous in andesite flows, are also nearly free of alteration in the freshest samples but are more commonly completely altered to chlorite. Augite and plagioclase occur mainly as isolated crystals but also form glomerocrystic aggregates distributed randomly throughout the rock. Fine grains of magnetite, not visible in hand specimen, constitute 1 to 3 volume percent of fresh andesite and give the rock a moderately magnetic character. In altered specimens magnetite is one of the earliest affected minerals and decomposes to leucoxene.

Andesitic debris flow rocks are most common in the lower part of Formation 3 where they are interbedded with andesite flows and become less common in the central and upper portions of Formation 3. Beds are massive, matrix-supported, and rarely over 3 m thick. They consist of poorly sorted, angular to sub-rounded fragments averaging 3 to 4 cm across in a finer grained groundmass. Coarse fragments comprise up to 70 percent of the rock and are almost entirely composed of porphyritic andesite with some rhyolite of Formation 2, and rare basement fragments. This unit resembles debris flow rocks of Formation 2, but lacks their abundant felsic and basement fragments.

Volcaniclastic sandstone occurs in the central and upper parts of Formation 3 as rare layers seldom more than 1 m thick interbedded with andesitic lapilli tuff and porphyritic andesite flows. Fresh surfaces are dark grey-green, similar to that of propylitically altered porphyritic andesite flows, and characterized by fine laminar interbedding of silt and sand-sized grains which are well-sorted and range in size from 0.2 to 2 mm. Clasts are exclusively andesitic. Coarse-grained beds locally contain interstitial quartz, sericite, calcite, and pyrite, indicating relatively high permeability. This unit resembles finer grained volcaniclastic sedimentary rocks of Formation 2 but lacks their maroon colour.

Andesite tuff is most common in the central and upper parts of Formation 3 where it forms beds of ash to lapilli tuff interbedded with porphyritic andesite flows. Beds range from 10 cm to 7 m thick, are massive, dark grey-green, and generally intensely altered due to a relatively high hydrothermal permeability. Angular to sub-angular lapilli to ash-sized

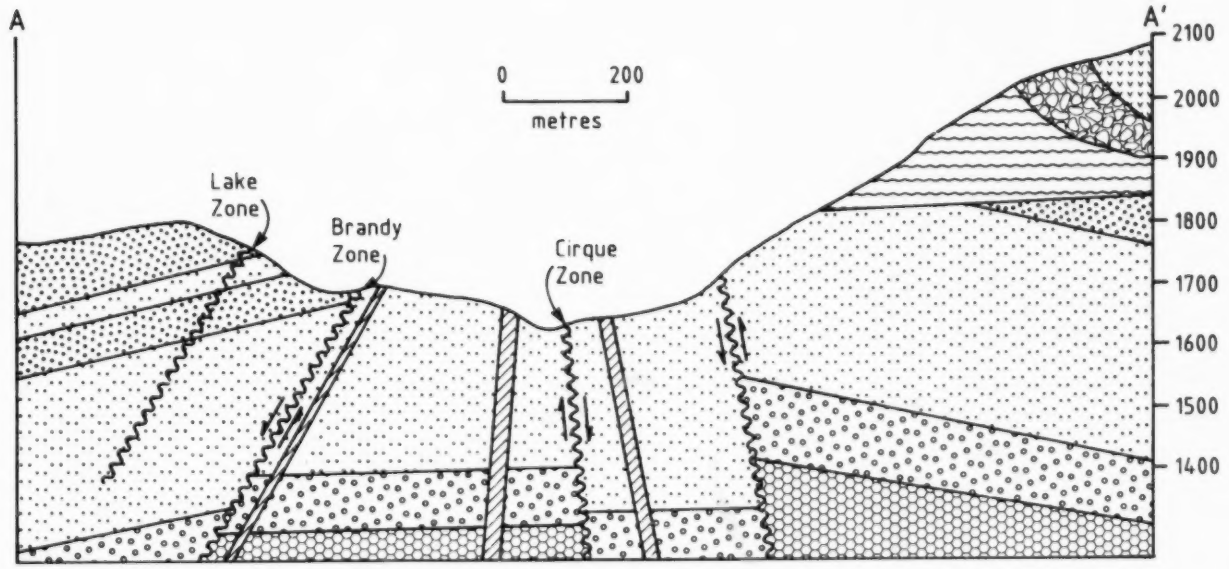

Figure 8 *Geologic cross section of Main Cirque. Section is based on field observation and the geologic map (Figure 7)*

cognate fragments of porphyritic andesite average 3 cm across in lapilli tuffs and rarely exceed 2 mm across in ash tuff. Coarser fragments are enclosed in a finer grained, bleached and, typically, more intensely altered matrix of angular lithic fragments of the same composition, as well as variable amounts of feldspar crystal fragments. Essential fragments are rare, except locally in the upper part of Formation 3 where they comprise up to 15 percent of the rock. Thin sections display intense silicification and sericitization of fragments and matrix with primary plagioclase completely replaced by sericite, calcite, and epidote, and pyroxene completely replaced by chlorite. Locally, intense alteration totally replaces original matrix constituents with quartz and pyrite.

Formation 4:

Formation 4 occurs at the highest elevations (1,900 to 2,100 m) on the eastern wall of Main Cirque (Figure 7). This formation represents a period of explosive felsic volcanism which followed a period of erosion after deposition of Formation 3. Formation 4 overlies Formation 3 unconformably and is composed of flow-banded rhyolite, felsic megabreccia, and a densely-welded felsic tuff.

Flow banded rhyolite forms the lower part of Formation 4, is over 200 m thick and dips gently east-southeast. The rhyolite is maroon, porphyritic, and displays fine flow-banding. Rare plagioclase, orthoclase and quartz phenocrysts are typically less than 3 mm across, and enclosed in an aphanitic felsic groundmass showing fine white and maroon flow-bands wrapped around large, locally abundant spherulites up to 6 cm across. Autobrecciation textures are locally abundant and display angular, maroon, flow-banded, breccia fragments enclosed in a matrix of aphanitic, maroon rhyolite. In the southernmost end of Main Cirque, a circular dome-shaped intrusion of similar composition may represent a feeder to the flow.

Felsic megabreccia occurs in the southeastern corner of Figure 7 where it lines a deeply cut bowl-shaped depression formed in the underlying flow-banded rhyolite. Enormous rotated blocks of flow-banded rhyolite of Formation 4, andesite of Formation 3, and interbedded epiclastics of Formation 2 are enclosed in a greenish-brown, unsorted matrix of finer breccia. This unit attains a maximum thickness of about 200 m with steep to vertical contacts against underlying rocks in the north and east. Some breccia blocks are several times the size of a large house — the largest are comprised of flow-banded rhyolite. This unit is interpreted to partially fill a volcanic crater with the largest blocks of flow-banded rhyolite formed

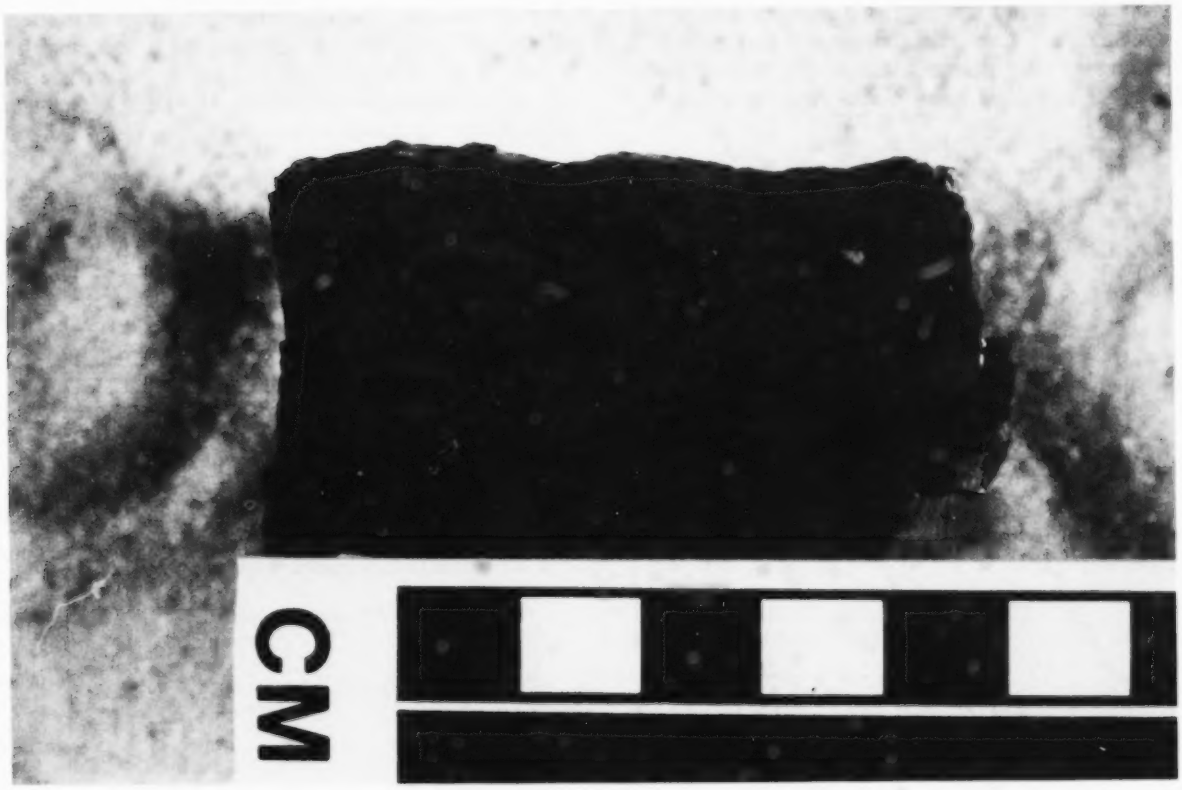

Figure 9 *Photograph of rhyolite ash tuff of Formation 2 showing concentrically layered accretionary lapilli.*

through slumping and collapse of the crater margins. More highly displaced blocks of Formations 2 and 3 may have been deposited during eruption.

Densely welded felsic tuff occurs at the highest elevations in Main Cirque where it overlies felsic megabreccia and fills the crater on the eastern wall of the cirque (Figure 7). The tuff is dark brown, up to 150 m thick, and displays a pronounced columnar jointing. In the crater bottom, where the basal contact is flat, the columns are vertical and straight. On the crater margins, particularly to the north where the basal contact is almost vertical, columns are near horizontal at the base and bend almost 90° to vertical near the top of the unit. The tuff contains abundant cognate and crystal fragments as well as elongate essential fragments with well-developed fiammé (Figure 10). It is interpreted to have formed as a single cooling unit which filled the crater from which it was erupted.

Igneous Intrusive Rocks:

Dykes and stocks of felsic to intermediate composition occur throughout Main Cirque. Intrusive rocks cut strata of Formations 2 and 3 and are interpreted as intrusive equivalents and feeders for volcanic rocks of Formations 3 and 4. Rhyolite, dacite and andesite dykes are recognized; all parallel nearby fault zones and dominant local fractures with common orientations of between 10° and 20° in the Main Cirque. Columnar - jointed porphyritic andesite dykes which cut similar andesitic flow rocks are the oldest intrusive rocks which formed feeders to the extensive andesite flows. Later rhyolite dykes were emplaced in zones of structural weakness, commonly also occupied by veins, which cross-cut porphyritic andesite and rhyolite dykes. Sparsely distributed aphanitic andesite and dacite dykes too narrow to be represented in Figure 7 were emplaced last, and cross-cut vein mineralization and other dykes.

Rhyolite dikes/stocks form large, irregular bodies intruding rocks of Formations 2, 3, and 4. Stocks and dykes are similar in texture and composition, with slight variations in grain size, are associated with mineralized zones, and commonly contain elevated gold values. Samples of rhyolite from Main Cirque and throughout the Mt. Skukum Caldera Complex commonly produce gold values as high as 100 ppb and values as high as 1000 ppb are not rare. The highest gold grades are commonly found in silicified, brecciated cooling margins and narrow, pyritic, silicified hornfels zones within 3 m of small stocks.

Two rhyolite stocks occur in the Main Cirque area, one in the southwestern corner of Figure 7 where it underlies a zone of red hematite staining known as Red Ridge, the other approximately 1.5 km north-northeast of the cirque. Rhyolite dykes form irregularly shaped, steeply dipping bodies up to 30 m thick that trend between N10°W and N35°E, parallel to local fault zones. The rhyolite is tan and massive, with feldspar phenocrysts from 2 to 5 mm across that are randomly oriented in an aphanitic to fine grained, locally flow-banded groundmass. In thin section, fresh groundmass occurs as minute, euhedral, prismatic needles of randomly oriented feldspar enclosed in a mosaic of coarser grained anhedral quartz.

Typically, sericite, calcite, and epidote completely replace phenocrysts and patchy to pervasive propylitization and phyllic alteration affect groundmass. The average mineralogical mode is in Table 2.

A thick marginal breccia flanks both sides of the most prominent rhyolite dyke in Main Cirque which occurs in the Main Cirque Fault Zone (Figure 7) and are common bounding rhyolite stocks and dykes throughout the volcanic complex. These breccias, up to 10 m thick, are composed of a siliceous matrix with up to 5 percent finely disseminated pyrite enclosing angular, tan rhyolite fragments up to 10 cm across. In larger marginal breccia zones, such as that associated with the prominent dyke in Main Cirque, fragment composition becomes increasingly andesitic away from dykes and, adjacent to andesite country rock, breccia fragments may be almost entirely andesite.

Rhyolite stocks and dykes in Main Cirque correlate with high-level porphyritic rhyolite intrusions which cross-cut all formations elsewhere in the Mt. Skukum Caldera Complex (Figure 3) and were probably intruded as a late-stage, resurgent event localized in fractures and faults formed through earlier caldera collapse. These intrusive rocks contain unusually high background levels of gold, are commonly spatially associated with gold - bearing veins, and may have been an important source for precious metals in veins.

Andesite dykes form steeply dipping, north to northeast trending bodies which cross-cut Formation 3. The dykes form two texturally and temporally distinct types which are too narrow to appear in Figures 7 and 8. The earliest and most widely distributed are porphyritic, recessive weathering, widely spaced bodies up to 5 m thick that commonly display a horizontal columnar jointing. These dykes resemble porphyritic andesite flows in colour and phenocryst size, abundance, and composition. They are typically massive, non-vesicular, display narrow chill margins, and are locally glomeroporphyritic. They probably formed feeders to porphyritic andesite flows in the upper part of Formation 3. The later dykes form narrow, steeply dipping bodies which rarely exceed 3 m across. These dykes are similar in composition to the early type but contain fewer plagioclase phenocrysts (average 3 percent). Amygdules comprise up to 5 percent of the rock and commonly display a concentric filling of quartz, chlorite, sericite and calcite. Propylitic and/or phyllic alteration are intense, probably as a result of the close proximity of these dykes to veins. Plagioclase phenocrysts are almost entirely replaced by sericite and carbonate with a patchy alteration of matrix minerals to sericite, calcite, epidote, and quartz. This amygdaloidal, sparsely porphyritic variety of andesite dyke cross-cuts rhyolite dykes in the Main Cirque Zone and quartz-calcite veins in the Lake Zone.

Dacite dykes are steeply dipping, trend north to northeast and are closely associated with amygdaloidal, sparsely porphyritic andesite dykes concentrated near the Main Cirque Fault Zone. These dykes are too narrow to appear in Figure 7 or 8. Dacite dykes are greenish-grey to tan and contain an average of 5 percent plagioclase, orthoclase, and quartz phenocrysts, all between 2 and 6 mm across in an aphanitic groundmass. Matrix feldspar crystals are interspersed with up to 20 percent quartz grains which average 0.26 mm across. Chlorite or calcite completely replace euhedral pyroxene phenocrysts. Amygdules may comprise up to 5 percent of the rock and are typically filled with calcite but locally contain sericite, chlorite and quartz. These dykes are probably penecontemporaneous with the late andesite dykes described above and form similar cross-cutting relationships with rhyolite dykes, but have not been observed to cross-cut veins.

Pebble dykes, typically between 10 and 30 cm and rarely exceeding 1 m across, occur throughout Main Cirque but are most common adjacent to faults which contain veins. These bodies dip steeply and trend parallel to faults and dominant local fractures. They are framework or matrix supported and composed of rounded to sub-angular clasts comprised mainly of porphyritic andesite of variable colour and phenocryst size and composition as well as clasts of granitic rock, rhyolite, pelitic schist, and marble. These fragments are typically 3 mm to 5 cm across, comprise 80 percent of the rock and display intense phyllic and propylitic alteration. Matrix consists mainly of fine-grained anhedral quartz with sericite, epidote and chlorite. Locally, cavities are lined with drusy quartz and calcite crystals up to 7 mm long. Pebble dykes cross-cut Formation 4, some pre-date mineralization but in many cases pebble dykes are closely related to gold-silver bearing veins.

Whole Rock Geochemistry of Igneous Rocks in Main Cirque

Forty-nine representative samples including 10 of fresh rhyolite, 3 of dacite and 36 of andesite from Main Cirque were analysed for major and trace elements by X-Ray Assay Laboratories, Don Mills, Ontario using X-ray Fluorescence (Appendix A). These three rock types comprise the fundamental elements of all epiclastic and pyroclastic rocks in the Main Cirque. Samples were chosen to avoid effects of hydrothermal alteration, however, oxygen isotopes indicate that all have been affected to some extent, even those perceived in hand specimen to be pristine. Complete data sets of chemical analyses used below are listed in Appendix A and B and summarized in Table 2.

Classification:

Igneous rocks from Main Cirque have been broadly

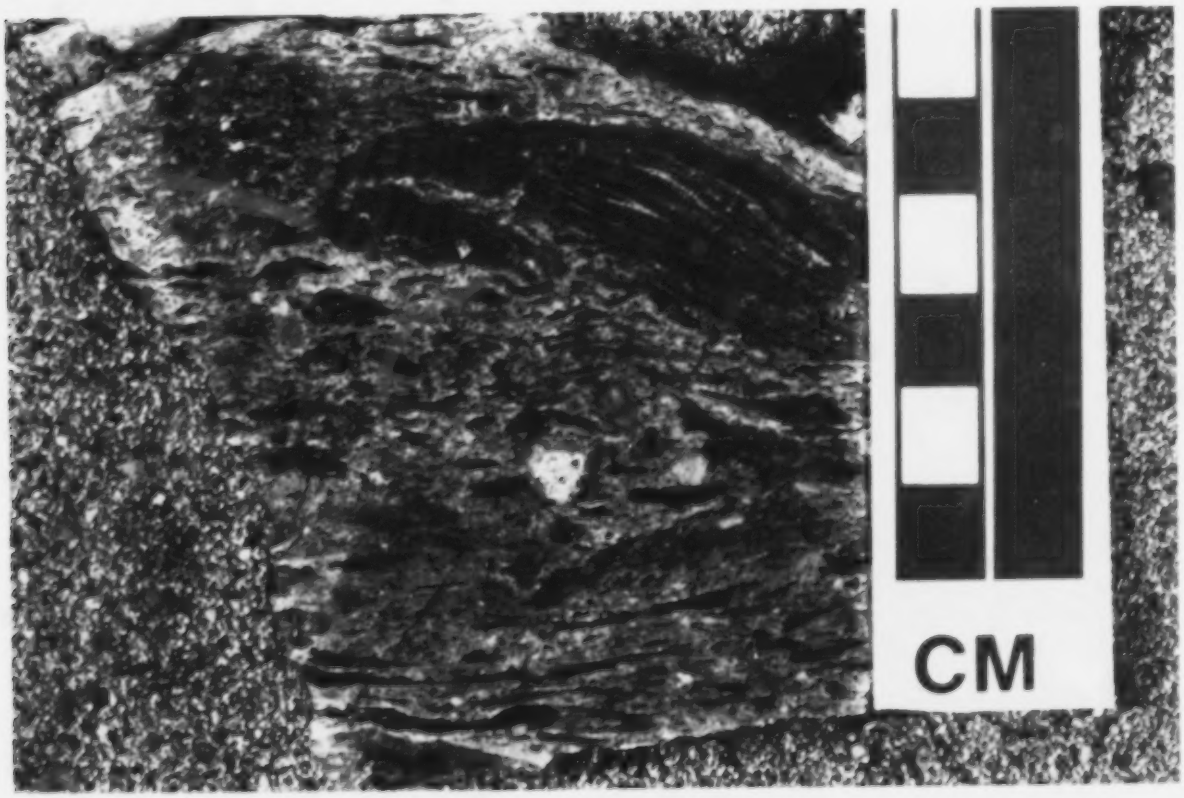

Figure 10 *Photograph of a hand specimen of densely-welded felsic tuff of Formation 4 showing elongate essential fragments and associated fiammé.*

classified using the AFM diagram of Irvine and Baragar (1971)(Figure 11). The close grouped, linear plot of the 49 samples shows a narrow range of hydrothermal alteration reflecting the relatively fresh nature of selected samples. All samples are calc-alkaline and display a discontinuous, curvilinear trend between two elongate clusters of points which probably represents a fractionation series. The tendency of points to cluster into two elongate groups rather than to form a continuous linear distribution is possibly a result of sampling over the restricted area of Main Cirque which represents merely a portion of the complete magmatic series in the complex. It may also indicate a bimodal volcanic suite. No basalts are present in the Main Cirque area.

The geochemical classification scheme of LeBas (1986) allows a more detailed characterization involving the plot Na_2O+K_2O vs. SiO_2 (Figure 12). Using this scheme the felsic and the more mafic rocks still form two clusters and most samples are slightly oversaturated in silica. Rocks named andesite on the basis of petrography cluster on the junction between four fields of intermediate composition and are evenly distributed between the basaltic andesite and andesite fields, but a few overlap into the basaltic trachyandesite and trachyandesite fields. Two specimens identified petrographically as dacite plot on the edge of the felsic cluster

Table 2. *Average major element geochemistry of the three igneous rock compositions found in Main Cirque, Mt. Skukum, Yukon Territory. Data is from Appendix 3.A.*

Elemental Oxides[1]	Porphyritic Andesite n = 36	Dacite n = 3	Rhyolite n = 10
SiO_2	57.1	63.8	72.0
Al_2O_3	16.4	15.4	13.22
CaO	5.86	3.14	0.81
MgO	2.76	1.36	0.24
Na_2O	2.73	4.02	2.88
K_2O	2.81	3.32	5.54
Fe_2O_3	7.20	4.30	1.82
MnO	0.13	0.08	0.04
TiO_2	0.99	0.65	0.17
P_2O_5	0.28	0.22	0.03
LOI	3.03	3.26	1.61
SUM	99.29	99.55	98.36
Zr	176	200	120

1. SiO_2 to LOI in weight %, Zr in ppm. Fe_2O_3 = Total Fe as Fe_2O_3.LOI = Loss on ignition. n = number of analyses, listed in Appendix A, used in calculation of average.

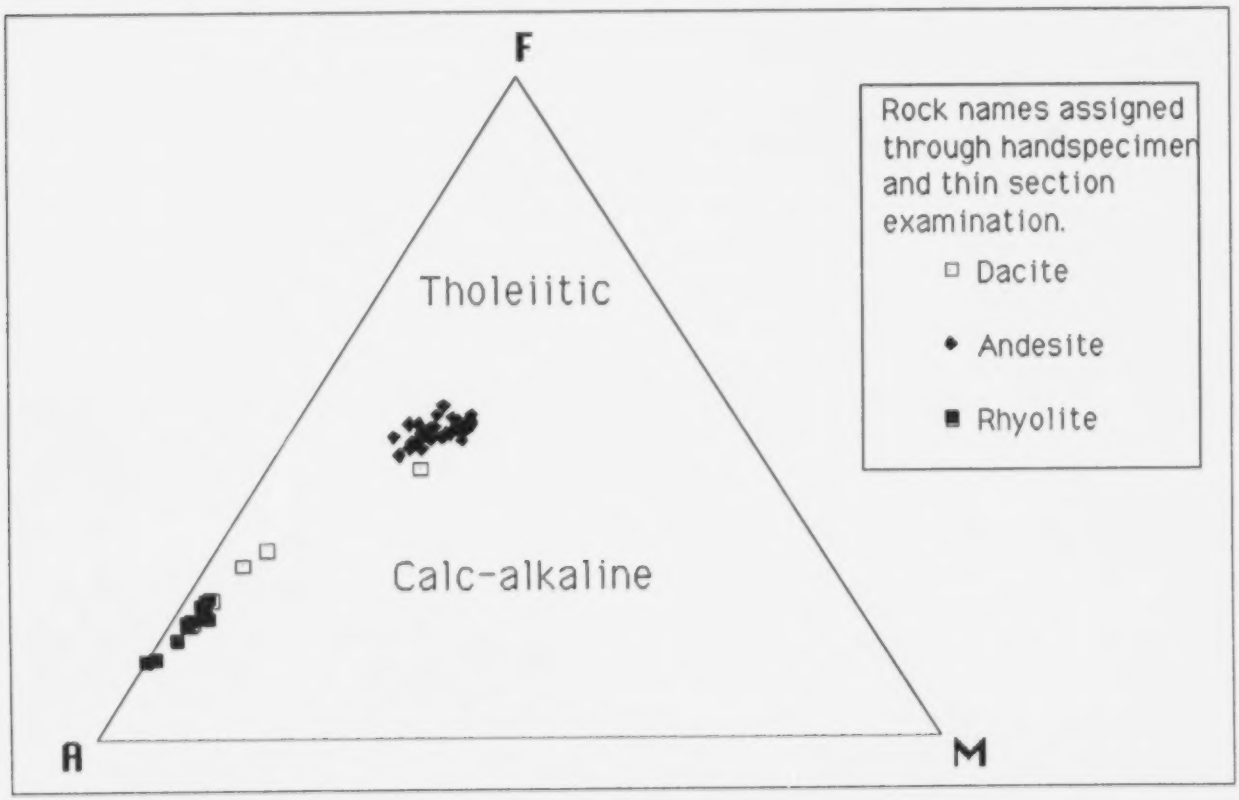

Figure 11 *AFM plot after Irvine and Baragar illustrating the calc-alkaline nature of igneous rocks at Mt. Skukum. Data is from Appendix 3.A. A = Na_2O+K_2O, F = Total iron, M = MgO.*

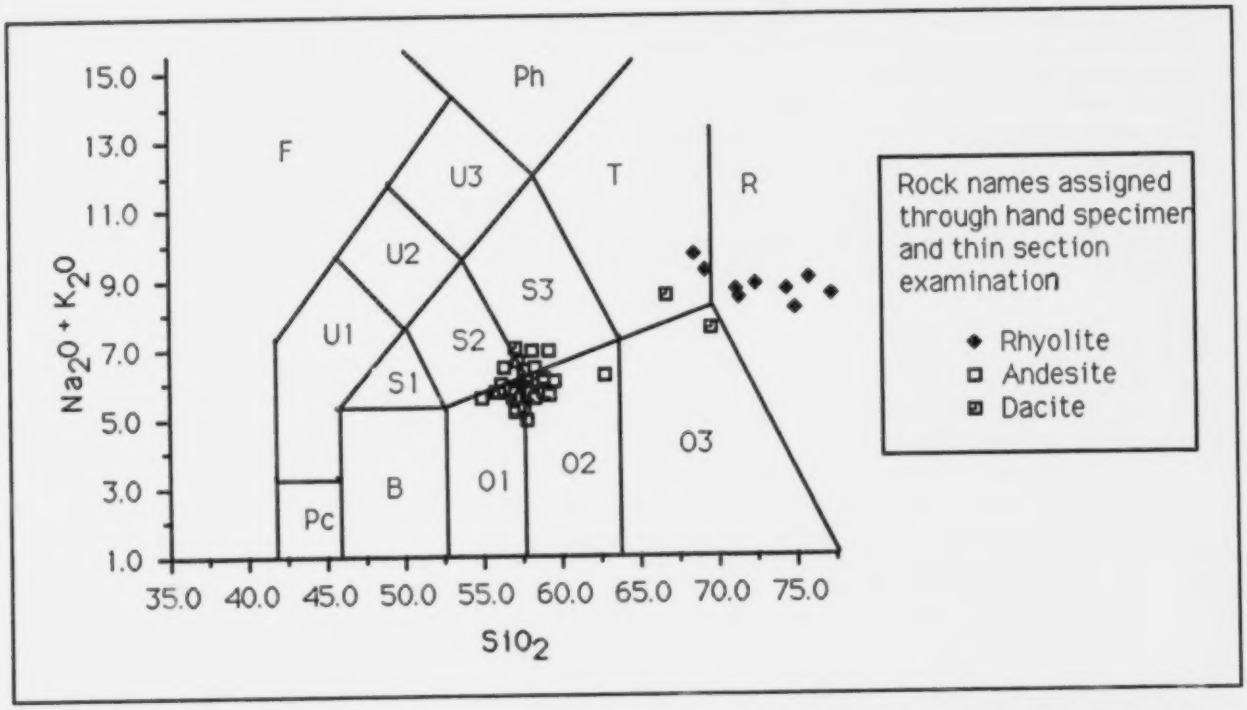

Figure 12 *Plot of Na_2O+K_2O and SiO_2 after LeBas (1986) illustrating the distribution of lithologies at Mt. Skukum, Yukon Territory using this geochemical classification scheme. Data is from Appendix 3.A. Abbreviations are as follows: F = foidite, Pc = picrobasalt, U1 = basanite-tephrite, U2 = phonotephrite, U3 = tephriphonolite, Ph = phonolite, B = basalt, S1 = trachybasalt, S2 = basaltic trachyandesite, S3 = trachyandesite, T = trachyte, O1 = basaltic andesite, O2 = andesite, O3 = dacite, R = rhyolite. The letters O, S, and U indicate the general state of silica saturation: O = oversaturated, S = saturated, and U = undersaturated.*

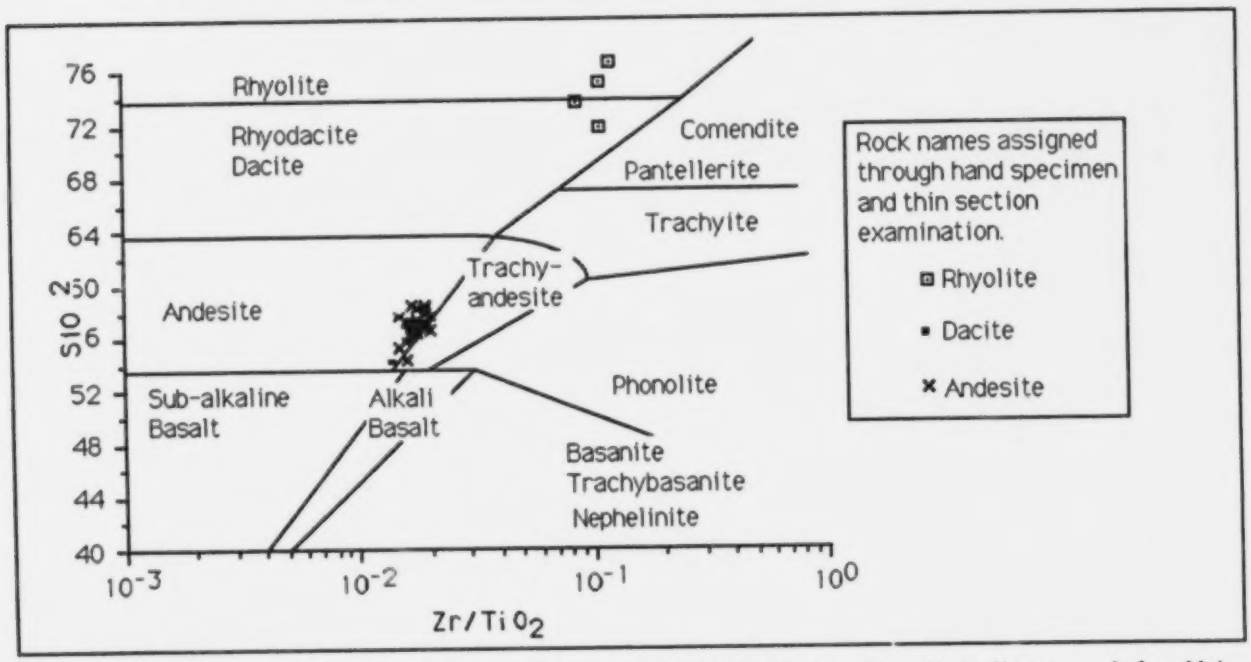

Figure 13 *Geochemical classification plot after Winchester and Floyd, 1977 showing the positions of igneous rocks from Main Cirque, Mt. Skukum, Yukon Territory. Data is from Appendix 3.A.*

straddling the boundary between the trachyte and dacite fields. Two specimens identified petrographically as rhyolite plot as trachytes; eight others plot in the rhyolite field. Once again, data in Figure 12 probably represents the volcanic products of fractionation. As in Figure 11, the lack of a continuous trend between data clusters may indicate a bimodal volcanic suite but may also be the result of sampling within the limited area of Main Cirque which restricted access to the full variety of rock types expected from differentiation. The relatively high concentration of sodium and potassium, as well as silica saturation rather than oversaturation of some rhyolite samples, may be due to an influx of hydrothermal fluids rich in potassium. As this process is shown to occur in highly altered rocks, the overlap of points into the trachyte and trachyandesite fields may not entirely reflect the original chemistry.

The classification scheme of Winchester and Floyd (1977), which involves the plot of SiO_2 vs. the ratio Zr/TiO_2 (elements usually considered immobile)(Figure 13), is intended to minimize the effects of hydrothermal alteration. Using this plot, most samples are subalkaline with several of the more mafic rocks lying inside of the mildly alkaline boundary. The data form two clusters, one in the andesite field with some specimens extending into the trachyandesite field, the other, on the rhyolite-rhyodacite border. The lack of a continuous trend between data clusters is possibly again the result of sampling within the limited area of Main Cirque, to which this study is restricted, but is inconclusive as to the likelihood of a bimodal volcanic suite.

Discussion:

The calc-alkaline character of Main Cirque igneous rocks (Figure 11) is consistent with the location and geology of the Mt Skukum Volcanic Complex. Calc-alkaline rocks are prominent throughout the North American Cordillera and other Circum-Pacific regions and are typified by basalt-andesite-dacite-rhyolite associations in andesitic volcanos (Irvine and Baragar, 1971). In Figures 12 and 13 igneous rocks of Mt Skukum were found to be generally oversaturated in silica, and sub-alkaline in nature, an observation that supports the calc-alkalic classification in Figure 11. The rock compositions cluster primarily as two lithological groups, one of andesite and one of rhyolite with minor dacite indicated in Figures 12 and 13. The possibility of minor hydrothermal enrichment of fresh rocks in potassium causing the artificial classification of some rocks in the more alkalic trachyandesite and trachyte fields in Figure 12 is reasonable due to the close proximity of these dykes to mineralized veins. In the Winchester and Floyd plot (Figure 13) secondary enrichment in mobile elements does not affect the fields rocks are plotted in, thus using this scheme, all felsic rocks plot in the subalkaline rhyolite and rhyodacite fields. Consequently, igneous rocks in Main Cirque are seen to trend between a sub-alkalic andesite through sub-alkalic dacite to sub-alkalic rhyolite.

Structure

A series of high-angle normal faults form an asymmetric graben centered on the Main Cirque Zone. Faults trend northeast with a series of splays branching north (Figure 7) which define at least three wedge-shaped blocks. The downward displacement of each block appears to increase progressively to the east resulting in a step-like topography (Figure 14) downward from west to east. The eastern and western walls of the cirque are marked by fault scarps which form the edges of the graben and describe two of three large faults in Main Cirque. The eastern bounding fault is inferred by displaced marker tuff horizons in Formation 2; the western bounding fault, known as the Saddle Fault, is visible as a prominent, recessive photo-linear and has been intersected in drill holes.

The eastern wall of the cirque is the largest fault scarp, rising steeply to a height of over 400 m to expose Formation 2, 3, and 4 on its northern face (Figures 7). Evidence of displacement up to 250 m along this fault is seen in the exposure of upper Formation 2 on the escarpment of the east wall approximately 250 m higher than 600 m to the west of this escarpment. Although an intervening, east-west trending fault is inferred to have down-dropped rocks to the north, a maximum displacement of 250 m is indicated.

The Saddle Fault, which trends about 20° along the foot of the western wall of Main Cirque, consists of a highly fractured zone of small, en echelon faults dipping about 60° west. Sense of displacement is unknown but is assumed to be east side down. The Brandy and Lake Zone veins parallel this fault within 100 m east and west of it respectively. A rhyolite dyke at least 700 m long intrudes the fault along its entire length.

The Main Cirque Fault Zone forms the third large fault in the cirque. It is visible in air photographs as a prominent linear depression that trends northeasterly across the central part of Main Cirque. The zone ranges from 20 to 30 m across and consists of two to three large faults and associated intense fracturing that is poorly expressed on surface but apparent in drill core as gouge 10 cm to 3 m wide. The fault is divided into southern and northern segments, each with slightly different orientations (Figure 7). The southern segment trends approximately 035° and dips eastward at 80°; the northern segment trends approximately 045° and also dips 80° to the east. Quartz-carbonate veins are thickest, felsic to intermediate dykes most common, and gouge material is best developed in the southern segment of this zone. The sudden change in attitude along this fault and the coincidental thickening of associated veins and enhancement of gold grade are probably genetically related as any transverse motion along this fault would allow development of large open spaces on the northern or southern segments of the fault dependent on the sense of motion.

Strata in and around Main Cirque tend to be flat-lying with dips less than 20°. Attitudes in the center of the cirque vary

from one down-dropped block to another reflecting the disjointed nature of these most highly displaced blocks. Strata on the west wall of the cirque dip 10° west and on the east wall dip 10° east. These divergent attitudes may reflect the original topography surrounding an eruptive center, or may indicate a doming of the area during insurgence of high-level rhyolitic stocks and dykes analogous to a resurgent doming event. Divergent dips displayed by major faults, and associated structurally controlled dykes and veins on the eastern and western sides of the cirque, support a resurgent doming event centered on Main Cirque after graben formation.

Summary

Evolution of the Mt. Skukum Volcanic Complex (Figure 15) began with deposition of lower conglomerate and debris flow rocks of Formation 1 that contain abundant basement fragments which reflect rapid erosion and instability of basement rocks associated with magmatic intrusion and incipient volcanism. Volcanic rocks of Formation 2, include lower thicknesses of felsic tuffs and debris flows that filled basement topography and reflects periods of violent volcanic eruption. These rocks grade upward from felsic to andesitic in composition, and represent the magmatic fractionation series produced by the parent magma. They also show a consistent decrease in content of accessory clasts as well as a decrease in grain size of associated epiclastic rocks; this reflects an increasing thickness of volcanic stratigraphy that filled and leveled off underlying basement paleotopography. Lithologies of Formation 3, include porphyritic andesite flows, andesitic pyroclastic rocks, and epiclastics considered to have formed as a proximal facies to an andesitic stratavolcano which covered the western and southern parts of the volcanic complex (Pride, in press) centered in the vicinity of Main Cirque. The uppermost monolithic andesite breccia unit of Formation 3 in the southeastern corner of the complex south and west of Main Cirque is interpreted to represent explosion and talus breccia and slump blocks formed on the inclined southeastern side of this volcano. Lithologies of Formation 4 are interpreted as part of a felsic volcanic event that occurred sometime after andesitic volcanism had ceased. Although this latest volcanic cycle appears to have been concentrated in the east, several isolated areas of Formation 4 are present in the west. Since erosion may have removed much of this felsic event in the western portion of the complex, it may have actually been widespread.

Structural and stratigraphic evidence in Main Cirque indicates a downward displacement of large blocks along

Figure 14 *Photograph of Main Cirque, Mt. Skukum, Yukon Territory, looking due south showing the fault scarps forming the east and west walls of the cirque and the step-like topography produced by down dropped blocks. The traces of several faults are visible on the escarpment at the front of the cirque.*

steeply dipping, north-trending normal faults. This produced a graben structure centered on the cirque. The collapse event which caused formation of this structure was probably related to depletion of a magma chamber at depth towards the end of intermediate volcanism. These faults provided an ideal locus for subsequent dyke intrusion and vein formation (Figure 15).

Emplacement of high-level porphyritic rhyolite stocks and dykes throughout the Mt. Skukum Volcanic Complex occurred after the last cycle of felsic volcanism. This is seen throughout the complex in cross-cutting relationships mapped by Pride (1985) and Doherty et. al. (1988) and in the structural control displayed by correlative rhyolite dykes and the stock in Main Cirque (Figure 7). Emplacement of these rhyolite intrusions probably coincided with doming of rocks in Main Cirque along a north-south axis represented by divergent dips observed in rocks of the eastern and western walls the cirque (Figure 7). This relation is compatible with dyke emplacement during an extensional reopening of normal faults by doming associated with a deeper rhyolitic intrusion under Main Cirque (Smith et al., 1961). Intrusion of minor intermediate dykes, followed emplacement of rhyolite dykes and vein formation (15d).

MINERALIZATION

The Mt. Skukum gold-silver deposits consist of low sulphide, electrum and native silver-bearing, quartz-carbonate-sericite veins which formed in an epithermal environment within several hundred meters of paleosurface. Historical reserves at Mt. Skukum totalled 230,000 tonnes of ore with an average grade of about 14 gms Au/tonne. Mineral and alteration assemblages resemble those found in adularia-sericite epithermal systems as described by Hayba et al. (1985). Veins representing all levels of mineral emplacement in a typical epithermal environment, are exposed in Main Cirque.

Economic veins occur in the south central part of the Mt. Skukum Caldera Complex in Main Cirque where they occupy several subparallel fault zones which trend N10°W to N50°E and dip between 80° east and 60° west. These vein systems are, from east to west, the Main Cirque Zone, Brandy Zone and Lake Zone. Separation between the zones is approximately 300 m. The Main Cirque Zone, the largest of these ore-bearing structures, forms a continuous zone of massive or stockwork veins traceable along strike for 1.5 km and down dip as a strong structure for over 100 m.

The veins have characteristic features of high-level emplacement such as crustification, chalcedonic quartz, brecciation textures with well-formed cockscomb quartz, and calcite crystals up to 15 cm in size. Large drusy cavities are common in framework supported breccias containing wall rock fragments and colloform layers of quartz. Two main types of veins are present in all precious-metal bearing zones; early, blue-grey, pyrite - bearing chalcedonic quartz veins, and later, gold-silver bearing, coarser grained quartz-carbonate veins. Barren early chalcedonic quartz occurs primarily as veinlets with pyritic selvages and envelopes and associated pervasive wall-rock alteration. The later, coarser grained, quartz-carbonate veins constitute most vein material in all gold-bearing zones, cross-cut earlier chalcedonic veinlets, and form a final filling in fractures already partially filled by chalcedonic material. These veins are characteristic of the Main Cirque area and contain most known gold but rarely contain sulphides.

The Main Cirque Zone, Brandy Zone, and Lake Zone, although generally similar, display slightly different styles of mineralization. The vein in the Main Cirque Zone contains variable proportions of quartz and carbonate with a 60 percent to 40 percent ratio of calcite to quartz predominant. Veins with at least 50 percent calcite tend to be favourable hosts to gold mineralization. The Brandy Zone consistently contains more carbonate minerals (generally more than 60% calcite) characterized by white to grey crystals up to 15 cm across in narrow, high grade, stockwork veinlets and parallel veins up to 0.4 m wide. Veins in this zone occupy a well defined, continuous fracture zone rarely more than 0.4 m wide. Lake Zone veins average 2 m wide, and contain abundant, coarse wallrock breccia up to 10 m across overgrown by colloform, 3 cm thick layers of coarse white and dark grey calcite. Sucrosic quartz and chalcedony fill remaining spaces between colloform layers leaving few open spaces within the veins. Sulphides, absent in other veins, are present locally in this zone, with sphalerite, galena, and rare chalcopyrite comprising up to 5 percent of vein material in rare "patches" up to 4 m across. Vein thickness varies dramatically with some areas swelling abruptly from a barren, 10 cm wide fault structure into a 7 m wide, vertically extensive, highly fragmental breccia pipe within the narrower, laterally extensive vein.

The Main Cirque Zone

The Main Cirque Zone constitutes the largest orebody yet found in the Mt. Skukum Volcanic Complex. It is centrally located in Main Cirque (Figures 3 and 4) in the Main Cirque Fault Zone, a 1 m to 40 m wide fault zone within one of the central blocks of a complex graben. This fault zone trends 035° in the southern part of Main Cirque but displays a sharp divergence to a strike of 045° in the northern part of Main Cirque. Veins have been traced along the known 1.5 km length and down-dip for over 200 m below surface along this strong, near-vertical vein-fault structure.

Vein material occurs along the entire length of the Main Cirque Fault both north and south of the prominent flexure. Veins typically occur as 0.5 m to 25 m wide zones of stockwork quartz-calcite veinlets 5 mm to 2.0 m wide, cross-cutting rhyolite and porphyritic andesite dykes, hydrothermal breccia zones, and pebble dykes within the fault zone. These veins narrow at depth, and only in one 200 m long interval, which extends immediately south from the flexure in the fault structure, does the vein system consolidate into a single, compact vein structure which contains four near-vertical ore shoots which

Figure 15 *Series of four schematic cartoons (a to d) illustrating the possible sequence of events forming the excellent ground preparation at Mt. Skukum, Yukon Territory, leading to formation of epithermal vein mineralization at Main Cirque. Each diagram represents a distance of about 15 km from west to east.*

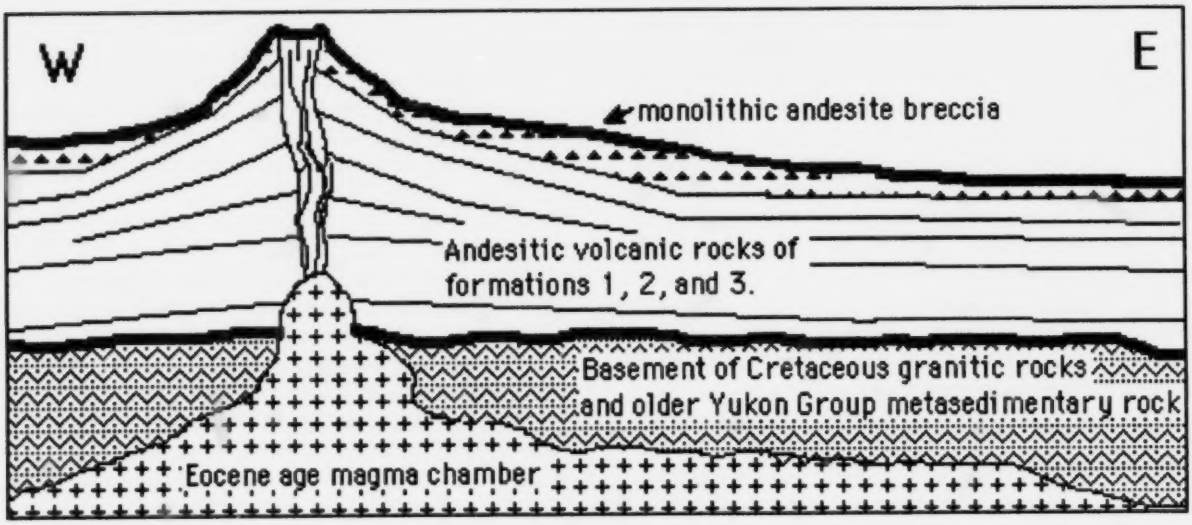

Figure 15a *Early deposition of volcanic rocks of formations 1, 2, and 3, lead to the development of an andesitic stratavolcano in the southwestern portion of the volcanic complex centered in the vicinity of Main Cirque and capped by a mantle of monolithic andesite explosion and talus breccia as well as slump blocks.*

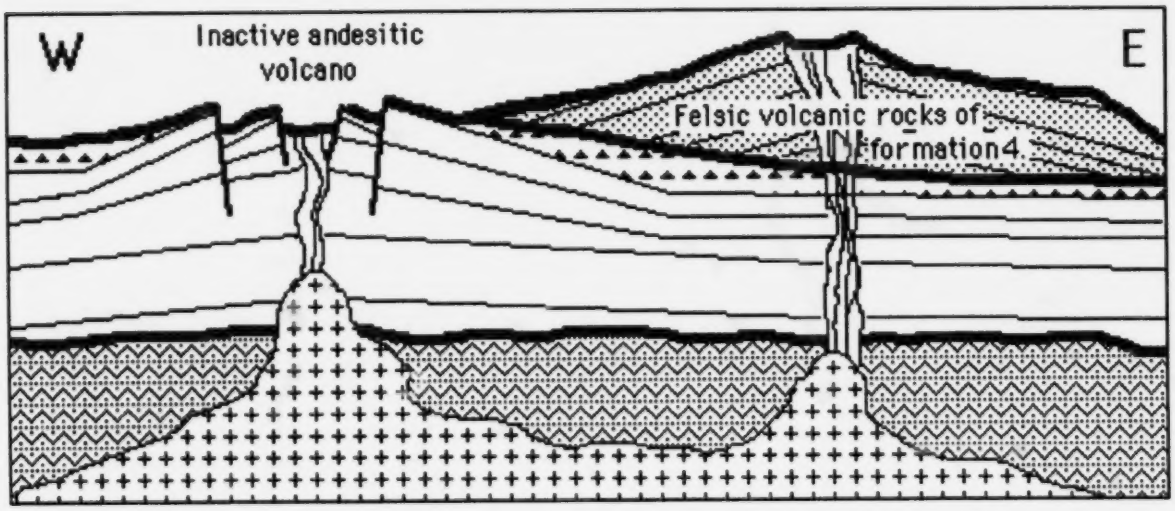

Figure 15b *A period of erosion following the end of andesitic volcanism was succeeded by a period of felsic volcanism centered mainly in the west which lead to deposition of formation 4.*

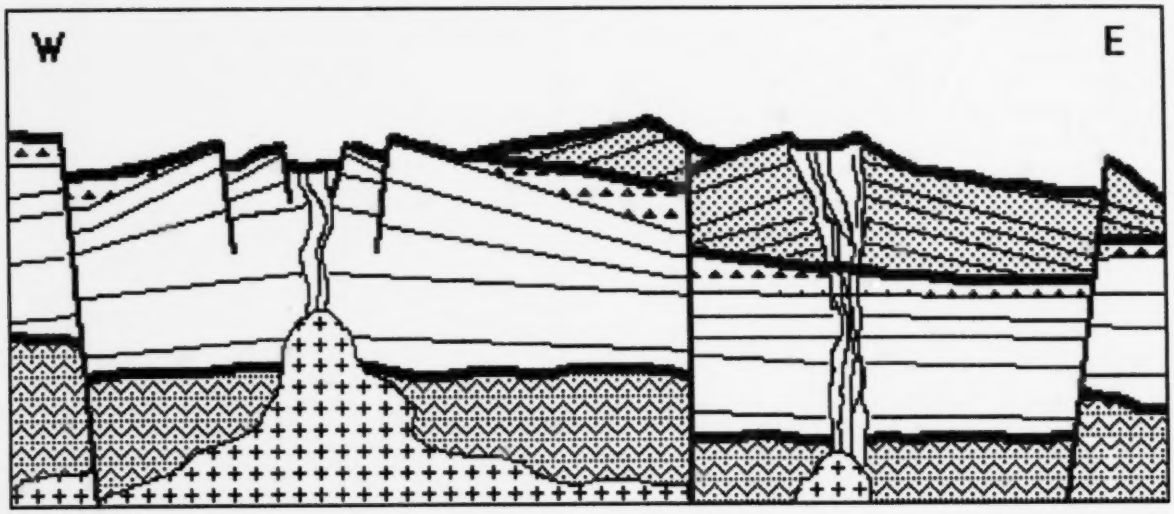

Figure 15c *This final cycle of felsic volcanism led to a depletion of the parent magma chamber at depth causing a regional subsidence of the volcanic complex and formation of a caldera bounded by high-angle normal faults. This was accompanied by the development of a major north trending fault dividing the volcanic complex in two with maximum displacement of rocks on the eastern side.*

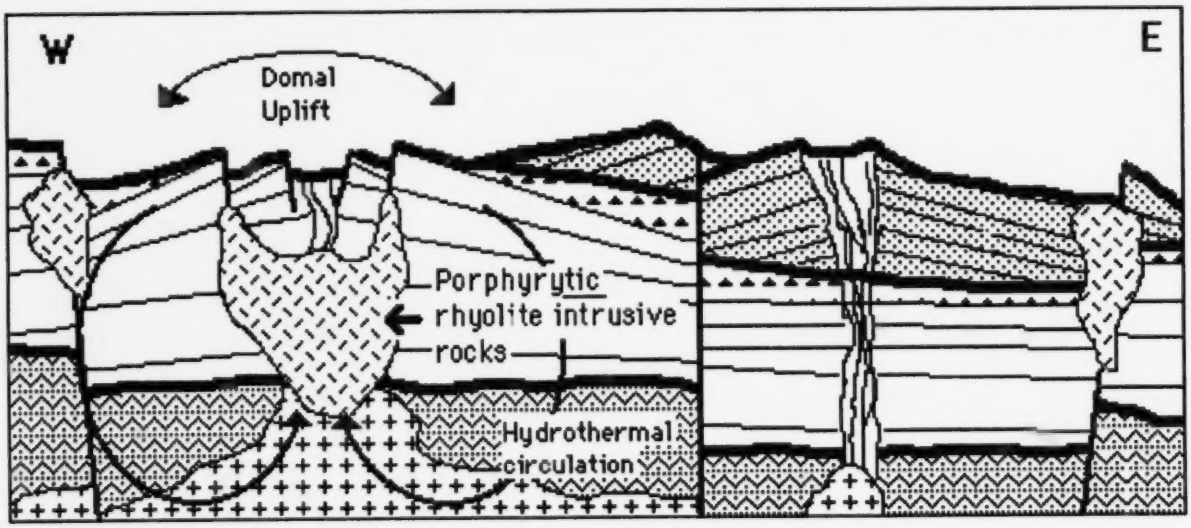

Figure 15d *Late stage intrusion of high-level porphyritic rhyolite stocks and dykes in structurally prepared sites caused an upward doming of volcanic stratigraphy at Main Cirque and provided a heat source to drive hydrothermal circulation that formed mineralized veins.*

contain grades up to 1,612 grams Au/tonne. Over this interval the vein averages 5 m wide and reaches a maximum width of 13 m. The extreme, consolidated thickness of vein material south of the fault flexure may be caused by the change in strike between the northern and southern segments, as even slight rotational or dextral strike-slip displacement brought about on the northeasterly-trending segment would open the southern segment as an enormous cavity which may have controlled ore deposition.

Three temporally, texturally and mineralogically distinct phases of vein mineralization are recognized in the Main Cirque Ore Zone. The two earliest phases are hypogene in origin and gold-bearing whereas the latest phase is supergene in origin and is barren. These three phases are detailed below.

The first and earliest phase of hypogene mineralization comprises blue-grey chalcedony veinlets , rarely more than 2 mm across, which display fine-grained selvages of intergrown pyrite and/or hematite and pyritic envelopes characterized by a narrow zone of silicification followed by a zone of argillic alteration. Coexistent pyrite and hematite , in the absence of supergene effects, indicate that they precipitated from solutions which fluctuated in oxidation state. Strong argillic alteration envelopes surrounding these veins are commonly up to 7 cm wide. Lithic fragments in the veins are commonly intensely silicified and argillically altered. Blue-grey chalcedony also fills hydrothermal breccias either as an early phase that coats fragments in framework-supported breccias, or filling myriad small hydrothermal breccias, typically no more than 10 cm across, which anastomose throughout andesitic volcanic rocks of the Main Cirque area. Blue-grey chalcedony veinlets are consistently barren, whereas chalcedony-filled breccias locally contain up to 60 grams Au/tonne.

Most gold occurs in the second, most common phase of hypogene veins. These veins characteristically consist of quartz with variable amounts of calcite and sericite, minor adularia and traces of albite. Other minerals present locally include, in order of abundance, fluorite (purple, green, and transparent varieties), ankerite, anhydrite, rhodochrosite, palygorskite, pyrite, barite, electrum, and native silver. Open-space filling textures are characteristic and include cockade and comb textured crystal growth around breccia fragments and lining vein walls (Figure 16), drusy cavities lined with variable layers of coarse grained quartz and calcite crystals, colloform layering, and ubiquitous breccia (Figure 17). These veins cross-cut all lithologies except late - stage andesite dykes and also cut pyritic, chalcedony veins described above. Quartz-carbonate veins range from 2 mm to 13 m across. The larger

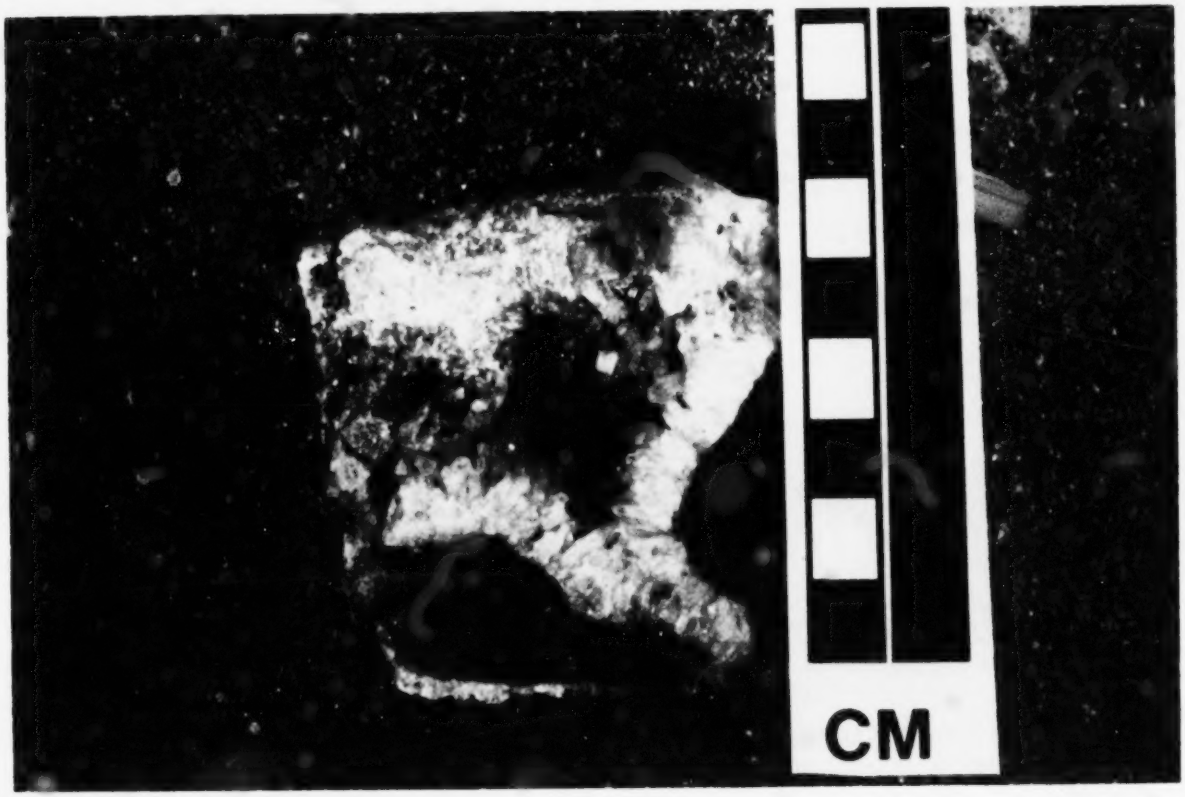

Figure 16 *Photograph of quartz-carbonate vein-breccia showing open-space filling textures in a drusy, quartz-lined cavity from the Main Cirque Ore Zone.*

bodies are continuous and strongly structurally controlled, bifurcating and changing attitude abruptly at the intersection of major fracture sets. Multiple emplacement episodes are indicated. Brecciated and recemented fragments of earlier-formed quartz-carbonate vein material are ubiquitous. Thin sections commonly reveal abundant fragments of coarse-grained, earlier formed vein material in a matrix of fine-grained quartz-carbonate-sericite in rocks which appear massive in hand specimen (Figure 18).

Wallrock breccia is characteristic of Main Cirque Zone veins with the abundance of wallrock fragments increasing toward vein margins. Typically, vein - wallrock contacts are transitional and wallrock breccia fragments increase in number and size towards the margins of the veins to form a jigsaw breccia which then grades into stockwork veins and then into undisturbed country rock. Some vein - wallrock contacts, however, form sharp faults.

The third phase of mineralization is uncommon and comprises barren veins and breccias. Veins of this phase occur in fractures cross-cutting earlier formed hypogene veins and andesitic host rocks. They contain crustiform and drusy coatings of gypsum, and palygorskite. Gypsum, the dominant mineral, is most common filling fractures in andesite, whereas palygorskite occurs exclusively in fractures cutting veins. Gypsum forms medium to coarse-grained euhedral crystals growing outward from vein walls with a cockade habit. Palygorskite forms a white, flexible, fibrous matte of crystals coating fractures. Gypsum and palygorskite are typical supergene minerals.

Ore Petrology

Ore in the Main Cirque Zone is exclusively in second phase, hypogene, quartz-carbonate veins. Typical hand specimens are white to pale green, (Figure 19), and composed of medium to coarse grained quartz and calcite which together make up 90 volume percent of the vein material with quartz the dominant mineral. Sulphides are rare but fine disseminations of pyrite occur in fragments of brecciated porphyritic andesite. A single grain of galena was identified in one polished section. No other sulphides have been identified in the Main Cirque or Brandy Zones, however, both galena.and sphalerite locally comprise up to 5 volume percent of vein material in rare patchy areas of the Lake Zone.

Two vein mineral emplacement styles, defined by differences in regularity of composition and texture, reflect mineral phases deposited prior to brecciation and later, as a

Figure 17 *Photograph of a quartz-carbonate vein showing the distribution and abundance of wall rock fragments in the Main Cirque Ore Zone.*

Figure 18 *Photograph of brecciated quartz-carbonate vein material re-cemented by a later phase of quartz-carbonate which illustrates the similarity of appearance and composition between early brecciated vein fragments and later matrix in*

Figure 19 *Photograph of a specimen of high grade ore showing wall rock fragments in relatively coarse-grained quartz and lamellar carbonate. The greenish-brown areas in the vein material reflect localized patches of abundant sericite. Specimen shown comes from an underground drift where assays of 1612.1 grams Au/tonne were obtained.*

Figure 20 *Photomicrograph of quartz-carbonate vein material showing the lamellar morphology of calcite crystals in the Main Cirque Zone. Magnification is 45 times.*

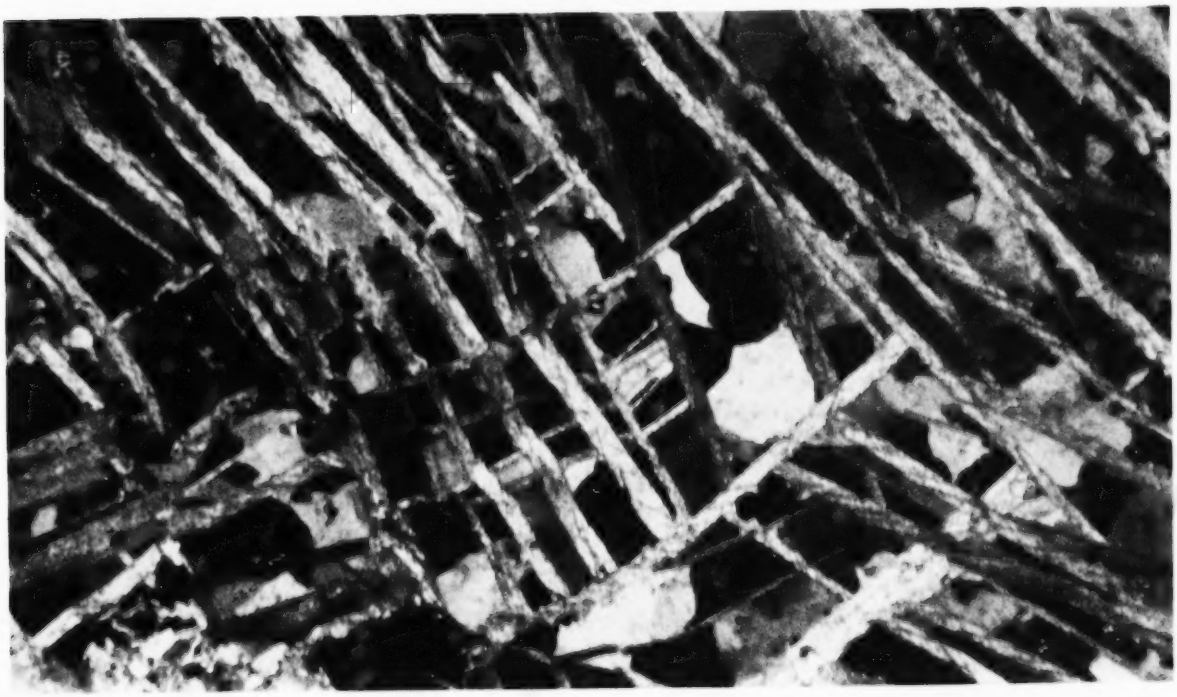

Figure 21 *Photomicrograph of quartz-carbonate vein material from the Main Cirque Zone, showing randomly oriented, bladed calcite crystals forming a skeletal lattice filled by later fine-grained sucrosic quartz grains. Magnification is 45 times.*

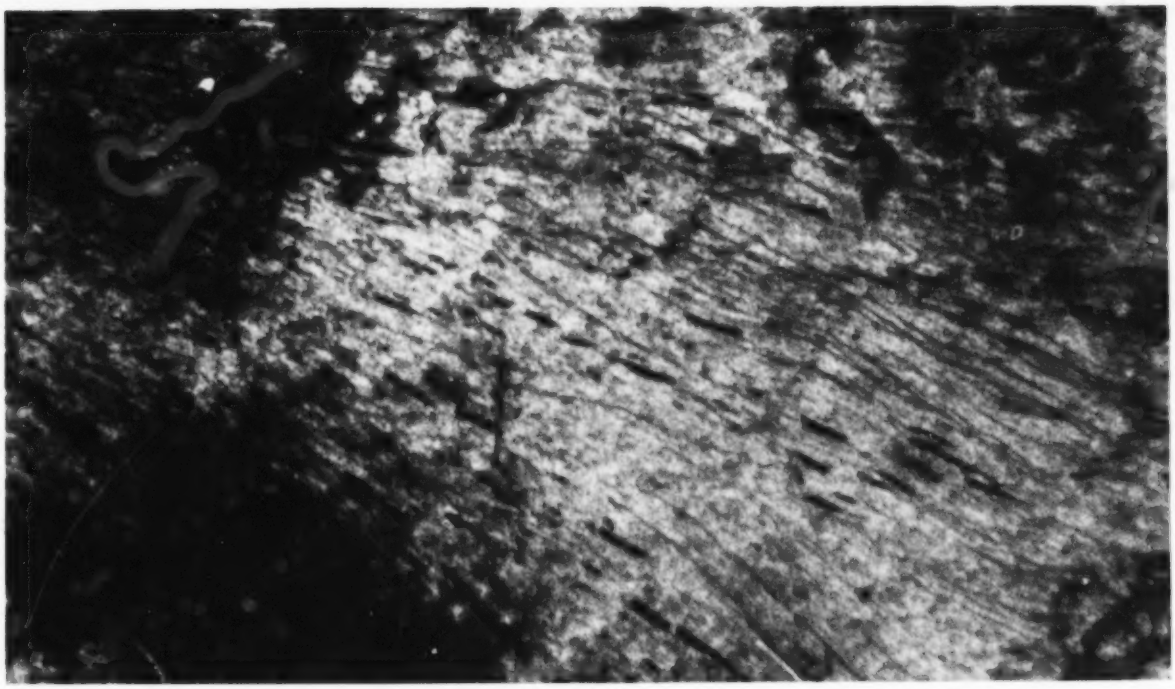

Figure 22 *Photomicrograph showing clusters of tightly packed bladed calcite crystals occuring in randomly oriented bundles distributed throughout the vein material from the Main Cirque Zone. Magnification is 45 times.*

Figure 23 *Photomicrograph of quartz-carbonate vein material showing exfoliation textures in bladed calcite clusters through replacement of calcite by quartz along cleavage planes and grain boundaries in elongate crystals from the Main Cirque Zone. Magnification is 175 times.*

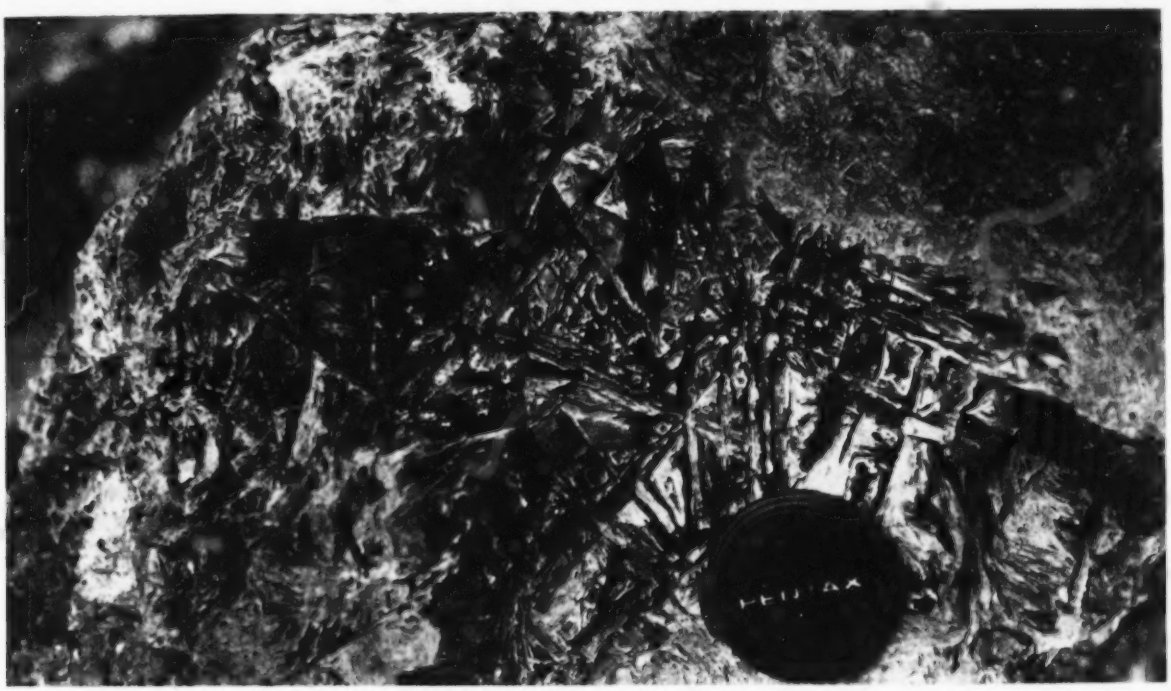

Figure 24. *Photograph showing prominent blades of equant, fine-grained quartz pseudomorphing calcite on weathered surfaces of quartz-carbonate veins from the Main Cirque Zone.*

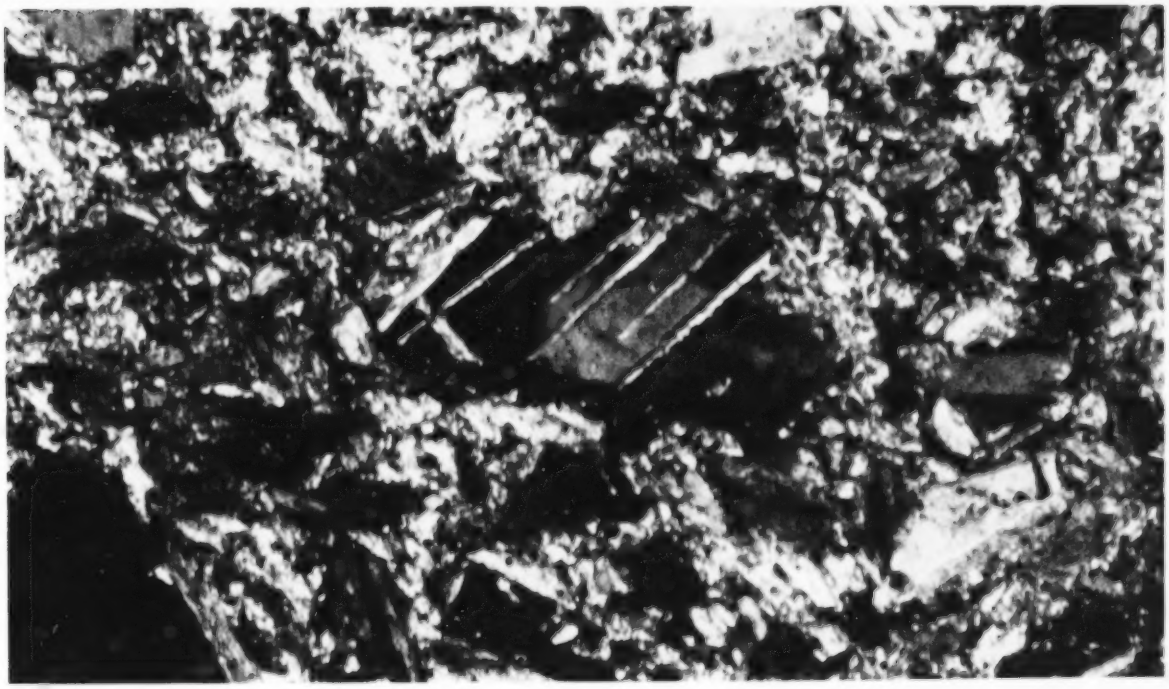

Figure 25 *Photomicrograph showing brecciated vein material re-cemented in a chaotic matrix of quartz-carbonate-sericite vein material. Magnification is 175 times.*

result of brecciation. These two styles are described below.

The first style is most widespread and shows a wide range of quartz-carbonate composition and appearance. Proportions of quartz and calcite vary. Crystals tend to be coarse to medium-grained and, on the scale of a single thin section, uniform in texture and composition. Calcite typically forms a striking, elongate, two dimensional, bladed or scalenohedral crystals (Figure 20) as long as 7 cm but less than 2 mm wide. Even hand specimens which seem to consist of equant, sucrosic quartz and carbonate, are found in thin section to contain calcite as minute bladed crystals clustered in radiating rosettes growing outward from central quartz grains. Where calcite occurs as coarse, elongate grains, individual blades intersect one another without truncation, to form a criss-crossed skeletal lattice of calcite crystals containing angular cavities filled by fine-grained sucrosic quartz (Figure 21). Where vein material is mainly calcite, these skeletal lattices develop as sheaves of many parallel, elongate, hair-thin blades packed together and oriented as random clusters of parallel crystals . Locally, quartz grains form cockade overgrowths on bladed calcite crystals and replace calcite along cleavage planes and boundaries between elongate crystals, thereby exfoliating the calcite sheaves (Figure 23). In some cases, bladed calcite crystals are replaced entirely by many fine, anhedral quartz grains that produce blade-like pseudomorphs which become prominent on weathered surfaces (Figure 24). The main feature distinguishing this first style of quartz-calcite mineralization from the second is the relatively undisturbed nature of crystal formation.

The second style of mineralization consists of breccia in a chaotic, fine-grained assemblage of equant calcite in greater abundance than quartz, accompanied by abundant sericite and adularia which forms irregular patches that appear to brecciate and flood earlier formed vein fragments (Figure 25). Brecciation caused by multiple vein emplacement events is apparent in most specimens of vein material.

Sericite, which most commonly forms a component of the breccia matrix, is the third most common vein mineral. It typically occupies about 2 volume percent of the early-formed style of vein material but locally constitutes up to 10 volume percent of the brecciated, recemented veins. It is a late mineral in the paragenetic sequence and typically forms minute clusters filling interstitial space between quartz and calcite grains, and locally occurs as rims around bladed calcite crystals. Sericite can be a major constituent of the quartz-carbonate breccia

Figure 26 *Photomicrograph showing a typical occurrence of fine-grained euhedral adularia grains intergrown with quartz in a brecciated specimen of quartz-carbonate material which was re-cemented by matrix material containing abundant adularia. Magnification is 175 times.*

filling described above (Figure 25); it also forms patchy to complete pseudomorphic replacement of adularia and albite in both veins and breccia matrix, and late-stage infillings in vugs in veins where it forms cockade coatings on cavities . Veins containing large amounts of sericite are pale green and similar to phyllically altered porphyritic andesite.

Adularia is also most common as a vein-breccia matrix mineral where it typically comprises 1 to 10 volume percent of vein material. Adularia forms clusters of fine euhedral grains averaging 0.2 mm across (Figure 26) that are rarely visible in hand specimen unless they are stained . Thin sections show that adularia characteristically occurs in quartz-calcite breccia as cockade coatings of crystals rimming brecciated fragments of earlier formed vein material, and also as bands lining late veins. Adularia is commonly replaced by pseudomorphic patches of sericite and, as a result, may have been abundant during the initial stages of vein formation.

Other vein gangue minerals in the Main Cirque Zone include ankerite, fluorite, albite, rhodochrosite, barite, anhydrite, and palygorskite. Ankerite and fluorite are locally abundant and can become a major constituent of veins at the expense of calcite. Albite and rhodochrosite are sparsely distributed as fine grains intergrown with quartz but rhodochrosite is most common in Lake Zone where it locally comprises up to 3 volume percent of veins. Trace amounts of barite, anhydrite, and palygorskite fill late fractures which cross-cut the larger veins.

Reflected light microscopy confirms the paucity of sulphides in the Main Cirque Ore Zone. Pyrite, the most abundant opaque mineral, is present only in trace amounts. Galena, the only other sulphide mineral observed in polished section occurred as a single grain in only one specimen. Electrum and native silver are present in trace amounts and are only slightly less abundant than pyrite. No other precious metal-bearing minerals were observed. All opaque minerals are fine grained and rarely visible to the eye usually because they are less than one millimeter in size and commonly range from 10 to 40 microns across. Electrum and native silver occur as irregular discrete grains interstitial to aggregates of either quartz or calcite; they show no systematic variations in abundance or morphology between the different styles of quartz-carbonate veins. Immiscibility between electrum and native silver is indicated by the local presence of minute grains of native silver within larger grains of electrum with textures similar to those produced through exsolution of chalcopyrite in sphalerite.

Distribution of Gold in the Main Cirque Ore Zone

The Main Cirque Ore Zone is characterized by gold to silver ratios of 1.2:1. Figures 27, 28, and 29 show the contoured distribution of gold values and vein thickness. Contoured values were obtained from routine sampling of underground workings during mining. A line of samples was taken across the vein every 2.5 m at the working face after each round. Individual samples were collected for each contrasting part of the vein; lithological divisions were sampled separately. Each sample location, therefore, produced one or more samples which were analysed for silver and gold at the mine by fire assay. Using this data base, the length-weighted average value of gold assays from each sample line was calculated to provide a representative value at each point. Vein thicknesses were obtained from test hole drilling along drifts at approximately 5m intervals.

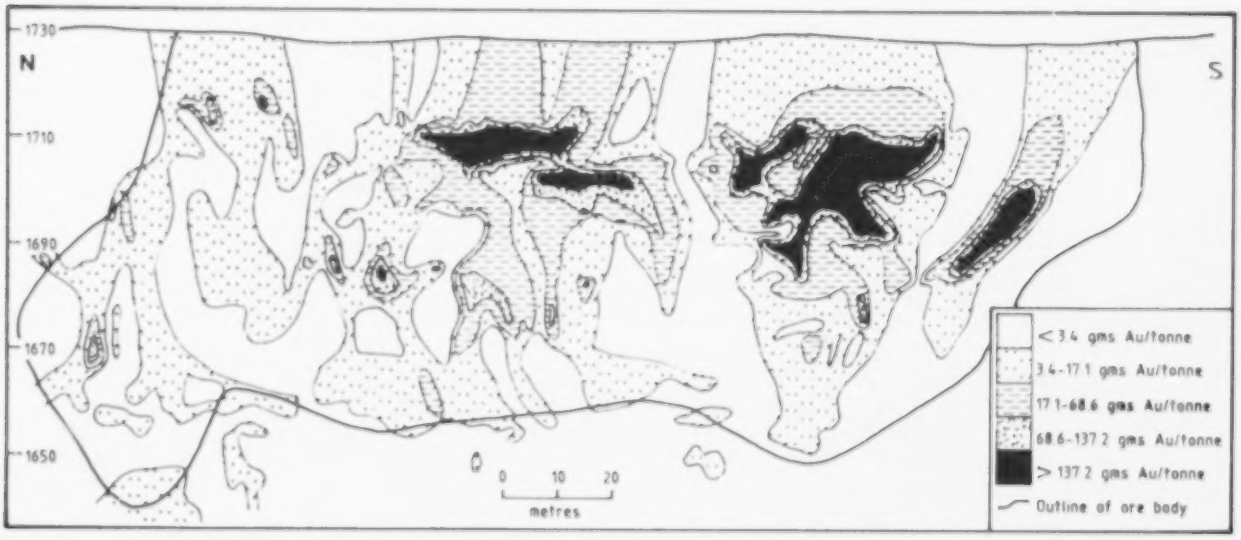

Figure 27 *Contour diagram showing distribution of gold values in the Main Cirque Zone (Figure 3). Gold occurs in elongate, irregular, vertically plunging ore shoots that increase in grade upwards. High-grade zones pinch out consistently downward near the 1676 sublevel. Data is from routine mine sampling during development.*

Gold in the Main Cirque Ore Zone is concentrated in four irregular, vertically-plunging zones each of which fan outward and become more laterally extensive with increasing elevation (Figure 27). The highest grade portions of all zones form a horizontal band about 60 m thick, between surface at about 1730 m elevation and the 1676 m sub-level of the mine.

Zones of maximum gold grade (Figure 27) correspond closely with zones of maximum vein thickness. The thickest part of the vein, in the southern part of the zone, appears to pinch out towards surface and at depth. At the southern end of this zone of maximum thickness, a near-vertical ore shoot is developed but also pinches out with depth. In the northern end of the ore zone an arcuate area of vein thickness extending from the top to the bottom of the ore zone curves around the bulls-eye pattern of isopachs formed by the zone of maximum vein thickness to the south and extends down-dip below the present level of the ore.

Figure 29 integrates both vein thickness and grade to illustrate the distribution of ore shoots in the Main Cirque Ore Zone. Three major, irregularly shaped oreshoots are delineated. Despite the prominent horizontal band of highest grade and vein thickness in Figures 27 and 28, all ore shoots plunge near-

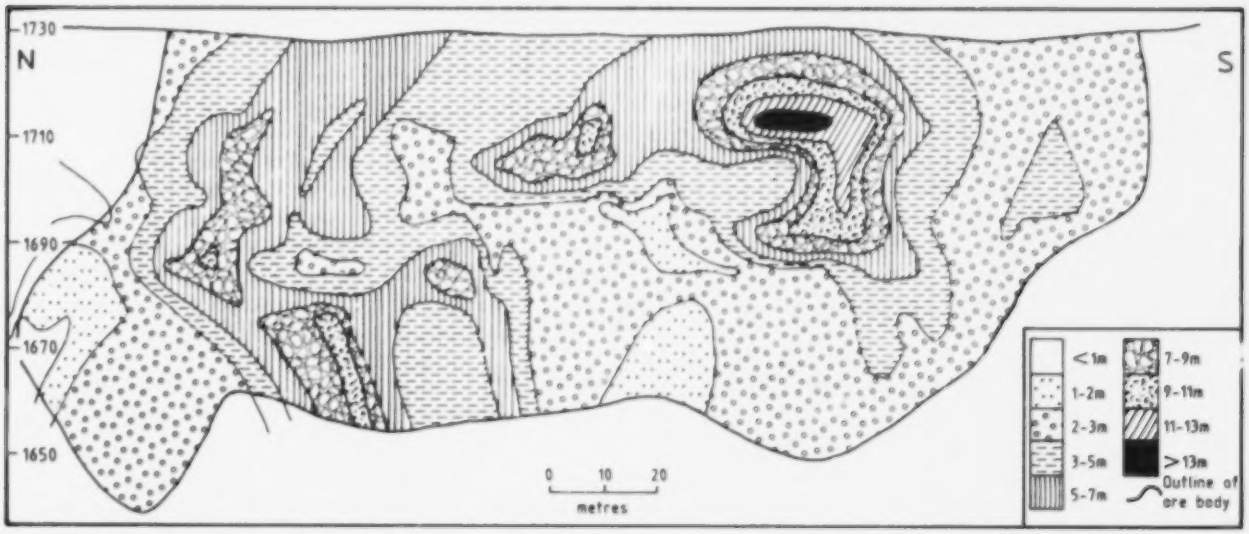

Figure 28 *Isopach diagram illustrating vein thickness in the Main Cirque Ore Zone (Figure 3). Zones of maximum thickness correspond with zones of maximum grade(Figure 27).*

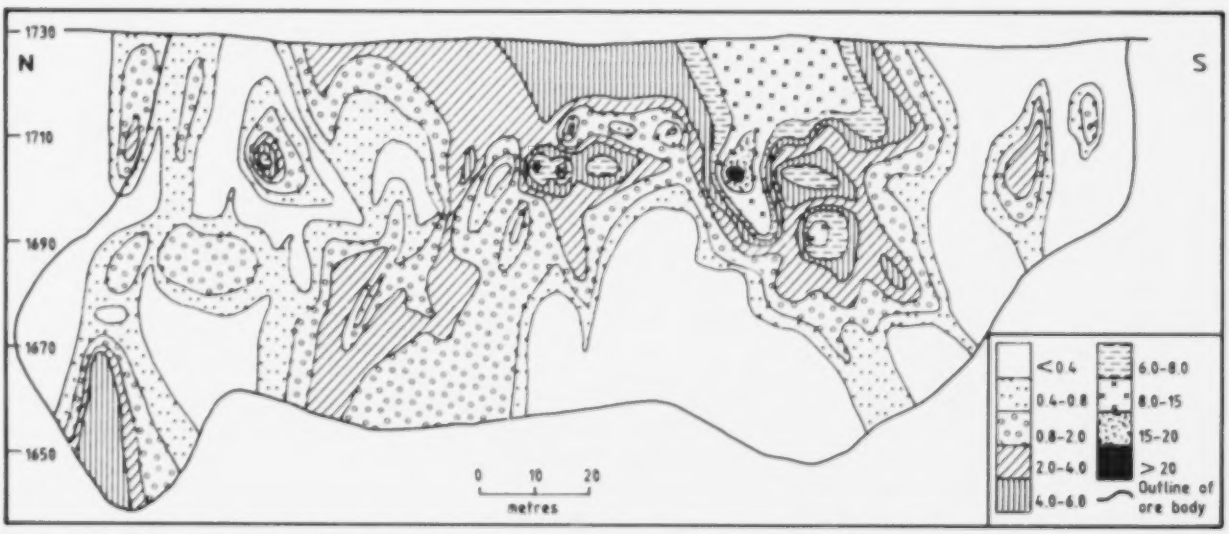

Figure 29 *Contour diagram of grade times thickness outlining zones of maximum vein width and gold grade. Gold occurs in three vertically plunging ore shoots that reflects the orientation of major hydrothermal channels indicating that fluid flow in the Main Cirque Ore Zone was directed vertically with little lateral flow.*

vertically and narrow with depth to coalesce in a single large body (Figure 29). Each ore shoot extends below the present level which has been mined, however, diamond drilling indicates that ore shoots quickly narrow and disappear below the lower levels of development.

No consistent textural or mineralogical guide to gold-rich vein material has yet been noted. However, favourable indicators include veins containing more than 50 percent coarse-grained calcite by volume, and/or abundant coarse-grained bladed calcite. Veins containing abundant massive, sucrosic quartz with little calcite commonly yield low precious metal contents.

Observations noted here as to gold distribution in the Main Cirque Ore Zone hold true for all veins developed in Main Cirque with the exception that electrum in Lake Zone veins is more silver rich than in other veins in Main Cirque.

Interpretation

Quartz-calcite veins in the Main Cirque Zone host all significant gold and silver. Open spaces formed through fault displacement acted as conduits for hydrothermal fluids. Breccias associated with gold and silver throughout the Main Cirque indicate that hydrothermal eruption accompanied vein emplacement — this is consistent with shallow depths of formation. Bladed calcite crystals forming a skeletal lattice is described in Oatman, Arizona by Lindgren (1933) as a characteristic form of crystal growth in epithermal deposits, known as lamellar ore; this also supports a shallow depth of formation and indicates a rapid rate of crystal growth possibly indicative of boiling. The local presence of chalcedony veinlets attests to periods of supersaturation of silica in hydrothermal fluids that may have been produced by a decrease of volatiles also possibly caused by boiling (Fournier, 1985). Boiling has been proposed as a mechanism of gold precipitation in many epithermal deposits, and may also have been a trigger for formation of mineralized zones at Mt. Skukum.

Electrum and native silver are concentrated in four, vertically-oriented ore shoots in the Main Cirque Ore Zone (Figure 29). The consistent depth to the base of the highest grade ore suggests that gold deposition was controlled by pressure decrease in fluids migrating upwards that allowed boiling at a depth dictated by the boiling curve for the hydrothermal solution (Haas, 1971). Grade times thickness contours (Figure 29) map zones of maximum vein width and grade which formed major channels within the conduit of the fault system. The orientation of these conduits suggests that fluid flow in the Main Cirque Ore Zone was directed vertically toward paleosurface. The correlation between areas of maximum vein thickness and maximum gold grade supports pressure decrease as a primary trigger for gold deposition. These zones probably existed as open cavities and permeable breccia zones created by fault displacement prior to vein mineralization. Upward migrating hydrothermal fluids encountering these cavities would undergo a rapid pressure decrease thereby initiating boiling with consequent gold precipitation in accordance with the throttling model of Barton and Toulmin (1961).

Mineralization at Mt. Skukum resembles that found in low-sulphur epithermal systems characterized by the presence of adularia, sericite, and high gold to silver ratios (e.g. Round Mountain, Nevada and Oatman, Arizona: Hayba et al., 1985). Bladed calcite textures similar to those at Mt. Skukum occur in other deposits of this type, including the Bodie Mining District, California, where they are visual indicators of high-grade gold mineralization (M. Silberman, 1985, pers. comm.). Vein textures and mineralogy at Mt. Skukum are consistent with ore deposition triggered by boiling from solutions rich in silica, potassium and carbon dioxide; groundwater mixing likely played a subordinate role. As pressure decrease causing boiling was probably a control of gold deposition, the horizontal band of highest grade gold values in the Main Cirque Ore Zone, may indicate the lower level of maximum economic potential below paleosurface. On a regional scale, this could delineate the depth below paleosurface at which an orebody could be located. Thus, if the depth below paleosurface of the Main Cirque Ore Zone can be determined, this information may help to define drill target depth to potential ore zones in vein structures located elsewhere in the Mt. Skukum Volcanic Complex.

ALTERATION

Both supergene and hypogene alteration affect rocks of the Main Cirque area. Both can be important exploration guides. Supergene alteration includes two facies, one characterized by brown and yellow-brown jarositic gossans and the other by bright red-orange limonitic gossans. Both occur in small zones throughout the Mt. Skukum Volcanic Complex. Hypogene alteration includes six facies which are directly related to veins and form an extensive halo surrounding the deposits in Main Cirque.

Supergene Alteration

Bright brown and yellow-brown supergene gossans on the east, south, and west walls of Main Cirque consist primarily of pervasive limonite, jarosite and clay alteration in and around fractures in silicified rocks containing disseminated pyrite.

The yellow-brown jarosite facies occurs as small gossans in brecciated or silica-flooded porphyritic andesite re-cemented or cross-cut by stockworks of early chalcedonic veinlets with pyritic selvages and envelopes. The pyrite, where exposed to oxidized surface waters, breaks down producing acid which alters plagioclase to kaolinite and produces bright, clay-rich, yellowish-brown, jarositic and limonitic gossans. Alteration is weak distal to fractures and the center of larger fragments, but is intense, and obliterates all primary textures near fractures or breccia fragments . Alteration is so intense in these areas that

present-day groundwater leaches clay from rocks exposed at surface and deposits it in stalactitic masses on the undersides of exposed ledges. As this alteration type is commonly associated with pyritic chalcedony veinlets generally low in precious metal content, it is not a specific guide to gold and silver mineralization, except in the Lake Zone where supergene limonite is derived from diffuse halos of disseminated pyrite which surround veins for several meters .

The red-orange limonitic supergene alteration occurs on the southwestern and southeastern walls of Main Cirque where bedrock contains disseminated pyrite. On Red Ridge (Figure 7), along the southwestern wall of the cirque (Figure 43), a porphyritic rhyolite stock contains up to 5 volume percent disseminated pyrite which has oxidized to produce clays and a bright reddish-orange gossan that covers the entire surface exposure of the stock. Iron oxides occur only in a very thin surficial zone involving the top 10 cm of soil overlying pyritic bedrock. Brightly coloured zones such as this are common throughout the Mt. Skukum Volcanic Complex and are located almost exclusively over pyrite-bearing rhyolite stocks. Soil samples from these areas are commonly anomalous in gold; they may contain up to 1000 parts per billion Au which is probably derived from the extremely high background gold content of these rocks.

Pyrite derived red-orange supergene alteration also occurs in areas of intense hypogene alteration and quartz-carbonate mineralization. In these areas, brightly coloured iron oxide forms intensely coloured gossans in the uppermost soil layers and as fracture coatings formed through oxidation of disseminated pyrite in rocks immediately below the surface. Two such areas are known in the Mt. Skukum region; one on the southeastern wall of Main Cirque, known as the Alunite Cap Zone (Figures 3 and 6), and the other at Vesuvius Hill (Figure 3), an extension of the Mt. Skukum Volcanic Complex to the northeast. Intense red-orange gossans cover about 300 m by 250 m at both locations; both are associated with pervasive hypogene alteration of underlying rocks to kaolinite, sericite, alunite, pyrophyllite and pyrite with minor local silicification . The Alunite Cap Zone occurs along a possible southern extension of the Main Cirque Fault Zone (Figure 3) along the eastern wall of Main Cirque and is an expression of near-surface acidic alteration caused by condensation of volatiles boiled off during hypogene hydrothermal activity. Similar alteration occurs beneath the red-orange gossan at Vesuvius Hill where drill holes have intersected significant quartz-carbonate veins and breccias. Thus, in both localities, important, recessive expressions of hypogene mineralization are clearly marked by supergene alteration. Although a promising target at Mt. Skukum, no precious-metal mineralization has yet been found associated with the Alunite Cap Zone.

Hypogene Alteration

Hypogene alteration is ubiquitous in porphyritic andesite of Formation 3, but is only intense adjacent to dykes and veins. Facies of pervasive hypogene alteration at Mt. Skukum (Figure 30) are characterized by the terms silicic, potassic, phyllic, argillic, and propylitic (Table 3), which represent mineral assemblages stable at progressively lower temperature conditions in the presence of hydrothermal fluid (Meyer and Hemley, 1967; Rose and Burt, 1979). Each facies may be subdivided into zones based on consistent mineral assemblages named after the dominant mineral components present.

Table 3. Hypogene alteration facies and zones in Main Cirque.

Facies	Zone	Mineralogy[1]
Silicic		Qz, Ms, Ad, Py, Cl, Ka
Potassic		Ad, Qz, Ms, Py, Ca, Cl, Ka
Phyllic		Ms, Qz, Ca, Cl, Ep, Py, Le, Ad
Argillic		Ka, Pr, Qz, Py, Ms, Al, Sm, Il
Propylitic	Chlorite	Cl, Ep, Ms, Qz, Ca, Py, Le
Propylitic	Epidote	Ep, Cl, Ms, Qz, Ca, Py, Le

1. Minerals are listed in order of abundance and are coded as follows: Ad = adularia, Ca = calcite, Cl = Chlorite, Qz = quartz, Ep = epidote, Ka = kaolinite, Le = leucoxene, Ms = Muscovite (sericitic), Py = Pyrite.

Silicic Alteration: One of the most common alteration types found in Main Cirque, silica flooding, forms envelopes up to 15 cm thick around veins. Wall-rock fragments in veins and breccia are also typically silicified. Silicification is closely associated with potassic alteration. Although both usually occur together adjacent to veins, potassic alteration does not invariably accompany silicification.

Silicification imparts a bleached appearance, obliterates primary textures, and contains disseminated pyrite. As silicification is fracture dependant, it commonly accompanies large-scale or micro-brecciation of the host rock. The importance of permeability to silicic alteration is seen in hydrothermal breccias where large rock fragments commonly display only a surficial rim of silicification whereas smaller fragments and matrix material are completely replaced by quartz and pyrite. Permeable horizons such as lapilli tuffs, brecciated flow tops and bottoms in andesite flows and coarse-grained volcaniclastic sedimentary rocks all display preferential silicification which can involve complete replacement of matrix material yet leave coarse fragments relatively unaffected. In thin section, fine-grained mosaics of equant anhedral quartz and euhedral adularia grains averaging about 5 to 10 microns across replace all minerals . In fragmental rocks, coarse, cockade-textured quartz grains, commonly oriented outward from the surface of fragments, completely replace surrounding matrix and produce prominent white halos around fragments. Silicification is invariably accompanied by 0.1 to 5 volume percent finely disseminated pyrite; there is a direct relation between intensity of alteration and the amount of pyrite. Primary feldspars and pyroxene may be partially or completely replaced by quartz

which can retain the pseudomorphic crystal shape of the original mineral grain. Minerals such as chlorite, epidote, and sericite, which are not characteristic of this alteration type, occur in silicified rocks because silicification tends to overprint other alteration types.

Potassic Alteration: Potassic alteration is more closely associated with veins than dykes and most commonly occurs in breccias that extend less than 15 cm into wallrock adjacent to veins. It forms local, narrow haloes, immediately surrounding veins or breccia infilling containing potassic minerals. Retrograde overprinting of phyllic alteration obscures identification in places.

Potassic alteration is common but limited in extent and is indistinguishable from silicification in hand specimen. Most commonly, potassic alteration is associated with silicification within 1 m of a fracture or permeable horizon as a fine-grained euhedral intergrowth of adularia crystals and quartz replacing primary minerals (Figure 26). Adularia commonly forms a border of cockade-textured crystals nucleated on relatively unaltered fragments in andesitic lapilli tuffs or breccia bodies where the matrix material has been completely replaced by adularia and quartz. Adularia is also common as a partial replacement of plagioclase in altered porphyritic andesite and felsic dykes. Although most common as a minor part of the silicification process, adularia can locally dominate silicification. Retrograde alteration of adularia to sericite may cause the original abundance of adularia to be underestimated. Masses of sericite have been observed in regular shapes consistent with those expected in pseudomorphs of adularia.

Potassic alteration affects all rock types including intermediate volcanic rocks which do not have a composition that allows such alteration under closed conditions. Consequently, potassic alteration represents a metasomatic process caused by exposure of the wall rock to hydrothermal fluids rich in potassium.

Phyllic Alteration: Phyllic alteration, the most common form of alteration directly associated with veins and dykes, occurs as haloes extending up to 4 m from veins or dykes but typically less than 1 m. Phyllic alteration is also common in brecciated rock fragments in veins and breccia bodies and on the margins of rhyolite dykes.

Phyllic alteration haloes are best developed in the Lake Zone where they extend up to 4 m away from veins; in the Main Cirque and Brandy zones they average 2 to 10 cm, and locally exceed 1 m.

In hand specimen, phyllic alteration is characterized by a mottled bleaching and pale apple-green colour , by unusually soft feldspar phenocrysts, and by traces of finely disseminated pyrite. Thin sections display consistently high abundances of calcite and variable amounts of introduced quartz and pyrite as well as minor pyrophyllite and illite. Plagioclase phenocrysts are characteristically clouded or completely replaced by sericite

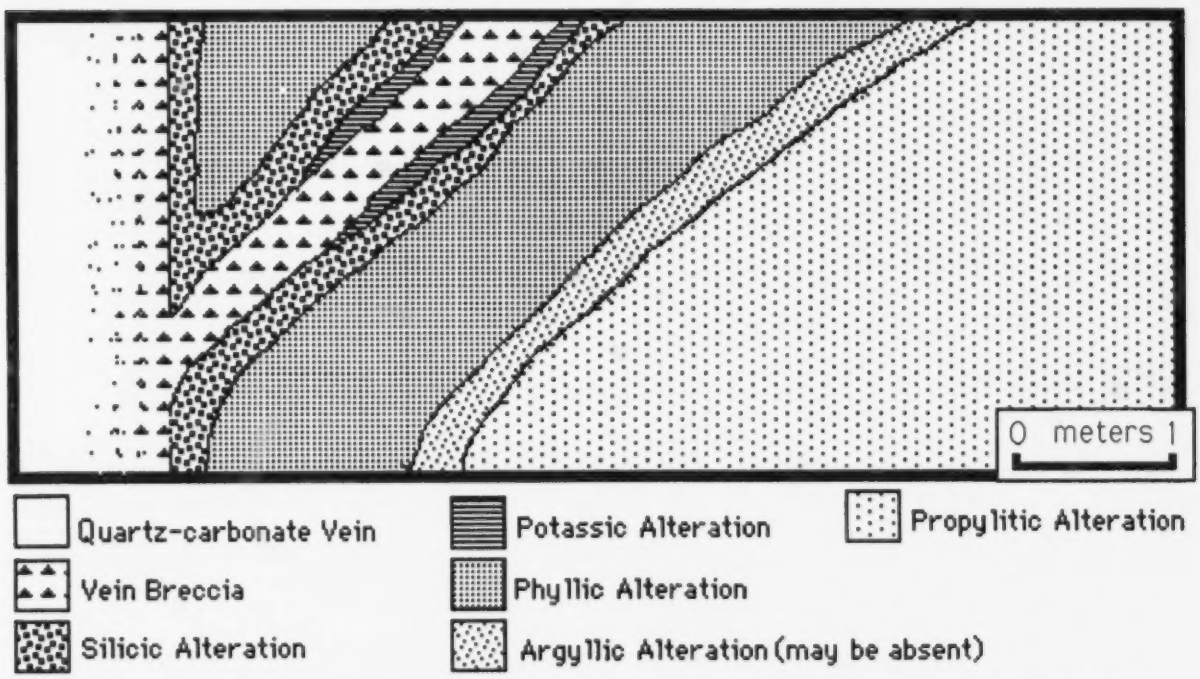

Figure 30 *Schematic illustration showing gradation between veins and zones of vein breccia and the distribution of hypogene alteration around quartz-carbonate veins and vein breccia in Main Cirque.*

and calcite locally with minor quartz and epidote . In areas of intense alteration, primary quartz phenocrysts may be rimmed and corroded by sericite and the groundmass of porphyritic rocks is commonly completely altered or mottled by patches of sericite, carbonate and quartz. Sericite and calcite also fill fine cross-cutting fractures and amygdules in intensely altered rocks. Phyllic alteration in felsic dykes is usually pervasive, but in some places, marginal zones of intense phyllic alteration are apparent which are probably caused by breakdown of fine-grained or vitric chill margins to sericite. The most intense phyllic alteration occurs in felsic dykes adjacent to large veins in the Main Cirque Zone and in the Alunite Cap Zone where the rock is reduced to a soapy-textured green coloured mass in which some coarse primary fragmental and flow-banded textures are preserved by differential silicification or alteration intensity.

Phyllic alteration is closely associated with veins and controlled by fracture intensity and rock permeability. It represents a metasomatic process of potassium enrichment that produced sericite in intermediate volcanic rocks and increased the abundance of sericite in felsic dykes.

Argillic Alteration: Argillic alteration forms infrequent alteration haloes around barren chalcedonic veinlets and rarely exceeds 1.5 cm across. It is also locally present in the Main Cirque Zone, where alteration envelopes in stockwork chalcedonic veinlets coalesce to form pervasive zones of argillic alteration. A large area of intense argillic alteration also occurs at high elevation on the southeastern wall of Main Cirque in the Alunite Cap Zone.

Argillic alteration is rare in the Main Cirque, Brandy and Lake zones where localized, narrow halos extend up to 4 cm from early chalcedonic veins. Silica envelopes adjacent to veins commonly pass outward into minor argillic alteration envelopes. Argillic alteration affects all rock types, obliterates all primary minerals, obscures primary textures, and reduces rock to a soft powdery white mass containing finely disseminated pyrite and is typically criss-crossed by chalcedonic veinlets. Thin sections display complete replacement of original mineralogy by fine-grained kaolinite, quartz and pyrite with some preservation of original porphyritic textures through kaolinite pseudomorphs of plagioclase or potassium feldspar phenocrysts. Up to 5 volume percent pyrite is common as finely disseminated grains in argillic envelopes that extend away from silica-flooded zones. Although argillic alteration in the Main Cirque Zone is a localized effect associated with pyritic chalcedony veinlets, the Alunite Cap Zone contains intense, widespread argillic alteration (Figure 31) which reduces the rock to a soapy textured white mass of soft kaolinite and

Figure 31 *Photograph of intense argillic alteration in rock of the Alunite Cap Zone, showing a gradual decrease in alteration intensity away from fractures and preservation of primary fragmental texture.*

pyrophyllite in an area where no pyritic chalcedony veinlets exist.

Argillic alteration in Main Cirque is caused by low pH conditions produced by condensation of volatile components (mainly CO_2, H_2S, and H_2O) released through boiling of hydrothermal solutions. The Alunite Cap Zone (Figure 7) represents a near-surface alteration cap, and localized argillic alteration zones associated with the Main Cirque, Lake, and Brandy zones indicate that boiling extended below these levels. Argillic alteration may have been produced in these zones by a localized mixing of oxidized surface waters with expelled volatile components in highly permeable fault zones allowing development of acidic conditions adjacent to boiling zones.

Propylitic Alteration: This alteration type forms the most widespread halo and is related to zones of maximum permeability. It is present in most andesitic volcanic flow rocks but is less pronounced in andesite dykes and many andesite stocks.

Propylitic alteration is present to some degree in all rocks of Main Cirque regardless of association with, or distance from veins. It is most abundant in the Main Cirque and Brandy zones, but it is also common in the Lake Zone. Propylitic alteration is uncommon in felsic dykes where phyllic alteration predominates. Most andesitic flow and pyroclastic rocks are affected by propylitic alteration. Permeable andesitic lapilli tuffs, ash tuffs, and flow top and bottom breccias appear to be more intensely altered than less permeable rocks of similar composition. In cliff exposures of multiple andesite flows, more highly altered brecciated flow tops and bottoms show a slightly bleached, greenish colour whereas the less fractured and altered flow centers remain dark grey, resulting in an alternating light and dark banding (Figure 6). The bleached, green colour is brought about by complete replacement of primary pyroxene by chlorite, and saussuritization of plagioclase. Magnetite is replaced by leucoxene. Transitional zones between the phyllic and propylitic facies are marked by abundant chlorite and the decrease and eventual disappearance of sericite and secondary quartz outward from the phyllic alteration zone. In hand specimen, this transition is seen as a subtle colour change from pale apple green, to a dark green marked by increasing amounts of epidote and chlorite, and decreasing amounts of pyrite, quartz, sericite, and calcite. Two types of propylitic alteration occur (Table 3). In Main Cirque, chlorite is the dominant alteration mineral in the propylitic suite; in the Brandy and Lake zones epidote is the dominant mineral. In thin sections, chlorite replaces pyroxene in both phenocrysts and groundmass: incipient, fine-grained epidote and minor calcite cloud plagioclase phenocrysts and microlites, and minor sericite replaces plagioclase phenocrysts in small patchy areas or occurs as fine envelopes along fractures and cleavage planes in the phenocrysts. In areas of propylitic alteration, amygdules in andesite flow rocks are commonly filled either entirely by rosettes of radiating chlorite crystals with minor epidote, or by a combination of chlorite and epidote rimming the amygdule followed by a final central infilling of quartz .

Propylitic alteration throughout the Mt. Skukum Volcanic Complex is developed mainly in andesitic volcanic rocks. Its distribution is controlled by primary permeability in fractured and volcaniclastic rocks. Propylitization represents a form of isochemical alteration produced by elevated temperature in rocks adjacent to hydrothermal conduits without the introduction of large amounts of volatile components such as potassium, silica, or carbon dioxide.

Discussion

Four of the five alteration facies described — silicic, potassic, argillic, and phyllic — result from the introduction of potassium, carbon dioxide, and silica along fractures and permeable zones to produce silicification, adularia, sericite, kaolinite, and calcite. The fifth alteration facies (propylitic alteration) represents an isochemical breakdown of primary minerals in response to increased temperatures and hydration. Propylitization is the most common of the five and is found throughout the Mt. Skukum Volcanic Complex. This alteration type is not specifically associated with mineralization although it does become most intense near veins and is associated with permeable zones in host rock. All the metasomatic forms of alteration are directly associated with veins and serve to indicate proximity to mineralization. Silicic and potassic alteration represent the most proximal facies and although potassic alteration is not identifiable in hand specimen, silicification is readily identifiable and is the most common form of alteration associated with veins. Phyllic alteration is not associated with all veins and can occur in areas where veins are not apparent. It is thereby an unreliable guide to mineralization. Argillic alteration associated with the Brandy, Lake, and Main Cirque zones forms envelopes of limited extent around barren chalcedonic veinlets as well as rare envelopes around precious-metal bearing quartz-carbonate veins.

Abundant argillic and phyllic alteration in the Alunite Cap Zone (Figure 7) may represent an important guide to vein mineralization as zones of quartz-carbonate filled hydrothermal breccia occur beneath a similar zone of alteration at Vesuvius Hill (Figure 3). In the Alunite Cap Zone intense alteration is centered around a vertically-dipping alunite > pyrophyllite > quartz vein. The presence of alunite (common in epithermal systems where high level oxidation occurs) and the abundance and intensity of argillic alteration in this zone suggest it may represent alteration at or near the paleo-surface at the time of mineralization in the Main Cirque Zone. This is supported by the high elevation of this area relative to the Main Cirque Zone (Figure 3).

Alteration facies and their distribution at Mt. Skukum are consistent with those which characterize a class of epithermal systems known as low-sulphur adularia-sericite deposits (Hayba et al., 1985; Bonham, 1986). Phyllic alteration assemblages

including sericite + illite + quartz + pyrite typically dominate these systems . Illite and smectite are also commonly present as mixed layer assemblages where illite layers dominate. Phyllic alteration in this class of deposit characteristically borders a silicified zone adjacent to veins and includes sericite as well as fine-grained potassium feldspar and/or chlorite disseminated throughout silicified wall rock. Away from veins, phyllic alteration assemblages grade outwards into a propylitic zone. Locally, argillic alteration separates phyllic and propylitic zones (Hayba et al., 1985). Several examples of this deposit type are Creede, Colorado; Pachuca, Mexico; and Oatman, Arizona. Each of these display a cap of sericitic alteration over the orebody that is interpreted to result from condensation of acidic volatiles (mainly H_2S and CO_2) released at depth during boiling (Barton et al., 1977; Buchanan, 1981). This description fits the observation of intense phyllic and argillic alteration in the Alunite Cap Zone remarkably well, especially since release of volatiles at depth through boiling can also cause intense argillic alteration in epithermal systems (Rose and Burt, 1979).

Thin section and x-ray study indicates that rocks at Mt. Skukum were altered by hydrothermal fluids rich in silica, potassium and carbon dioxide. The presence of calcite as an alteration mineral present in all alteration facies, particularly phyllic and silicic zones, indicate metasomatism by fluids rich in CO_2. In phyllic alteration zones, formation of calcite largely through replacement of plagioclase indicates that Ca^{2+} was not added to the system but was recombined with externally derived CO_2. In addition, chloritic amygdules found locally in andesitic flow rocks may be due to the interaction of CO_2-rich fluids with host-rock de-stabilizing Ca^{2+} to form chlorite (Grunsky, 1986). Saussuritization of plagioclase in propylitic zones is indicative of a lack of CO_2, and is consistent with its location away from the fractures and veins which channeled hydrothermal fluids. The presence of adularia and abundant sericite in intermediate volcanics which are relatively low in primary potassium minerals suggests that potassium was introduced by hydothermal fluids.

FLUID INCLUSIONS

Fluid inclusions were studied to determine the temperature of deposition, the salinity of depositional fluids, depth of mineral emplacement, volatile components, and evidence of boiling in the hydrothermal fluids.

Data Collection

Ten specimens of quartz-carbonate vein material, some from high-grade gold areas and others from relatively barren zones, were selected over a broad vertical and lateral extent of the Main Cirque Ore Deposit (Appendix B). Three of the ten specimens were devoid of usable inclusions. Paragenetic separation of vein specimens was not possible because textural evidence for age relationships are obscure.

A total of 63 fluid inclusions were analysed using a Chaixmeca heating-freezing stage. Measurements were calibrated using calibration curves derived from nine standards (Appendix D). These curves (Figure D.1) demonstrate an accuracy of measurement to within 6.7°C with a precision of 0.6°C (1 s) for the temperature range -100° to +40°C. Temperatures in the range +40° to +420°C (Figure D.2) show an accuracy to within 5.3°C and a precision of 2.2°C (1s).

Inclusions in quartz grains yielded the most reliable data. These inclusions occur in two forms. The first consists of quartz grains hosting enormous quantities of minute inclusions of all classifications (see Roedder, 1984). These are invariably too small to work with (<2μm across) because optical interference from surrounding inclusions make measurements difficult, and abundant fracture planes in these grains attest to disturbance after emplacement which might have caused leakage. Inclusions of the second form are relatively easy to measure because they occur in clear quartz grains, and are sparse, isolated and moderately sized (2 to 25 μm).

Inclusions in calcite are commonly very large, some exceeding 20 μm across. However, although some useful measurements were obtained, problems were encountered with optical interference from cleavage planes, poor clarity in calcite crystals, and leakage along cleavage planes during heating.

Fluid inclusions were classified as (Roedder, 1979): primary (P), pseudo-secondary (PS), or secondary (S). Primary inclusions were identified by their solitary location or presence on a crystal growth zone, and the lack of any associated fracture planes; these inclusions commonly took a negative crystal or ovoid shape. Pseudo-secondary inclusions, also commonly of negative crystal habit, occurred along fracture planes truncated by crystal boundaries. Secondary inclusions with highly irregular, two dimensional shapes, occurred along fracture planes that crossed crystal boundaries. The above characteristics, insufficient alone to uniquely categorize a fluid inclusion, formed the basis of classification of inclusions described in Appendix E.

Fluid inclusions studied ranged from 28.3μm to 5.0μm across in their longest dimension. All contained at least two phases, a liquid and a vapour phase. The amount of vapour phase present, determined using visual estimation tables (Roedder, 1984), ranged from 1 to 20 volume percent (Appendix E) around an overall mode of 5 volume percent gas (Figure 36).

Homogenization Data

A total of 48 measurements of homogenization temperature (T_h) are in Appendix E and summarized in Table 5. Homogenization invariably took place through disappearance of the vapour phase. To obtain the recorded homogenization temperature, each inclusion was heated three times to obtain an average T_h. If leakage of fluid, decrepitation or disparate T_h

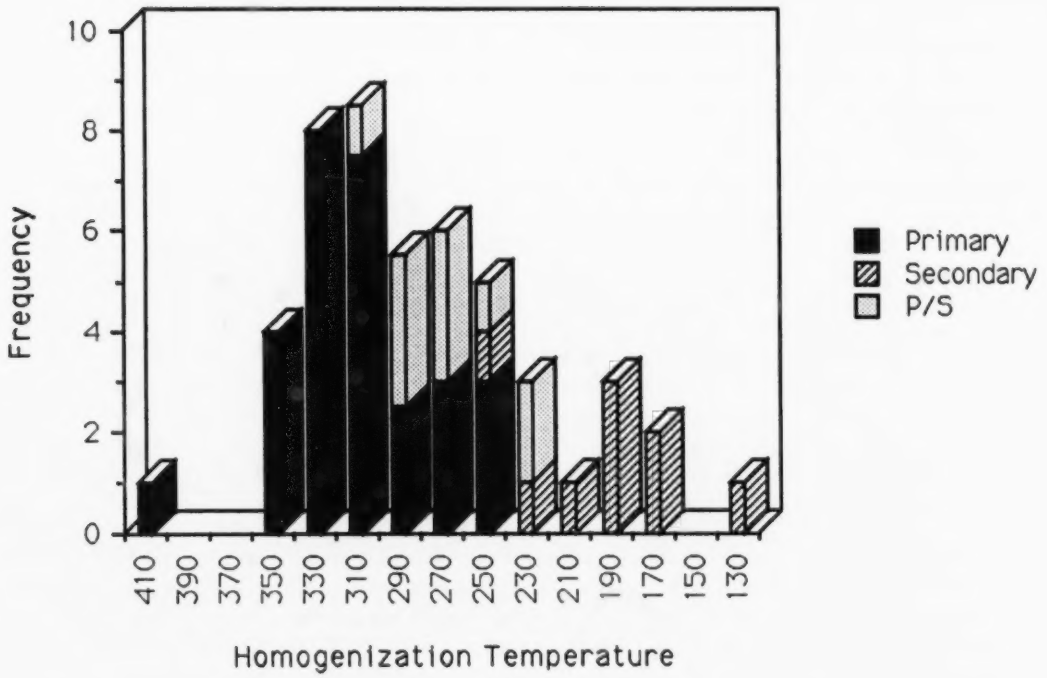

Figure 32. *Fluid inclusion homogenization data from the Main Cirque Zone, showing the distribution of primary, secondary, andpseudo-secondary (P/S) inclusions from vein material. A tri-modal distribution with peaks near 310°C, 270°C, and 190°C is indicated. Data are from Appendix D.*

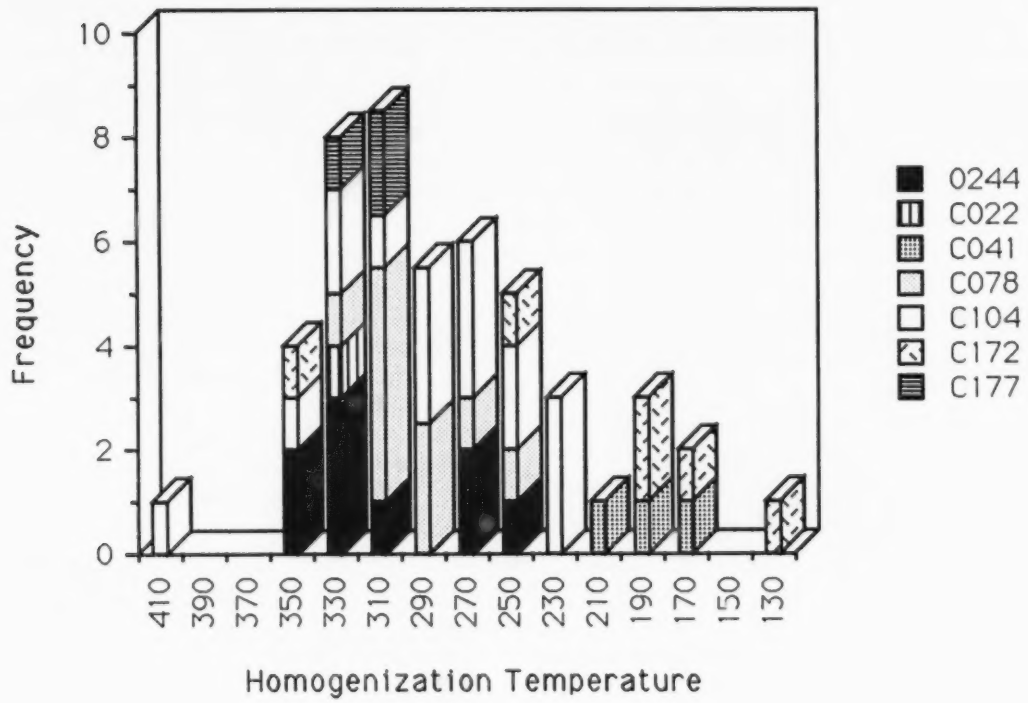

Figure 33. *Fluid inclusion homogenization data obtained from individual samples of vein material from the Main Cirque Zone. Data are from Appendix D.*

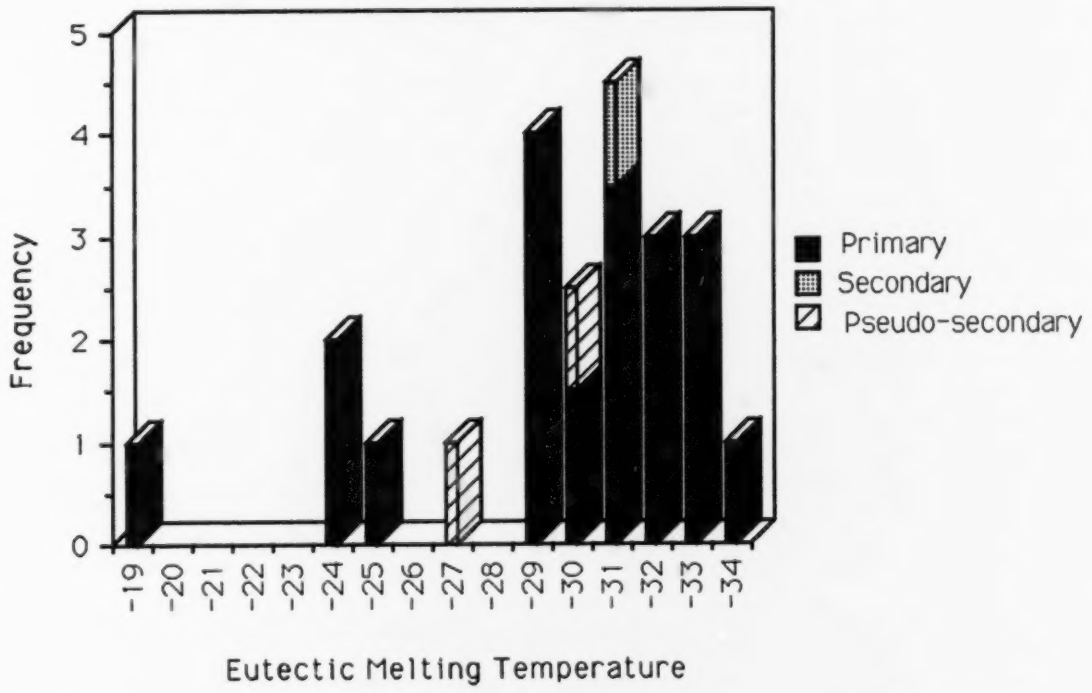

Figure 34. *Eutectic melting temperatures by distribution of inclusion types (primary, pseudo-secondary, and secondary) in vein material from the Main Cirque Zone. Data are from Appendix D.*

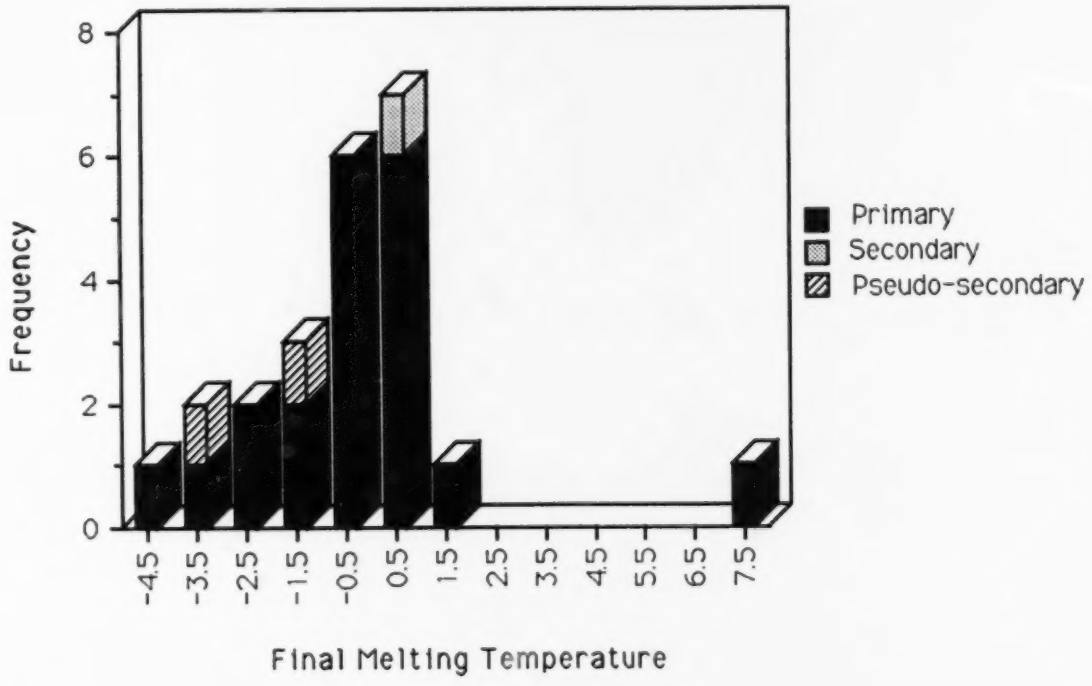

Figure 35. *Final melting temperatures of fluid inclusions by distribution of inclusion types (primary, pseudo-secondary, and secondary) in vein material from the Main Cirque Zone.*

determinations occurred, no measurements were recorded. Homogenization temperature data are plotted in Figures 32 and 33.

Table 4. Summary of homogenization temperature (T_h) data from fluid inclusions in vein samples from the Main Cirque Zone.

Inclusion Type	Number of Measurements	Ave T_h°C[1]
Primary	29	313.5 ± 6.5
Pseudo-secondary	10	269.1 ± 8.0
Secondary	9	196.8 ± 11.5

1. Arithmetic means with standard error.

Freezing Data

Freezing temperatures and phase changes were observed in 23 fluid inclusions. The temperature of eutectic melting T(e) as well as the temperature of final melting T(m) are in Appendix E. Results, plotted in Figures 34 and 35, are summarized in Table 5.

Table 5. Summary of freezing data from fluid inclusions in vein samples from the Main Cirque Zone.

Inclusion Type	Number of Measurements	T(e)°C[1]	T(m)°C[1]
Primary	20	-29.6 ± 0.9	-0.4 ± 0.5
Pseudo-secondary	2	-28.4 ± 1.8	-2.4 ± 1.3
Secondary	1	-31.4	+0.1

1. Arithmetic mean with standard error, where calculable

The temperature at which liquid in fluid inclusions commonly froze during cooling was approximately -46.5°C. Although nucleation of a clathrate was never observed during the freezing process, appearance of minute amounts of liquid at approximately -56°C was consistently observed. This observation possibly indicates, but does not substantiate, the presence of some CO_2. This liquid appears in such small quantity that it would have gone un-noticed but for a minute "frantic" boiling action displayed at that temperature.

Pressure Correction

Homogenization data are not corrected for the effects of pressure. Features of the deposits such as vuggy veins, chalcedony, and extensive fracturing indicate a high level of emplacement. Abundant hydrothermal breccias adjacent to and surrounding the deposit attest to hydrostatic pressure conditions for at least short periods. This is only possible near surface where lithostatic loads are low. In addition, alunite-clay alteration in the Alunite Cap Zone (Figure 3), no more than 320 m above the deposit, represents alteration which probably formed less than 200 m below paleo-surface. Its presence constrains the minimum depth of emplacement at 320 m. A large fault inferred to pass between the Main Cirque Zone and the Alunite Cap Zone is interpreted to have dropped the Main Cirque Zone block down with respect to the Alunite Cap Zone by a minimum of 200 m. Therefore, the minimum depth of emplacement of was probably less than 320 m. Thus, a hydrostatic pressure of approximately 31 bars may have affected this fluid. Pressure corrections to measured homogenization temperatures in inclusions subjected to this hydrostatic pressure in a solution of 1 weight percent NaCl equivalent are no more than 8°C (Potter, 1977) indicating that the actual temperature of deposition probably would be less than 8°C higher than reported homogenization temperatures.

Interpretation

Inclusions examined at room temperature contain at least one liquid and one vapour phase. As these inclusions freeze at -46.5°C, a slight contraction of the vapour bubble occurs which is consistent with inclusions being H_2O-rich. After being frozen, two distinct melting events occur during warming. One at approximately -56°C, indicates the presence of CO_2 (Hollister et al., 1981), the other at about -0.4°C (Table 6) indicates the presence of minor amounts of dissolved salts (Hollister et al., 1981). Although the presence of CO_2 is indicated by the melting event at -56°C, no clathrate was seen to nucleate upon cooling. This suggests that clathrates were obscured in the bubble meniscus, and that only low partial pressures of CO_2 are involved.

Homogenization temperatures from inclusions in the Main Cirque Zone range from a maximum of 412.7°C to a minimum of 139.2°C but show a tri-modal distribution (Figure 32). The three modes at approximately 310°C, 270°C, and 190°C correspond to clusters of primary, pseudo-secondary, and secondary fluid inclusions respectively. These modal temperatures are consistent with findings in other epithermal deposits formed in sub-aerial conditions where characteristic temperatures range from 200° to 330°C (i.e. Sunnyside, Colorado at 300°C; Finlandia, Peru at 270°C; Tonopah, Nevada at 300-250°C (Roedder, 1984; Spooner, 1981; Kamilli and Ohmoto, 1977)). The three modal temperatures might reflect three major mineralizing events related to periods of peak fluid flow. The first event probably occurred at the highest emplacement temperature where precipitating minerals preserved the event mainly as primary inclusions. The second event, at a lower temperature of 270°C, was preserved partly in primary inclusions of precipitated minerals and partly in pseudo-secondary inclusions in fractures caused by some associated activity. The final pulse, at a temperature of 185°C, was also associated with activity which fractured earlier mineralization to form secondary inclusions. No marked difference in homogenization temperature was noted between inclusions in

calcite and quartz. An overall decay is apparent in filling temperatures in Figure 32, from the peak of 310°C to the low of 130°C. This smooth decay in filling temperatures, frequently observed in other hydrothermal deposits, reflects the gradual decline in temperature and activity of the hydrothermal cell as the heat source cools (Spooner, 1981). As a result, this decay may record the thermal history of the system from its beginning at temperatures of 350° to 410°C, to its peak at 310°C, followed by a waning of activity and fluid temperatures.

The presence of low concentrations of dissolved salts in fluids of primary inclusions from Mt. Skukum was determined by the melting point depression of 0.4°C. Eutectic melting in these inclusions at -29.6°C is very close to the metastable eutectic melt in the H_2O-NaCl system (—28°C) indicating that salinity can be largely attributed to NaCl (Roedder, 1984). Using the experimentally derived curve for the H_2O-NaCl system of Potter et al. (1978) , the average final melting point depression of 0.4°C corresponds to a dissolved salt content of 0.7 weight percent NaCl equivalent. Eutectic and final melting temperatures for pseudo-secondary and secondary inclusions show minor variations from data for primary inclusions but data are too few to be conclusive (Figures 34 and 35). As found at Mt. Skukum, salinities of epithermal fluid inclusions are typically lower than that of sea water and range from 0.1 to 3.6 weight percent NaCl equivalent (Spooner, 1981) with inclusions from most epithermal deposits between 0.5 and 1.0 weight percent NaCl equivalent (i.e. Mount Kasi, Fiji at <2 weight percent NaCl (Turner, 1986); Au-quartz-adularia veins in Nevada at <2.1 weight percent NaCl equivalent (Nash, 1972)). Similar temperatures and salinities are also recorded in modern geothermal systems (Ellis, 1979). Consequently, the average salinity of 0.7 weight percent NaCl equivalent at Mt. Skukum is within expected limits for epithermal deposits, and indicates that large amounts of meteoric water with a low initial salt content passed through the hydrothermal system and maintained a dilute salt content in its passage through the rock. The presence of CO_2, noted above, will increase the apparent salinity of the inclusions (Hedenquist and Henley, 1985) indicating that the actual salinity may be even lower than measured. Hedenquist and Henley (1985) found that a solution containing 1 weight percent NaCl equivalent and 1 weight percent CO_2 at 300°C shows an apparent salinity of approximately 1.7 weight percent NaCl equivalent.

Liquid to vapour (L:V) ratios of primary inclusions are highly variable and bi-modal (Figure 36) with peaks at 2 and 20 volume percent vapour. No evidence of necking, which could account for this variation, was observed. Figure 37 shows that the average homogenization temperature for each of the volume percent gas class intervals in Figure 36 are remarkably similar. The only minor deviation occurs in inclusions which contain 2 and to a lesser extent 5 volume percent gas each of which display slightly lower homogenization temperatures. Widely ranging L:V ratios with similar homogenization temperatures such as these are generally considered symptomatic of a

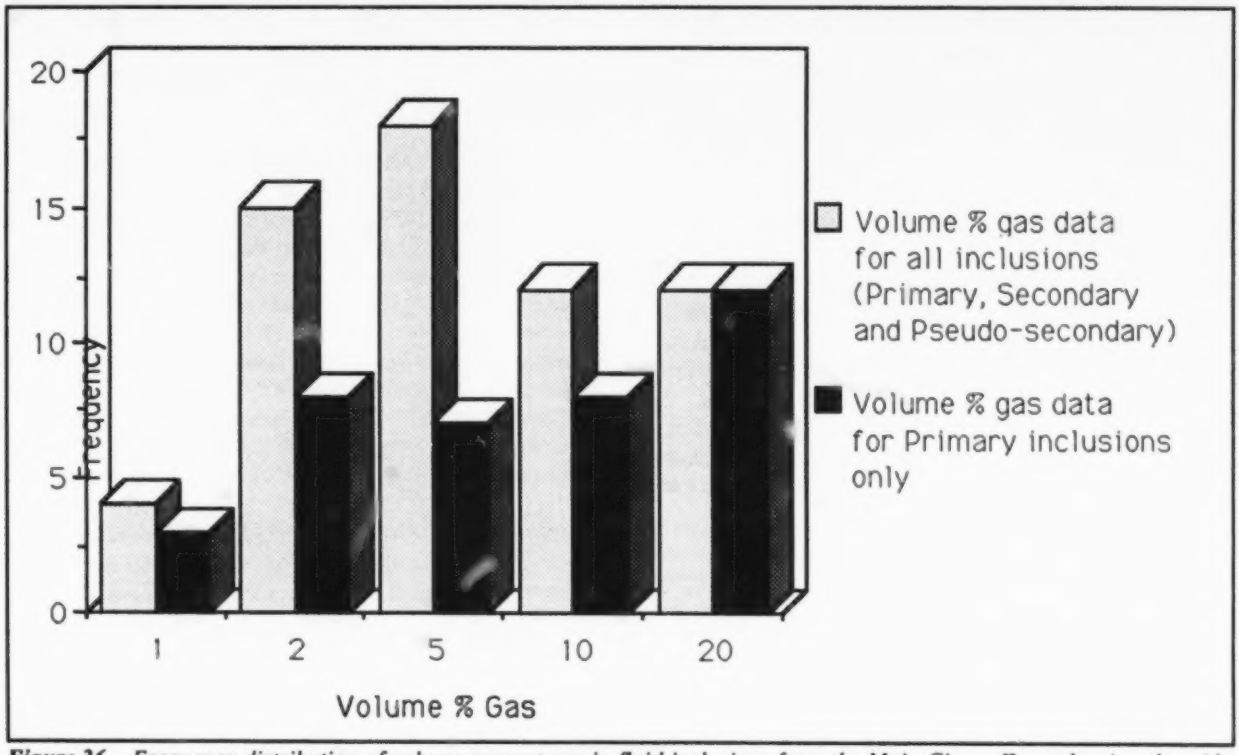

Figure 36. *Frequency distribution of volume percent gas in fluid inclusions from the Main Cirque Zone showing the wide variationin L:V ratios and their bi-modal distribution in primary inclusions at 2 and 20 vol. percent gas. The overall mode is at 5 vol. percent. Data is from Appendix D.*

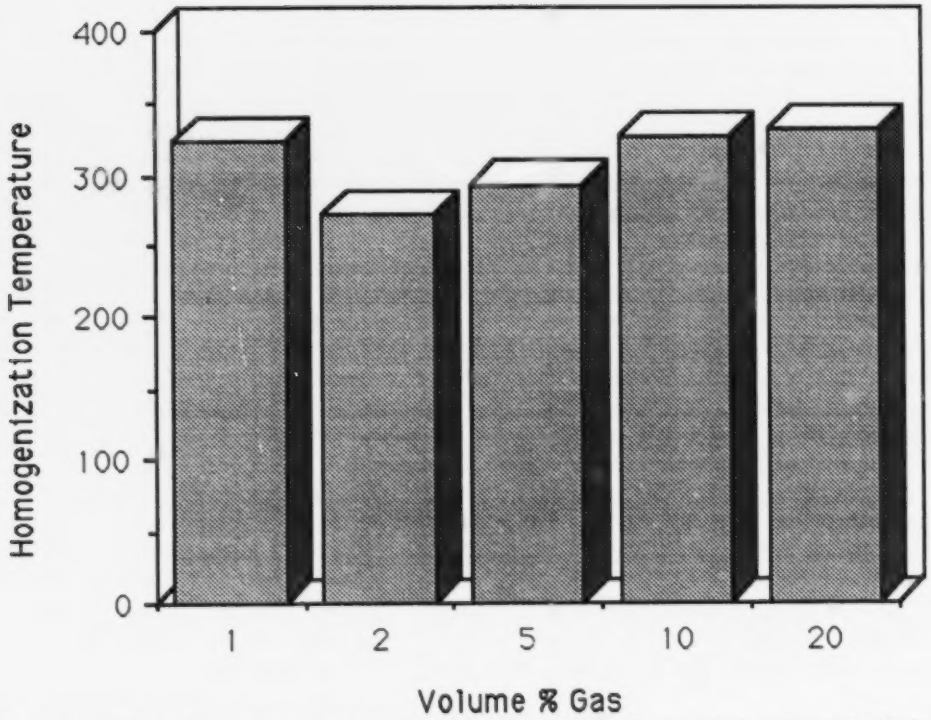

Figure 37 *Homogenization temperature versus L:V ratio for primary fluid inclusions from the Main Cirque Zone. This histogram illustrates the generally consistent homogenization temperatures of inclusions with a wide range of volumes*

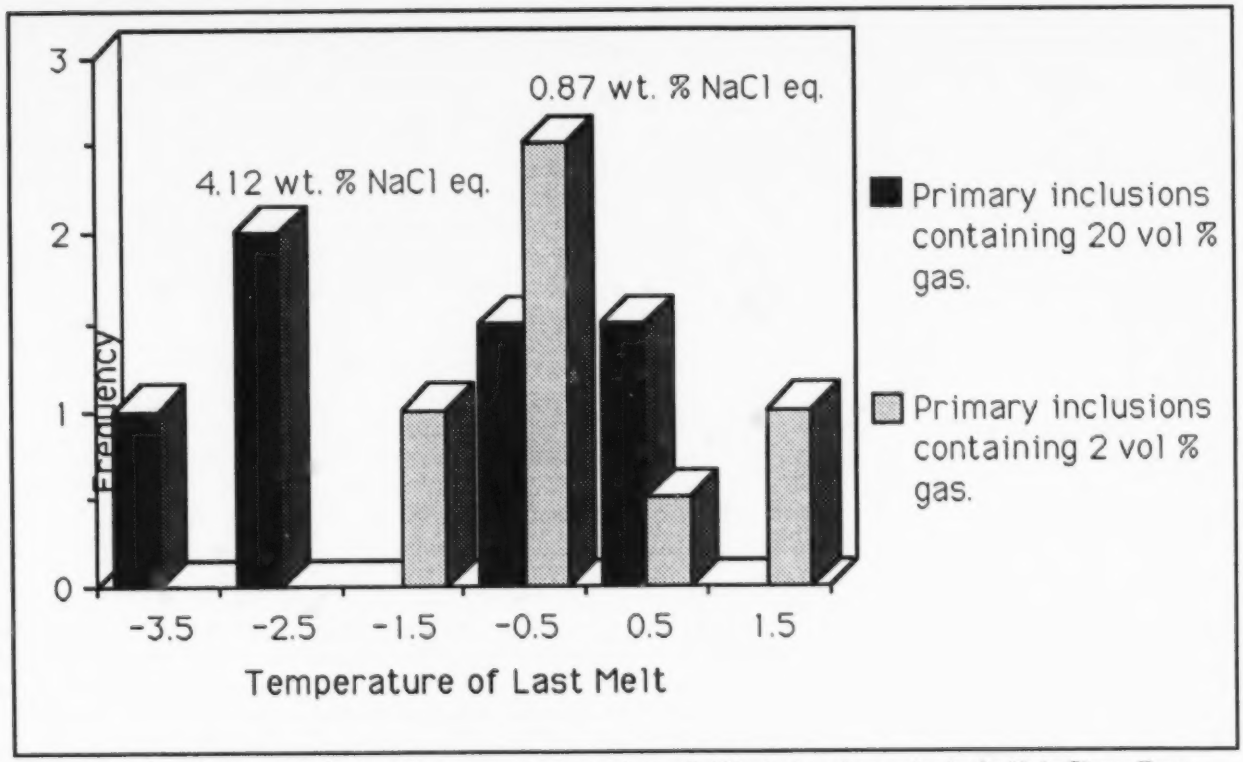

Figure 38 *Distribution of the last melting temperature of primary fluid inclusions from veins in the Main Cirque Zone, showing that those containing different gas contents have different apparent salinities. Data are from AppendixD.*

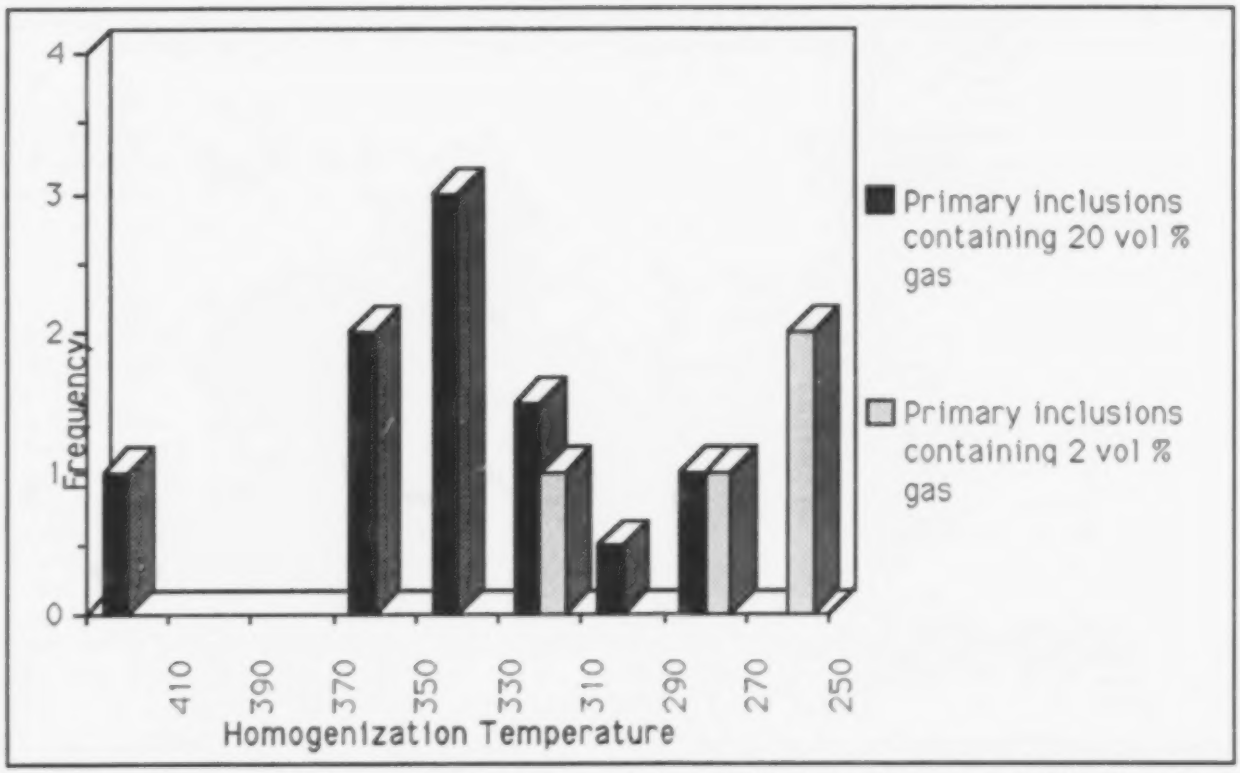

Figure 39 *Distribution of the homogenization temperature of primary fluid inclusions from veins in the Main Cirque Zone, showing that those containing different gas contents had different minimum temperatures of emplacement. Data are from Appendix D.*

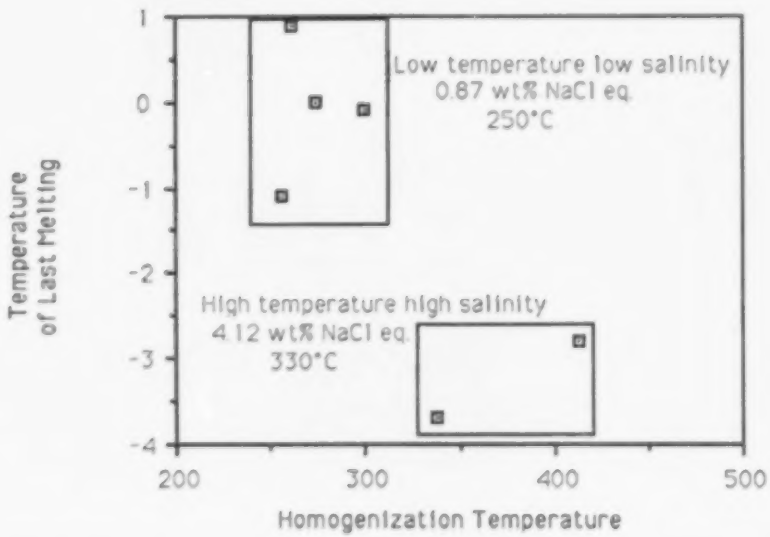

Figure 40 *Primary fluid inclusion data for temperature of last melt vs. homogenization temperature from veins in the MainCirque Zone, shows two fluid types, a low temperature, low salinity fluid and a high temperature, high salinity fluid. Points plotted represent all those inclusions for which both homogenization temperature and temperature of last melt were obtained and thus represent only a part of the total data set. Fluid temperature and salinities for each cluster are from Figures 37 and 38 which represent complete data sets. Data are from Appendix D.*

boiling event. However, these variations might also be due to several stages of vein emplacement from fluids of varying composition. No additional fluid inclusion evidence of boiling, such as coexisting liquid-rich and vapour-rich inclusions, was found. Nevertheless, breccia textures in veins and abundant breccia bodies associated with ore indicate that boiling probably was common during mineralization and may be responsible for variable L:V ratios.

The bi-modal distribution of gas content in primary inclusions corresponds with subtle differences in homogenization temperature and apparent salinity (Figures 37, 38 and 39). This indicates that at least two different fluids were responsible for mineralization; one relatively high in gas content, salinity, and temperature; the other relatively low in all of these.

Plotting the homogenization temperature vs. final melting temperature for those primary inclusions in which both were obtained illustrates this relationship (Figure 40).

As the fluids were at or near boiling (see Mineralization and Alteration), the data for the two clusters in Figure 40 allow calculation of depths of emplacement based on the boiling curves of Haas (1971) using the different modal salinities and homogenization temperatures for each cluster. Although the points plotted in Figure 40 represent only inclusions for which both homogenization temperatures and final melting temperatures were obtained, they coincide with the two modal salinities and homogenization temperatures in Figures 38 and 39 that represent complete data sets. Using this evidence, the maximum depth of emplacement for each fluid can be calculated for both lithostatic and hydrostatic pressure conditions. The high temperature fluid in Figure 40 has a modal temperature and salinity of 330°C and 4.12 weight percent NaCl equivalent respectively (Figures 38 and 39), while the low temperature fluid in Figure 40 has a modal temperature and salinity of 250°C and 0.87 weight percent NaCl equivalent respectively (Figures 38 and 39). Salinities and temperatures of these fluids indicate densities of 0.789 ± 0.002 gms/cm^3 for the low temperature, low salinity fluid and a density of 0.675 ± 0.002 gms/cm^3 for the high temperature, high salinity fluid if both are considered to lie on the boiling curve (Haas, 1971) at 250°C and 330°C respectively. Calculated vapour pressures for the low and high temperature fluids are 39.5 bars (± 0.5 percent) and 125.2 bars (± 0.5 percent) respectively; these are equal to the confining pressure on the respective liquids during deposition at the maximum depth of boiling. As confining pressure may be hydrostatic or lithostatic, different maximum depths of emplacement can be calculated. For hydrostatic conditions, maximum depths of emplacement are 460 ± 4 m for the low temperature fluid and 1,600 ± 19 m for the high temperature fluid. For lithostatic conditions, assuming a mean rock density of 2.7 gms/cm^3, the maximum depth of emplacement for the low temperature solution is 149 ± 4 m and for the high temperature solution 473 ± 19 m. The coincidence of calculated lithostatic and hydrostatic depths at about 465 m is consistent with: 1) stratigraphic evidence(p. 4 to 7), 2) the epithermal character of the veins, and 3) Lindgren's (1933) estimate that epithermal veins form at depths of less than 1 km. The depth of 1,600 m obtained for the high temperature, high salinity fluid under hydrostatic conditions exceeds the reasonable range of depths expected in an epithermal deposit that exhibits the abundance of open-space filling textures observed at Mt. Skukum, and also contradicts the depth of emplacement indicated by stratigraphic evidence. From the same stratigraphic evidence, the calculated depth of 149 m for the low temperature fluid under lithostatic pressure is unreasonably shallow. This introduces the possibility that these are perhaps not different solutions but rather high pressure and low pressure equivalents of the same hydrothermal fluid. Formation of a silica cap sealing movement of fluids in the Main Cirque Zone would cause an increase in fluid pressure towards lithostatic conditions. Minerals deposited during these sealed periods reflect higher pressure conditions through lower L:V ratios and higher temperatures of emplacement. Breaking of this seal, perhaps explosively, would allow sudden releases of pressure, and trigger boiling events which would be reflected in a decrease in fluid temperature accompanied by rapid mineral precipitation and loss of volatiles. The result is seen as lower homogenization temperatures and higher L:V ratios in inclusions from mineral phases formed at this time.

Periods of free fluid flow might also be accompanied by widespread mixing of upwelling hydrothermal fluids with cooler groundwater which may contribute to the relatively dilute dissolved salt content found in lower temperature inclusions. A wide variation in liquid to vapour ratios in inclusions and abundant zones of hydrothermal brecciation also supports the occurrence of boiling in the deposit as do localized zones of argillic alteration surrounding veins and the occurrence of an alteration cap zone. Consequently, fluid inclusion evidence suggests that boiling occurred during vein formation and may have been important in mineral precipitation. It also indicates that mixing of hot hydrothermal fluids with cooler in situ groundwater may have played a part in mineral precipitation as the solubility of gold decreases rapidly below 250°C and with decreasing salinities (Helgeson and Garrels, 1968). High homogenization temperatures averaging about 315°C support the presence of an igneous body at depth which supplied thermal energy to drive hydrothermal circulation.

Carbon dioxide clathrates formed in fluid inclusions from the Main Cirque Zone indicate that a moderate partial pressure of CO_2 existed in the depositional fluid. Only where CO_2 pressures within the inclusion lie between 10.4 and 45 bars (Figure 41) will a CO_2 clathrate ($CO_2 \cdot 5.75\ H_2O$: Roedder, 1984) form as the inclusion is cooled below 10°C. This partial pressure corresponds to a molal concentration at $P_{CO2} = 10.4$ bars of at least 0.85 molal (Hedenquist and Henley, 1985). Where P_{CO2} is greater than 45 bars (2.2 molal) a liquid CO_2 phase will be visible within inclusions at room temperature (Figure 41). As this phase was not observed in inclusions from Mt. Skukum, the maximum molal concentration of CO_2 present

must be less than 2.2 molal. The minor quantities of clathrate present in inclusions from Mt. Skukum indicates a CO_2 concentration close to the lower of these limits, probably about 1.0 molal or 4.4 weight percent (i.e. just above the minimum concentration required for clathrate formation). Moderate concentrations of CO_2 in fluid inclusions of epithermal deposits are common as phase equilibria in the H_2O-CO_2 system allows almost complete miscibility over a wide range of temperature and pressure above 300°C and a high degree of immiscibility at lower temperatures. Homogenization temperatures determined above, indicate that fluids at Mt. Skukum were sufficiently hot to carry large amounts of CO_2 in solution as seen in several active geothermal systems (Ngawha and Broadlands, New Zealand) where carbon dioxide dominates the dissolved gases in geothermal fluids and in some cases exceeds chloride as the major dissolved component (Hedenquist and Henley, 1985).

Fluid inclusion evidence from the Main Cirque Zone

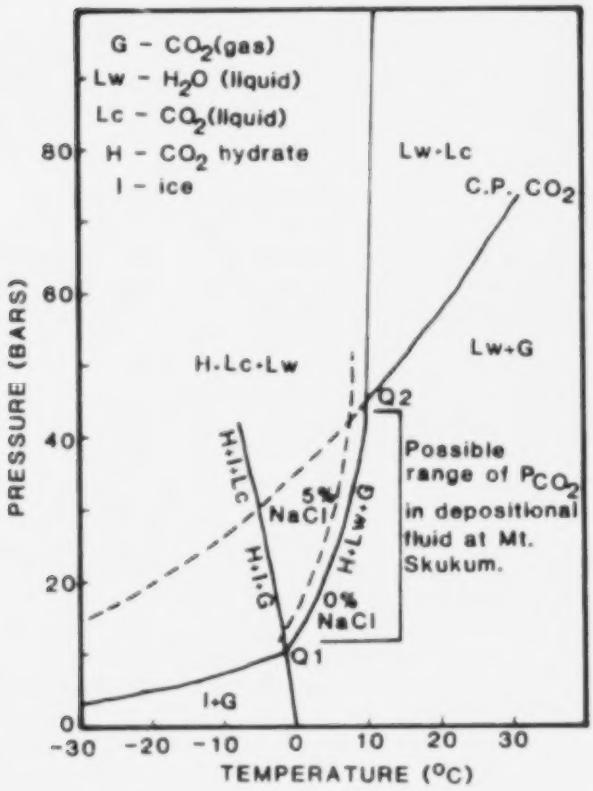

Figure 41. Phase equilibria in the lower temperature part of the system H_2O - CO_2 showing the limitations of CO_2 content in depositional fluids at Mt. Skukum (after Roedder, 1984). Q1 = CO_2 vapour, H_2O liquid, CO_2 clathrate, and ice at = -2°C and 10.4 bars. Q2 = CO_2 vapour, H_2O liquid, CO_2 liquid, and CO_2 clathrate at = 10°C and 45 bars. The equivalents of curve Q1 - Q2 for 5 percent added NaCl is also shown.

indicates that fluids responsible for mineralization were of low salinity and contained an apparent average of 0.7 weight percent NaCl equivalent. These fluids, which contained approximately 1.0 molal CO_2, deposited minerals at an average temperature of about 313°C at depths of about 470 m below paleo-surface. Mineral precipitation was probably controlled by boiling events brought about through tectonic activity that fractured overlying rocks thus allowing sudden releases of pressure. Mineral deposition may have been enhanced by mixing of upwelling hot hydrothermal fluids with cooler ground water near surface. At least three major episodes of mineral deposition are recognized; the first involving fluids at 310°C, the second at 270°C, and the third at 190°C. The presence of significant CO_2 in depositional fluids at Mt. Skukum explains the abundance of carbonate minerals occurring as gangue in the deposit and as wall rock alteration. Its presence has been found to cause a decrease in the measured salinity of fluid inclusions which may decrease the calculated emplacement depth of mineralization by as much as 23 percent (107 m). Carbon dioxide may have been incorporated into the hydrothermal system by deep fluid circulation and dissolution of marble in basement rocks.

STABLE ISOTOPE COMPOSITION OF HYDROTHERMAL MINERALS,FLUIDS, AND SURROUNDING HOST ROCKS

Knowledge of the origin of water, which is the dominant component of any hydrothermal fluid,is essential to any theory of ore formation. Systematic differences in the ratios of deuterium to hydrogen (D/H), and ratios between oxygen isotopes ($^{18}O/^{16}O$) and carbon isotopes (^{13}C and ^{12}C) allows the derivation of naturally occurring waters to be classified broadly into categories of meteoric, metamorphic and magmatic. Calculations concerning the temperature and salinity of depositional fluid, the isotopic composition and origin of the fluid, and considerations of scale involving possible water to rock ratios and total water volumes may also be made.

Estimation of the conditions of deposition involves many assumptions as to equilibrium and other factors; however, theoretical guidelines serve to place useful constraints on the size and character of the hydrothermal system. This information may be used to assess the likelihood of additional, similar deposits in areas adjacent to the mine and may provide insight into previously untried exploration techniques.

Direct measurements of the isotopic composition of extinct hydrothermal systems may be made by crushing fluid inclusion-bearing hydrothermal minerals and measuring the isotopic composition of minute amounts of liquid contained therein. An alternate method, used in this study, involves analysis of oxygen-bearing hydrothermal minerals and the application of experimentally derived equations to calculate the isotopic composition of the depositional fluid.

The objectives of the oxygen and carbon isotope study were to: a) determine the source of hydrothermal fluids which formed the deposit; b) calculate the isotopic composition of the mineralizing fluids, c) define constraints on the water to rock ratio operative in this hydrothermal system and thereby estimate its size, and d) calculate an isotopic temperature of deposition for minerals in the deposit.

Oxygen Isotopes

Fourteen analyses from ten samples from the Mt. Skukum deposit area were used, including three whole rock samples and eleven mineral separates. Two samples of altered wall rock, one of fresh wall rock, two pairs of quartz and calcite mineral separates from coexisting assemblages in quartz-carbonate veins, two of veins containing quartz only, two of early chalcedonic veinlets, and three independently analysed samples were used (Appendix F). Individual results and analytical methods are listed in Appendix F.

Isotopic Composition of Hydrothermal Fluids

The isotopic species of oxygen (^{18}O and ^{16}O) become fractionated between a mineral and its depositional fluid during precipitation through mass-dependant differences in chemical and physical behaviour. The degree of fractionation varies inversely with temperature and independently of pressure in a predictable way (Field et. al., 1985; Taylor, 1979). Consequently, if an independent estimation of temperature for the depositional fluids can be made through fluid inclusions or other means, the isotopic composition of that fluid may be calculated using analytical isotope data from a mineral and the fractionation coefficient between that mineral and water at the temperature of deposition.

Primary fluid inclusions from the Main Cirque Zone yield an average temperature of homogenization of approximately 315°C (see Fluid Inclusions, p. 119). Using this independent estimation of temperature (temperature of formation estimates using oxygen isotope analysis of mineral pairs on page 48 appear to be invalid) and isotopic data from analyses of quartz and calcite in the veins, the original isotopic composition of the depositional fluids can be calculated using the following two equations:

1. Quartz-H_2O

$$1000 \ln a_{(quartz\text{-}water)} = 3.34 \times (10^6/T^2) - 3.31$$

where: T = Temperature (°K)

Temperature range=250-500°C

(Matsuhisa et al, 1979)

2.Calcite-H_2O

$$1000 \ln a_{(calcite\text{-}water)} = 2.78 \times (10^6/T^2) - 2.89$$

where: T = Temperature (°K)

Temperature range = 0-500°C

(Friedman and O'Neil, 1977)

The $d^{18}O$ values of whole rock can also be used to calculate the composition of depositional fluids. According to Taylor (1979), it is reasonable to assume that $d^{18}O_{rock}$ in equilibrium with hydrothermal fluids is equal to the $d^{18}O$ value of plagioclase (An_{30}). Therefore, the following plagioclase-H_2O equation can be used:

3. Plagioclase(An_{30})-H_2O

$$1000 \ln a_{(plagioclase\text{-}water)} = 2.68 \times (10^6/T^2) - 3.5$$

where: T = Temperature (°K)

Temperature range = any reasonable geologic temperature.

(O'Neil and Taylor, 1967)

Table 6. *Oxygen isotope composition [1] of hydrothermal fluids at Mt. Skukum, Yukon Territory .Calculations are from data in Appendix E and equations 1, 2 and 3 in text.*

Sample Number	Material	$d^{18}O$ value of material	Calculated $d^{18}O$[1] of depositional fluid
ASTN-15	Unaltered Andesite	-6.8	-11.0
ASTN-13A	Altered Andesite	-6.7	-10.9
ASTN-10A	Altered Andesite	-7.2	-11.4
C049-Qtz	Quartz	-3.5	-9.8
C049-Cal	Calcite	-6.9	-12.0
C005-Qtz	Quartz	-4.3	-10.6
C005-Cal	Calcite	-6.8	-11.9
C042	Quartz	-4.3	-10.6
C040	Quartz	-4.0	-10.3
C072	Quartz	-5.2	-11.5
M1	Quartz	-4.71	-11.1
M2	Quartz	-4.3	-10.6
M3	Calcite	-8.6	-13.7
		Average (n = 13) is	-11.2

[1] Error in calculated values ± 0.0008

In the above three equations, $1000 \ln a_{(a\text{-}b)} \approx d_a - d_b$. Consequently, they may be used to calculate the $d^{18}O$ composition of depositional fluids for all data in Appendix F. Results of these calculations (Table 6) display a very narrow spread of isotopic composition in the depositional fluids of between $d^{18}O$=-9.8 and -13.7 $‰$. The average value for calculated $d^{18}O$ composition is -11.2 $‰$; analytical error gives an uncertainty of ± 0.0008 $‰$.

Water to Rock Ratio

Unaltered andesites have a well-known $d^{18}O$ value of +6.5 ± 1 $‰$ (Taylor, 1979). The extent to which $d^{18}O$ values of the andesites surrounding the deposit have been lowered from this norm depends on temperature, extent of isotopic equilibrium between wall rock and fluids, the $d^{18}O$ value of circulating

Table 7. Water to rock mass ratio calculations for Mt. Skukum, Yukon Territory. Calculations are from data in Table 6 and equation 4 in text.

Sample Number	Calculated $d^{18}O$ value of water in equilibrium with sample (Table 6)	Calculated water: rock mass ratio
ASTN-15	-11.0	0.80
ASTN-13A	-10.9	0.78
ASTN-10A	-11.4	0.86
	Average (n = 3) is 0.81 ±0.0008 ‰	

fluid, and the water to rock ratio (i.e. the amount of exposure the rock has had to the fluids). Since isotopic equilibrium is assumed and the remaining three variables are known — one from independent observation and the others determined above — the remaining unknown may be calculated using the following equation (after Ohmoto and Rye, 1974, and Field and Fifarek, 1985):

$$4. \quad d^{18}O_{f_w} = \frac{7 - D_{r-w} + (1.8R)(d^{18}O_{i_w})}{1 + (1.8R)}$$

where: r = rock, w = water, f = final, i = initial, R = water to rock mass ratio, and D = calculated fractionation coefficient for isotopic exchange between rock and water

This equation assumes continuous re-circulation and re-equilibration of the water in a closed system. Although this cannot be rigorously true, it is probably closer to reality than an open system would be (Taylor, 1979). Results of applying the above equation to the available whole rock isotope data are in Table 7; they indicate an average water to rock ratio for the Main Cirque Zone of 0.81. Factors other than simple fluid-rock exchange that may affect the isotopic composition of the fluids include boiling and mixing with unexchanged meteoric water, neither of these conditions are compensated for in the equation (Field and Fifarek, 1985).

Geothermometry

Two minerals deposited in isotopic equilibrium from the same fluid will contain different quantities of ^{18}O due to temperature dependant fractionation between the two minerals. Assuming that equilibrium was preserved and knowing variations in fractionation factor with temperature from experimental data it is possible to calculate temperature of deposition for the two minerals. In this study, quartz and calcite were used as the mineral pair to determine the isotopic temperature of deposition. The fractionation factor ($D_{quartz-calcite}$) between these two minerals in relation to the temperature of deposition can be expressed as follows (Field and Fifarek, 1985):

$$5. \quad T(°K) = (0.74 \times 10^3) + (D_{quartz-calcite} + 0.42)^{1/2}$$

Temperature range = (250-500°C)

where: $D_{quartz-calcite} \approx d^{18}O_{qtz} - d^{18}O_{cal}$

Two mineral pairs from samples C005 and C049 were chosen as they both contained intimately intergrown quartz and calcite, a feature supporting the assumption that the mineral assemblage was deposited in isotopic equilibrium. Applying the above formulae to data from these samples results in the calculated temperatures of deposition in Table 9 of 160°C and 106°C or an average of 133°C.

Table 8. Calculated isotopic temperature of deposition [1] from mineral pairs obtained from the Main Cirque Zone. Calculations use data from Appendix F and equation 5 in text.

Sampled Number	$^{18}O_{quartz}$	$d^{18}O_{calcite}$	$D_{quartz-calcite}$	Calculated T(°C)[1] deposition
C005	-4.3	-6.8	2.5	160°
C049	-3.5	-6.9	3.4	106°
		Average (n = 2) is	133°	

[1] Error in calculation 0.001 ‰

Discussion

A significant feature of all analytical results regardless of the mineral or sample type is a consistent depletion in ^{18}O with respect to SMOW. Whole rock analyses show average $d^{18}O$ values at Mt. Skukum of -6.9 ‰; analyses of quartz show average $d^{18}O$ values of -4.6 ‰; and calcite analyses show average $d^{18}O$ values of -7.4 ‰. As the lower boundary of $d^{18}O$ for normal igneous rocks on the earth and moon is +5.5 ‰ (Taylor, 1968; Taylor and Epstein, 1970), these materials are depleted in ^{18}O by 10 to 13 ‰. An average of -6.9 ‰ for the whole rock data is 13.4 ‰ below normal for an unaltered andesitic igneous rock (Taylor, 1979). This is indicative of isotopic exchange at elevated temperature with large volumes of hydrothermal solutions of low ^{18}O content. Such isotopic exchange occurs during alteration of country rock by meteoric hydrothermal fluids; the degree of isotopic exchange at Mt. Skukum is symptomatic of host rocks being completely saturated in this fluid.

Calculation of the original ^{18}O content of the hydrothermal fluid from $d^{18}O$ values for the resultant quartz and calcite give an average $d^{18}O$ of -11.2 ‰. As this fluid must have interacted with country rocks considerably higher in ^{18}O content than itself, its original isotopic composition can only have had an even lower $d^{18}O$ value than the post-equilibration value calculated above. In comparing the calculated $d^{18}O$ value for depositional waters to fields for naturally occurring waters in Figure 42, it is apparent that regardless of the dD composition, a fluid this low in ^{18}O content can only have originated from meteoric water with little or no contribution from magmatic or metamorphic sources.

The $d^{18}O$ composition of meteoric water in the Mt.

Skukum area today can be calculated using the relation cited by Craig (1966).

6. $dD\ (‰) = 8\ d^{18}O\ (‰) + 10$

where: dD = deuterium values in meteoric water at any given point on earth

Figure 43 indicates that present-day dD values for meteoric water in the Mt. Skukum area are approximately -155 ‰. Applying this data to the above equation indicates a $d^{18}O$ value of -20.6 ‰ for naturally occurring meteoric water in the area today. Although the isotopic composition of meteoric waters in any area does not remain constant through time, analyses of Tertiary supergene mineral assemblages indicate only minor changes involving a 1 to 2 ‰ shift toward heavier values for $d^{18}O$ since Tertiary time (Taylor, 1974; O'Neil and Silberman, 1974; Field and Fifarek, 1985). This assumption is reasonable in that as meteoric isotope composition reflects latitude and elevation(Figure 43), no significant changes have occurred since pre-Tertiary time. Therefore, depositional fluids at Mt. Skukum, having had an original $d^{18}O$ composition of -20.6 per mil, were enriched by 9.4 ‰ during interaction with the country rock. This enrichment in ^{18}O composition of the fluid almost exactly matches the ^{18}O depletion in the surrounding country rocks. This supports the hypothesis that groundwater was the major and probably only constituent of mineralizing fluids; if this was not so there would be some discrepancy between the amount of depletion of ^{18}O in country

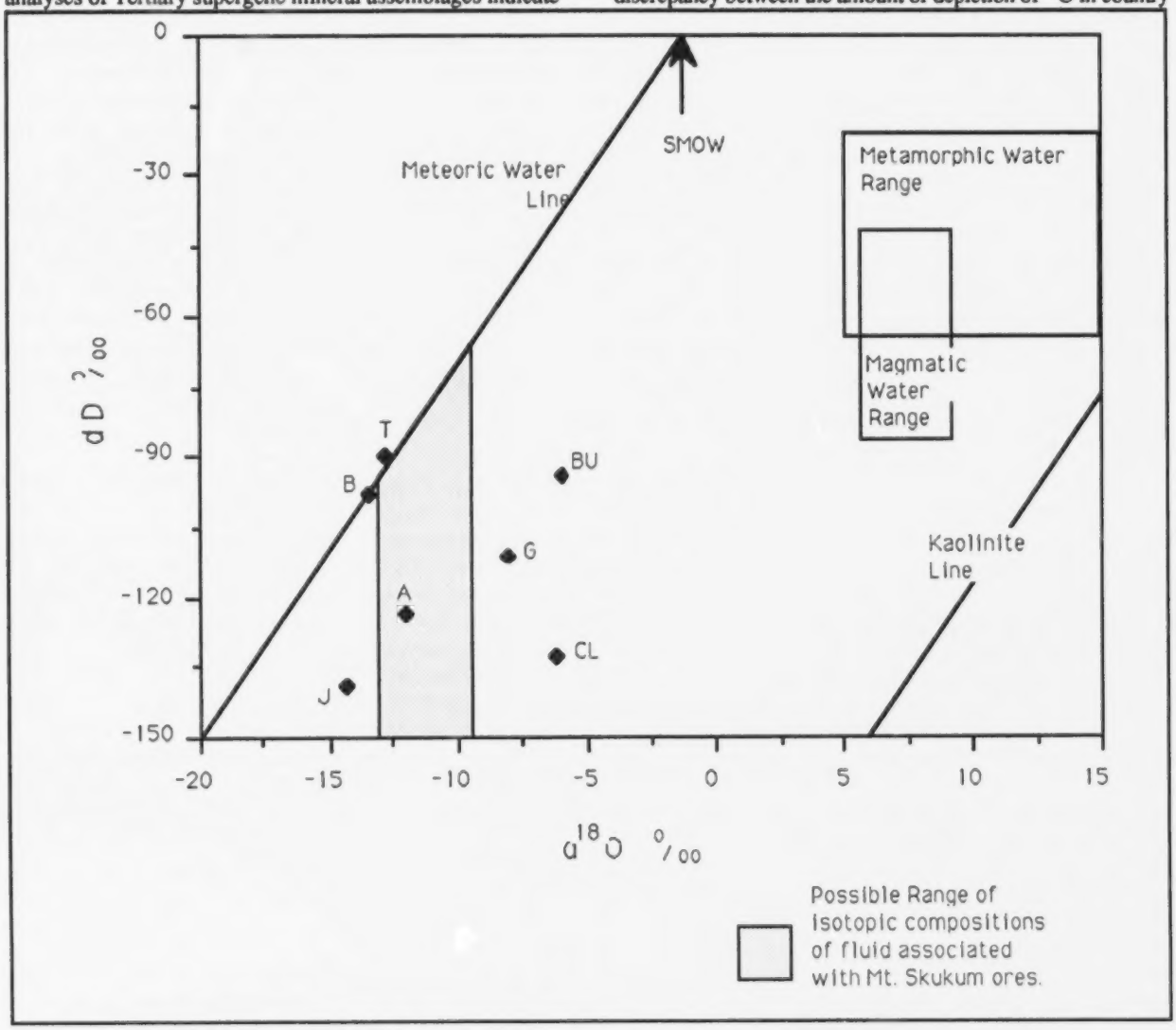

Figure 42. *$d^{18}O$ vs. dD values showing fields for magmatic and metamorphic water and the possible range of depositional fluid composition in the Main Cirque Zone. Values for some Tertiary volcanic-hosted epithermal deposits of the Basin and Range region of the U.S. also shown are: Bullfrog (BU), Aurora (A), Jarbidge (J), Gilbert (G), Tonopah (T),Bodie (B), Comstock Lode (CL). SMOW indicates the position of Standard Mean Ocean Water. All values in per mil (‰). Modified after Taylor (1979) and Field and Fifarek, (1985).*

rocks and the amount of enrichment in depositional fluids from the pristine meteoric state. Reciprocal shifts in isotopic composition of this sort in both host rocks and meteoric fluids have been noted around the world both in modern geothermal systems such as Wairakei, New Zealand and Steamboat Springs, Nevada (Taylor, 1979; White, 1981) and in their fossil equivalents Bodie, California; Tonopah, and Goldfield, Nevada (Taylor, 1973, 1974; O'Neil et al., 1973; Field and Fifarek, 1985). These areas are all characterized by highly jointed, permeable volcanic rocks associated with high-level igneous intrusions, usually Tertiary in age, which act as heat engines driving the circulation of meteoric water over a broad area. Volcanic country rocks characteristically show depletions in ^{18}O of between 10 and 13 $^{0}/_{00}$ around centres of hydrothermal activity (Taylor, 1971).

Calculations of the mass ratio of water to rock which prevailed at Mt. Skukum show that for every gram of rock in the area of the deposit, 0.81 grams of water have moved through the system. This represents a minimum figure considering that at least some of the water passing through the system may never have made contact with the walls and that water in the latter phases would only contact wall rock which had already equilibrated with the fluid. Although this represents an enormous amount of water considering the aerial extent of hydrothermal alteration, it is consistent with values obtained in many epithermal districts in the western U.S. where reported water to rock ratios range from 0.2 to 2 (Taylor, 1974). Low salinities in fluid inclusions support a high water to rock ratio to maintain dilution of the dissolved salts. Modern geothermal systems have similar water to rock ratios such as 0.45 to 1.3 at the Salton Sea, and 4.3 at Wairakei (Clayton and Steiner, 1975). Typical porosities for host rocks of these deposits limit the water:rock ratio to generally less than 0.1 (Field and Fifarek, 1985). This implies that mineral deposition at Mt. Skukum must have occurred in an open system of fractures and fault zones to allow passage to such large quantities of fluid.

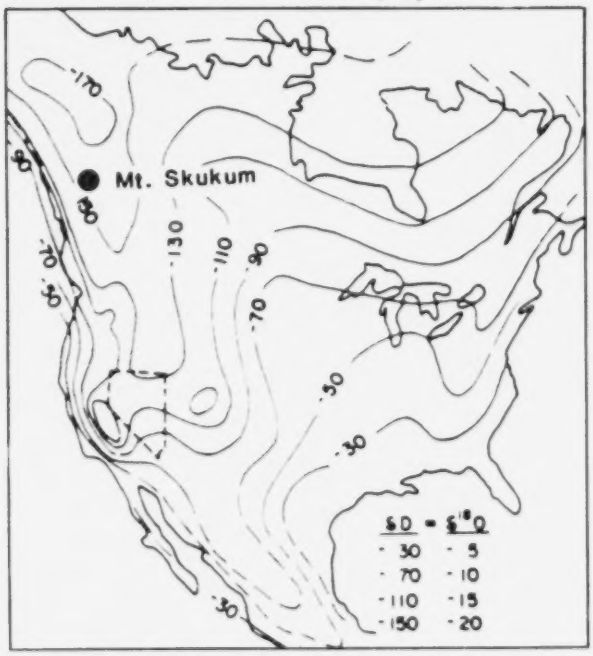

Figure 43 *North America with contours of dD values in meteoric surface waters (from Taylor, 1979).*

Two attempts to calculate an isotopic temperature of mineral deposition yielded divergent results of 106° and 160°C. Not only are these numbers not in agreement with those obtained using fluid inclusions, but they are both below the lower limit of temperatures required to cause the regional propylitic alteration observed. Calculations of temperature based on isotopic evidence requires not only isotopic equilibrium between the depositional fluid and each mineral considered, but also equilibrium between the minerals themselves. As isotopic temperatures are radically lower than homogenization temperatures of fluid inclusions ($T_h \approx 315$°C: Section 5.2), the assumptions of equilibrium and contemporaneity are invalid. Despite the apparent intimate relationship between the quartz and calcite, they may have been deposited at different times by fluids of slightly differing isotopic composition. Thus, the intimate textures displayed by the quartz-calcite pairs probably result from replacement rather than equilibrium. Unfortunately, in an epithermal environment, equilibrium conditions that allow temperature calculations are the exception rather than the rule. The other calculations using isotopes are still valid as each relies not on mineral-mineral equilibria but mineral-fluid equilibria.

Carbon Isotopes

Carbon isotopes provide an indirect method of determining hydrothermal conditions in a fluid. Although carbon is not as fundamental a part of the hydrothermal fluid as oxygen, carbon-bearing species such as CO_2, HCO_3^-, H_2CO_3, and CH_3 are commonly present in hydrothermal fluids. The isotopic ratio between ^{13}C and ^{12}C in minerals deposited from a hydrothermal fluid can supply information about the rocks it moved through and equilibrated with during its history in the hydrothermal system. Unfortunately, isotopic signatures of many varieties of rocks are similar and commonly cannot be satisfactorily distinguished. Also, the occurrence of carbon as either oxidized or reduced species leads to very different isotopic compositions in rocks that are genetically similar (Ohmoto and Rye, 1979). Despite these difficulties, some useful information was obtained from these studies.

Data

Analyses from carbonates in vein material were obtained from three specimens. All samples were analysed by K. Muehlenbachs at the University of Alberta. Two of the samples were collected and prepared by the author. The third sample was independently collected by K. Muehlenbachs. Results are reported in Table 9 as $d^{13}C$ per mil ($^{0}/_{00}$ representing the deviation from the marine carbonate carbon standard (PDB).

Table 9. Carbon isotope composition of hydrothermal minerals at Mt. Skukum, Yukon Territory.

Sample #[1]	Mineral Analysed	$d^{13}C$ ‰
C005	Calcite	-10.3
C049	Calcite	-10.3
M3[2]	Calcite	-10.7
	Average (n = 3)	-10.4

1. Descriptions of samples are in Appendix D. All samples were analysed by K. Muehlenbachs at the University of Alberta.
2. Collected and analysed by K. Muehlenbachs.

Conclusions

Calcite analyses in Table 9 exhibit an extremely narrow isotopic range with an average $d^{13}C$ value of -10.4 ‰. Due to the relation $d^{13}C_{calcite} \approx d^{13}C_{fluid}$, which applies at temperatures greater than 200°C (Ohmoto and Rye, 1979), the ^{13}C composition of the depositional fluid must also have been approximately -10 ‰. This result falls within the overall range in carbon isotope compositions in epithermal deposits which vary world wide from -10 to +1 ‰ (Field and Fifarek, 1985). In addition, $d^{13}C$ values in CO_2 emanating from geothermal sources today range from -8 to -11 ‰, values that encompass those in calcite at Mt. Skukum.

Determining the source of carbon based on carbon isotopic compositions alone is difficult due to the lack of discrimination among isotopic compositions for carbon from different sources. Nevertheless, calculated isotopic compositions at Mt. Skukum of -10 ‰ are well below average values of $d^{13}C$ for igneous, metamorphic and sedimentary rocks at about -5.5 ‰ (Ohmoto and Rye, 1979). This indicates significant enrichment in the lighter isotope relative to these rocks. Abundant carbonate minerals present in veins at Mt. Skukum and the presence of carbon dioxide in fluid inclusions indicates that much of this carbon occurred in the system as carbon dioxide. Marble present in underlying Yukon Group metasedimentary rocks has been proposed as a probable source of this component through dissolution in deeply circulated hydrothermal fluids.

From the relation given above $d^{13}C_{calcite} \approx d^{13}C_{fluid}$ (Ohmoto and Rye, 1979), the fractionation coefficient between carbon isotopes in basement marble and interacting hydrothermal fluids is assumed to be unity. This suggests that if these fluids had equilibrated with basement marble, then calcite deposited from these fluids should have the same isotopic composition as that of the marble, which is expected to be about -5.5 ‰. As carbon isotopes in vein material from Mt. Skukum display values almost twice as negative as that expected in any of the surrounding metamorphic or igneous host rocks, other factors must have affected isotopic compositions. Equilibration with reduced carbon is an effective way to drive carbon isotopic compositions towards significantly lower $d^{13}C$ values. Thus, the presence of disseminated graphite in pelitic schists in underlying Yukon Group metasedimentary units may be the cause of the unusually light carbon isotopic composition of calcite at Mt. Skukum. Abundant evidence that these rocks were exposed to and commonly involved in much of the hydrothermal activity is indicated by frequent inclusions of both marble and pelitic schists in hydrothermal breccias in the area.

Preliminary study of carbon isotopes in calcite from Mt. Skukum veins indicates that carbon was incorporated into a deeply circulating hydrothermal system through leaching of volcanic and graphitic metasedimentary country rock. It existed in solution in an oxidized state as reflected by the abundance of carbonate minerals in the deposit. Marble, which comprises a significant proportion of these metasediments, may have been a primary source for carbon along with significant contributions from reduced carbon (graphite) which resulted in unexpectedly negative $d^{13}C$ values in vein material.

DEPOSIT MODEL

The model proposed for the Mt. Skukum epithermal gold-silver deposit is depicted in Figure 44. Characteristics of this deposit closely fit those described as low-sulphur, adularia-sericite type epithermal deposits (Heald et al., 1987, Hayba et al., 1985; Bonham, 1986; Buchanan, 1981; Berger and Eimon, 1983). Emplacement of veins forming the Mt. Skukum deposit was probably caused by development of a hydrothermal circulation cell driven by the porphyritic rhyolite intrusion inferred below rocks of Main Cirque. Considering the broad extent of propylitic alteration which affects porphyritic andesite flow rocks over an area of at least 66 square km, this hydrothermal cell was probably regional in extent covering the entire western portion of the volcanic complex. Hydrothermal outflow may have been centered on different areas at different times, one of which was Main Cirque where previous block-faulting, reactivated and dilated by resurgent doming, provided excellent ground preparation. In addition, the presence of a heat source centered below the cirque, focussed hydrothermal discharge in the area (Figure 15).

Mineralization in Main Cirque was deposited in veins structurally controlled by major fault zones between down-dropped blocks (Figure 8). The largest mineralized zone is the Main Cirque Zone which occurs in a large fault in the keystone block of the Main Cirque graben. Veins in the southern segment of this zone achieve thicknesses of up to 13 m and are paralleled by an equal thick rhyolite dyke which continues northward past the point at which the Main Cirque Fault Zone assumes a more easterly trend and cross-cuts this rhyolite dyke (Figure 7). The extreme thickness of vein material present in the southern segment of the Main Cirque Zone, as opposed to that in the northern segment, may be caused by two factors. Arching, which reactivated faults in Main Cirque creating

dilatant cavities for vein formation, occurred through a broad folding of strata about a north-trending axis which would tend to dilate north-trending faults by a greater amount than those trending north-east. In addition, if even slight rotational or dextral strike-slip displacement was brought about on the northeasterly-trending segment of the Main Cirque Fault Zone (Figure 7) during doming, the southern segment would be opened as an enormous cavity due to the change in strike between northern and southern segments, allowing a greater thickness of vein material to be deposited.

Vein textures take the form of open-space fillings with abundant associated brecciation. This indicates deposition in a near-surface environment where lithostatic pressure conditions were low enough to allow open cavities produced by faulting to be maintained for prolonged periods of time. Hydrothermal breccias are common throughout the Main Cirque indicating that at times pressures were built up and released in explosive events leading to localized fracturing of rocks in the area and precipitation of mineralization. Precious metal distribution within the Main Cirque Zone forms a mineralized horizon of maximum values extending over a vertical depth of 59m to a base elevation of 1,676 m; this supports a pressure-related precipitation mechanism limited by depth to a boiling curve (Haas, 1971) dictated by the temperature and salinity of the hydrothermal fluid. Grade-thickness plots of the Main Cirque Zone (Figures 27, 28 and 29) show that mineralization is deposited in steeply dipping ore shoots filling large conduits suggesting that fluid flow in this zone was directed upwards toward paleosurface. This further reinforces pressure decrease as a viable trigger for mineral precipitation.

Fluid inclusion study indicates that vein minerals formed from fluids under two pressure régimes at a common depth of about 470 m. Two populations of salinity and temperature are clearly demonstrated by inclusion measurements ; one population characterized by homogenization temperatures of approximately 330°C and a salinity of 4.12 weight percent NaCl, and the other by homogenization temperatures of approximately 250°C and a salinity of 0.87 weight percent NaCl. A coincident depth of formation (within error margins) can be calculated for these different fluids assuming that high temperature, high salinity fluids were trapped in minerals formed under lithostatic pressure whereas fluids of lower temperature and salinity were trapped in minerals formed under hydrostatic pressure. Postulation that these populations of temperature and salinity formed at a common depth is consistent with sudden boiling events caused by tectonic release of near-lithostatic pressure built up against a sealed alteration cap near the surface. A wide variation in liquid to

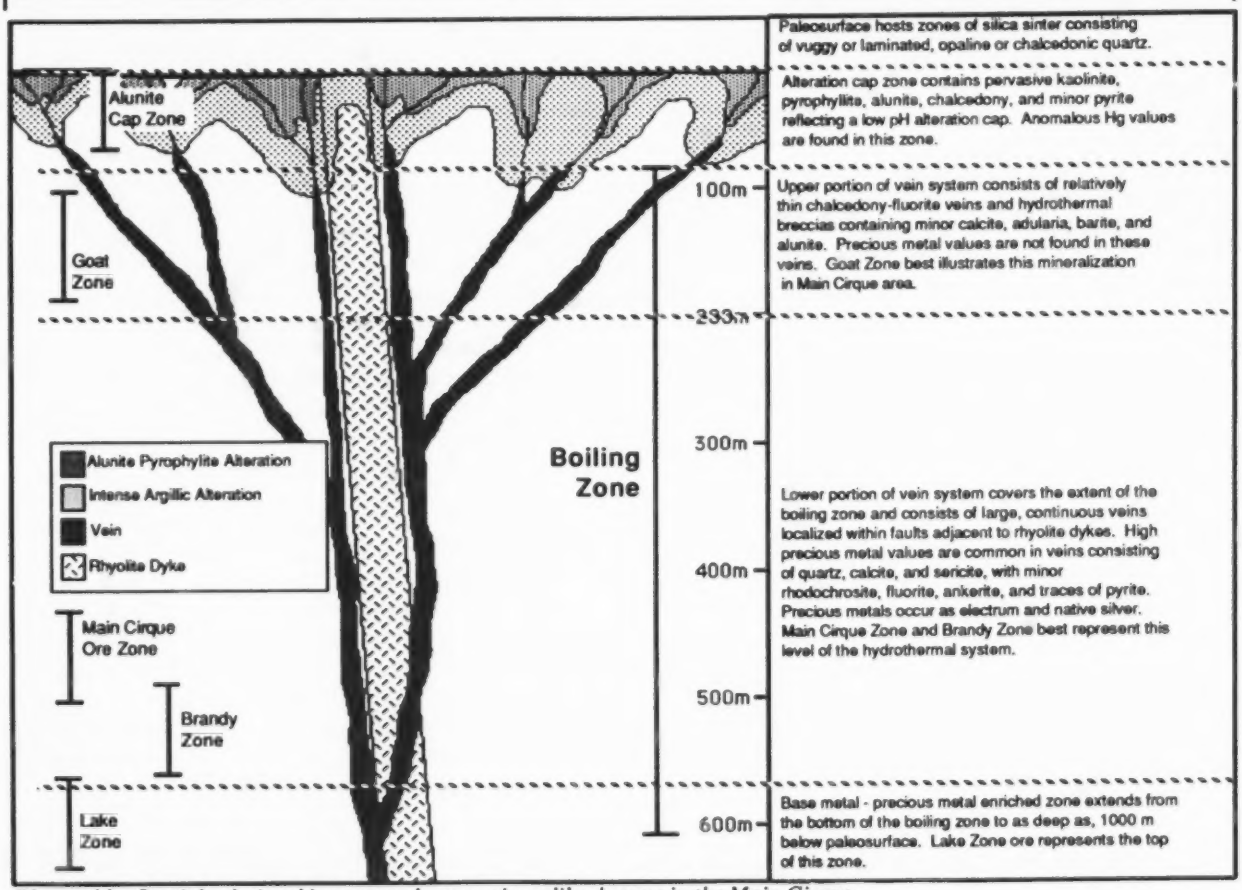
Paleosurface hosts zones of silica sinter consisting of vuggy or laminated, opaline or chalcedonic quartz.
Alunite Cap Zone
Alteration cap zone contains pervasive kaolinite, pyrophyllite, alunite, chalcedony, and minor pyrite reflecting a low pH alteration cap. Anomalous Hg values are found in this zone.
100m
Goat Zone
Upper portion of vein system consists of relatively thin chalcedony-fluorite veins and hydrothermal breccias containing minor calcite, adularia, barite, and alunite. Precious metal values are not found in these veins. Goat Zone best illustrates this mineralization in Main Cirque area.
233m
300m
Boiling Zone
Alunite Pyrophylite Alteration
Intense Argillic Alteration
Vein
Rhyolite Dyke
Lower portion of vein system covers the extent of the boiling zone and consists of large, continuous veins localized within faults adjacent to rhyolite dykes. High precious metal values are common in veins consisting of quartz, calcite, and sericite, with minor rhodochrosite, fluorite, ankerite, and traces of pyrite. Precious metals occur as electrum and native silver. Main Cirque Zone and Brandy Zone best represent this level of the hydrothermal system.
400m
Main Cirque Ore Zone
500m
Brandy Zone
Lake Zone
Base metal - precious metal enriched zone extends from the bottom of the boiling zone to as deep as, 1000 m below paleosurface. Lake Zone ore represents the top of this zone.
600m

Figure 44. Spatial relationships among known mineralilzed zones in the Main Cirque.

vapour ratios in inclusions and abundant zones of hydrothermal brecciation also supports the occurrence of boiling in the deposit as do localized zones of argillic alteration surrounding veins and the occurrence of an alteration cap zone. Fluids trapped below a sealed cap would maintain a relatively high temperature and salinity as represented by the high temperature, high salinity population of fluid inclusions at Mt. Skukum. When the cap was fractured, released pressure allowed boiling to occur causing rapid precipitation and mixing of hot hydrothermal fluids with cooler groundwaters during a rapid return to hydrostatic conditions as solutions circulated freely to the surface. Boiling alone causes a decrease in temperature and may account for the temperature difference between inclusion populations; however, the significant decrease in salinity observed suggests interplay between hydrothermal fluids and in situ groundwater which may have both cooled and diluted hydrothermal solutions. The conclusion that inclusion populations represent common solutions under different pressure régimes is supported by stratigraphic evidence which indicates that the determined depth of 470 m is not unreasonable. Consequently, fluid inclusion evidence suggests that boiling occurred during vein formation and may have been important in mineral precipitation. It also indicates that mixing of hot hydrothermal fluids with cooler in situ groundwater may have played a part in mineral precipitation as the solubility of gold decreases rapidly below 250°C and with decreasing salinities (Helgeson and Garrels, 1968). High homogenization temperatures averaging about 315°C support the presence of an igneous body at depth which supplied thermal energy to drive hydrothermal circulation.

Stable isotope composition of minerals in the Mt. Skukum deposit indicate that they have undergone isotopic exchange at elevated temperature with large volumes of hydrothermal fluid. Although the presence of a rhyolitic magmatic body at depth is indicated as a heat engine driving hydrothermal circulation, oxygen isotope evidence clearly shows that circulating solutions were meteoric in origin with little or no contribution from magmatic sources (Figure 42). The magnitude of this hydrothermal system is indicated in calculations of the mass ratio of water to rock which shows that for every gram of altered rocks in the area, a minimum of 0.81 grams of water moved through the system in its lifetime. Considering the area of altered rock covers approximately 66 square km to a depth exceeding the thickness of the volcanic complex (850 m), an enormous volume of water is represented. As an example, assuming that 50 percent of the rocks in this volume are affected, an unreasonably small quantity, the minimum amount of water indicated is 7.22×10^{13} kg.

A preponderance of evidence suggests that boiling of an upward moving low-salinity, hydrothermal fluid at Mt. Skukum was a common phenomenon during mineral deposition and may have been important in precious metal precipitation. Hydrothermal fluids interacting with oxidized surface and groundwaters caused pervasive clay alteration of rocks at the site of hydrothermal discharge which, combined with precipitation of quartz, effectively sealed-off hydrothermal discharge causing pressure below this sealed cap to approach lithostatic conditions. Periodic re-activation of faults in the area fractured these sealed caps and allowed sudden release of pressure as described by the throttling model of Barton and Toulmin (1961); this process likely led to repetitive boiling events extending significantly deeper than could be expected under normal hydrostatic conditions (Buchanan, 1981; Henley, 1985). This would be accompanied by mineral deposition over a relatively broad range of elevations brought about by free interaction of in situ groundwater with hydrothermal solutions. During periods where this seal restricted flow to the surface, lithostatic pressures which built up are reflected in high temperature, high salinity inclusions containing CO_2. This alternating fracture and seal mechanism of precipitation provides an efficient means of gold deposition and aids in the understanding of complexes involved in transporting gold to this location. The complex $Au(HS)_2^-$ has been found to be a dominant complexing agent of gold in hydrothermal fluids and allows a relatively high gold solubility in near-neutral pH, low saline solutions at temperatures lower than 350°C (Seward, 1973; Lewis, 1982; Henley, 1985). The dominant dissolution reaction involving this gold species is

$$Au + 2H_2S = Au(HS)_2^- + H^+ + 0.5H_2 \qquad \text{(Henley, 1985)}$$

Consequently, increasing H_2S increases the solubility of gold carried as sulphide and bisulphide thio complexes. Boiling events cause CO_2 and H_2S to be rapidly partitioned into the vapour phase, and formation of only a few percent of vapour allows the loss of more than 90 percent of dissolved CO_2 with an accompanying increase in pH and loss of H_2S (Henley, 1985). This leads to supersaturation of gold and silver sulphide and bisulphide thio complexes causing deposition of precious metals. The premise of sulphur complexes forming a ligand allowing transportation of precious metals is reasonable in that although the system is generally low in sulphur, significant amounts of sulphides are present in alteration envelopes and associated with some veins. In addition, the presence of abundant alunite in the Alunite Cap Zone is indicative of significant amounts of sulphur in the system that was released through a boiling process then cooled and condensed near the surface to form a low pH cap over the hydrothermal system. Due to the small amounts of precious metal required to make a viable deposit, a large supply of sulphur is not necessary for economic amounts of gold to be deposited in a system leaving only trace amounts of sulphide minerals.

This boiling model reflects mineral precipitation under two main pressure régimes and explains the observed mineral paragenesis in veins of early-formed skeletal bladed calcite later filled and partially to completely replaced by fine-grained equant quartz crystals locally forming cockade overgrowths on these blades. During periods where hydrothermal circulation was sealed at the surface, precipitation of minerals from the relatively hot hydrothermal fluid under lithostatic pressure resulted in widespread deposition of calcite which is relatively

insoluble in high temperature solutions (Fournier, 1985a). Upon initiation of boiling following tectonic rupture of the sealed cap, a sudden decrease in temperature of the hydrothermal solution caused supersaturation in silica and an attendant increase in solubility of calcite (Fournier, 1985b) thereby initiating rapid precipitation of fine-grained anhedral quartz in skeletal interstices between calcite blades as well as replacement of calcite by quartz.

Evaluation of many epithermal deposits (Henley, 1985) has led to the conclusion that the availability of a recognized source of precious metal components found in the deposit is of little consequence considering the volume of solution which moves through a typical epithermal system such as Mt. Skukum and the area of rock affected. Any rock type contains sufficient quantities of these metals in trace amounts to supply the total metallic content typically found in these deposits many times over. Consequently, the source of precious metals at Mt. Skukum was probably a combination of the Tertiary volcanic pile and underlying basement rocks. Extremely high background gold values in late-stage rhyolite stocks and dykes indicate that there was some pre-existing gold concentration in the Caldera Complex which may have contributed significantly through further concentration by hydrothermal means. The availability of a suitable structure which focused the discharge of hydrothermal fluids is perhaps the most important factor in concentration of precious metals to form an epithermal deposit; this occurs at Mt. Skukum in the form of large block faults centered over the graben structure at Main Cirque.

Following models of other precious metal districts (Buchanan, 1981; Berger and Eimon, 1983; Hayba et al., 1985) a zone of base metal enrichment may be expected at and below the base of the boiling zone with an accompanying decrease in precious metal values. Although this zone is not reached in the Main Cirque Ore Zone, elevated base metal contents encountered in the Lake Zone and a higher observed silver : gold ratio may reflect the upper portion of this base metal zone, and the lowest extent of the boiling zone.

SUMMARY AND CONCLUSIONS

1) The Mt. Skukum epithermal gold deposit occurs in an early Eocene caldera complex in the southern Yukon Territory which forms the northernmost expression of a large belt of volcanic rocks extending into northern British Columbia known as the Sloko Volcanic Province.

2) Rocks of the Mt. Skukum Volcanic Complex are divided into four formations reflecting three cycles of volcanic activity:

a) Felsic rocks of Formations 1 and 2 form the first cycle of volcanic activity.

b) Andesitic rocks of Formation 3 deposited conformably over Formation 2 form the second cycle.

c) Rhyolitic volcanics of Formation 4, deposited unconformably over Formation 3, represent a return to Felsic volcanism in the third cycle.

3) Post-depositional block faulting, probably associated with depletion of a large inferred magma chamber at depth, caused downward displacement of the entire volcanic complex along major faults on the eastern and southern margins of the complex .

4) A final magmatic resurgence caused emplacement of gold-enriched, high-level, tan coloured, porphyritic rhyolite stocks and dykes throughout the volcanic complex, as well as several irregular intrusions surrounding the complex.

5) Characteristics of the Mt. Skukum epithermal gold-silver deposit closely fit those described as low-sulphur, adularia-sericite type epithermal deposits (Heald et al., 1987, Hayba et al., 1985; Bonham, 1986; Buchanan, 1981; Berger and Eimon, 1983).

6) Emplacement of veins forming the Mt. Skukum deposit was probably caused by development of a hydrothermal circulation cell driven by a porphyritic rhyolite intrusion inferred below rocks of Main Cirque. Hydrothermal outflow was centered on Main Cirque where previous block-faulting, reactivated and dilated by resurgent doming, provided excellent ground preparation.

7) Precious metals in the Main Cirque Zone form a mineralized horizon of maximum values extending over a vertical depth of 59 m to a base elevation of 1,676 m with maximum grades found in discrete vertically-extensive ore shoots. This supports a pressure-related precipitation mechanism limited by depth, intensified by throttling effects, and dictated by the temperature and salinity of the hydrothermal fluid.

8) Fluid inclusion study indicates that veins formed at a depth of 470 m. Two populations of salinity and temperature are clearly demonstrated by inclusion measurements; one population characterized by homogenization temperatures of approximately 330°C and a salinity of 4.12 weight percent NaCl, and the other by homogenization temperatures of approximately 250°C and a salinity of 0.87 weight percent NaCl. Indications that these two populations of inclusion temperature and salinity formed at a common depth is consistent with sudden boiling events caused by tectonic release of near-lithostatic pressure built up against a sealed alteration cap near the surface.

9) Oxygen isotope evidence clearly shows that circulating solutions were meteoric in origin with little or no contribution from magmatic sources.

10) Gold was probably transported through the Mt. Skukum hydrothermal system as sulphide or bisulphide thio

complexes. The complex $Au(HS)_2^-$ has been found to be a dominant complexing agent of gold in hydrothermal fluids and allows a relatively high gold solubility in near-neutral pH, low saline solutions at temperatures lower than 350°C (Seward, 1973; Lewis, 1982; Henley, 1985). Consistent pyritic alteration envelopes surrounding veins and the presence of argillic alteration envelopes and cap zones support the presence of acidic conditions created when boiling causes CO_2 and H_2S to be rapidly partitioned into the vapour phase. Formation of only a few percent of vapour allows the loss of more than 90 percent of dissolved CO_2 with an accompanying increase in pH and loss of H_2S (Henley, 1985). This causes gold precipitation.

11) The source of precious metals at Mt. Skukum was probably a combination of the Tertiary volcanic pile, particularly rhyolite stocks and dykes, and underlying basement rocks. A specific source is not necessary however, considering the volume of solution which moves through a typical epithermal system and the area of rock affected. Any rock type contains sufficient quantities of these metals in trace amounts to supply the total metallic content typically found in these deposits many times over. The availability of a suitable structure in the form of large block faults centered over the graben at Main Cirque which focussed discharge of hydrothermal fluids is perhaps the most important factor in concentration of precious metals at Mt. Skukum.

REFERENCES

Barton, P.B., Jr., and P. Toulmin, 1961, Some mechanisms for cooling hydrothermal fluids: U.S. Geological Survey, Professional Paper, 424-D, p.348-352.

Barton, P.B., Jr., P.M. Bethke, and E. Roedder, 1977, Environment of ore deposition in the Creede mining district, San Juan Mountains, Colorado: Part III. Progress toward interpretation of the chemistry of the ore forming fluid for the OH vein: Economic Geology, vol. 72, p. 1-24.

Berger, B.R., P.I. Eimon, 1983, Conceptual models of epithermal precious-metals deposits; in Shanks, W.C., III (ed.), Cameron Volume on Unconventional Mineral Deposits: Society of Mining Engineers, A.I.M.E., p. 191-205.

Bloom, M.S., 1979, Calibration and collection of fluid inclusion data on the chaixmeca heating/freezing stage: Unpubl. paper, U.B.C., 20p.

Bloom, M.S., 1983, Geochemistry of fluid inclusions and hydrothermal alteration in vein and fracture controlled mineralization, stockwork molybdenum deposits: Unpubl. PhD. Thesis, U.B.C.

Bodnar, R.J., T.J. Reynolds, and C.A. Kuehn, 1985, Fluid inclusion systematics in epithermal systems; in Berger, B.R, and P.M. Bethke, (eds.), Geology and Geochemistry of Epithermal Systems: Society of Ec. Geol.,p. 73-97

Bonham, H.F., Jr., 1986, Models for volcanic - hosted epithermal precious metal deposits; a review; in Proceedings of Symposium 5: Volcanism, hydrothermal systems and related mineralization: International Volcanological Congress, New Zealand, p. 13-17.

Bostock, H.S., 1941, Mining industry of Yukon, 1939 and 1940; Geol. Surv., Canada, Mem. 218

Buchanan, L.J., 1981, Precious metal deposits associated with volcanic environments in the southwest; in Dickinson, W.R. and W.D. Payne, (eds.), Relation of Tectonics to Ore Deposits in the Southern Cordillera: Arizona Geological Society Digest, vol. 16, 292 p.

Burruss, R.C., 1981, Analysis of phase equilibria in C-O-H-S fluid inclusions; in Hollister, L.S., M.L. Crawford, (eds.), Short course in Fluid Inclusions: Applications to Petrology: Mineralogical Association of Canada, p. 39-74.

Cairnes, D.D., 1912, Wheaton District, Yukon Territory; Geological Survey of Canada, Mem. 31.

Cairnes, D.D., 1916, Wheaton District, Yukon Territory; Geological Survey of Canada, Supplement to Sum. Rept. for 1915, p. 36-49.

Clayton, R.N., and A. Steiner, 1975, Oxygen isotope studies of the geothermal system at Wairakei, New Zealand: Geochimica et Cosmochimica Acta, vol. 39, p. 1179-1186.

Craig, H., 1966, Isotopic composition and origin of the Red Sea and Salton Sea geothermal brines: Science, vol. 154, p. 1544-1548.

Crawford, M.L., 1981, Phase Equilibria in Aqueous Fluid Inclusions; in Hollister, L.S., M.L. Crawford, (eds.), Short course in Fluid Inclusions: Applications to Petrology: Mineralogical Association of Canada, p. 75-100.

Doherty, R.A., et. al., 1981, Mount Skukum Project, 1981 Exploration Activities; in Southwestern Yukon Projects - 1981; Agip Canada Ltd. private company report.

Doherty, R.A., et. al., 1988, Preliminary Geological Map of Fenwick Creek Map Area (105 D/3), Open File 1988-2, Indian and Northern Affairs Canada Geological Services Division.

Eimon, P.I., 1983, Exploration for epithermal gold and silver deposits: the epithermal model; in Eimon, P.I., (ed.), A Collection of Unpublished Papers on Epithermal Silver - Gold Deposits.

Ellis, A.J., 1979, Explored geotherma systems; in Barnes, H.L., (ed.), Geochemistry of Hydrothermal Ore Deposits, Second Edition: John Wiley and Sons, New York, p. 632-683.

Field, C.W., and R.H. Fifarek, 1985, Light stable-isotope systematics in the epithermal environment; in Berger, B.R. and P.M. Bethke, (eds.), Geology and Geochemistry of Epithermal Systems: Society of Economic Geologists, p. 99-128.

Fisher, R.V. and H.-U. Schmincke, 1984, Pyroclastic Rocks, Springer-Verlag, New York, 472p.

Fournier, R.O., 1985a, Carbonate transport and deposition in the epithermal environment; in Berger, B.R. and P.M. Bethke, (eds.), Geology and Geochemistry of Epithermal Systems: Society of Economic Geologists, p. 63-72.

Fournier, R.O., 1985b, The behaviour of silica in hydrothermal solutions; in Berger, B.R. and P.M. Bethke, (eds.), Geology and Geochemistry of Epithermal Systems: Society of Economic Geologists, p. 45-62

Giles, D.L., C.E. Nelson, 1983, Principal features of epithermal lode gold deposits of the Circum-Pacific rim: Circum-Pacific Energy Minerals Conference, Honolulu, Hawaii, August 22-28, 1982.

Godwin, C.I., 1975, Imbricate subduction zones and their relationship with Upper Cretaceous to Tertiary porphyry deposits in the Canadian Cordillera: Canadian Journal of Earth Sciences, vol. 12, no. 8, p. 1362-1378.

Grunsky, E.C., 1986, Recognition of alteration and mineralization in volcanic terrains; in Proceedings of Symposium 5: Volcanism, Hydrothermal systems and related mineralization: International Volcanological Congress, New Zealand, p. 13-17.

Haas, J.L., 1971, The effect of salinity on the maximum thermal gradient of a hydrothermal system at hydrostatic pressures: Economic Geology, vol. 66, p. 940-946.

Harland, W.B., A.V. Cox, P.G. Llewellyn, C.A.G. Pickerton, A.G. Smith, and R. Walters, 1982, A Geologic Time Scale; Cambridge Earth Sciences Series, Cambridge University Press, 131p.

Hayba, D.O., P.M. Bethke, P. Heald, and N.K. Foley, 1985, Geologic, mineralogic and geochemical characteristics of volcanic-hosted epithermal precious-metal deposits; in Berger, B.R. and P.M. Bethke, (eds.), Geology and Geochemistry of Epithermal Systems: Reviews in Economic Geology, vol. 2, S.E.G., p.129-167.

Heald, P., N.K. Foley, D.O. Hayba, 1987, Comparative anatomy of volcanic-hosted epithermal deposits: acid-sulphate and adularia-sericite types: Economic Geology, vol. 82, no. 1, p. 1-26.

Hedenquist, J.W. and R.W. Henley, 1985, The importance of CO_2 on freezing point measurements of fluid inclusions: evidence from active geothermal systems and implications for epithermal ore deposition: Ec. Geol., vol. 80, no. 5, p. 1379-1406.

Helgeson, H.C. and R.M. Garrels, 1968, Hydrothermal transport and deposition of gold: Economic Geology, vol. 63, p. 622-635.

Henley, R.W., 1985, The geothermal framework for epithermal deposits; in Berger, B.R. and

P.M. Bethke, (eds.), Geology and Geochemistry of Epithermal Systems: Society of Economic Geologists, p.1-25.

Hollister, L.S. et al, 1981, Practical aspects of microthermometry; in Hollister, L.S., M.L. Crawford, (eds.), Short course in Fluid Inclusions: Applications to Petrology: Mineralogical Association of Canada, p. 278-295.

Irvine, T.N. and W.R.A. Baragar, 1971, A guide to the chemical classification of the common volcanic rocks: Canadian Journal of Earth Sciences, vol. 8, p. 523-548.

Kamilli, R.J., and H. Ohmoto, 1977, Paragenesis, zoning, fluid inclusion, and isotopic studies of the Finlandia Vein, Colqui district, central Peru: Economic Geology, vol. 72, p. 950-982.

Lambert, M.B., 1974, The Bennett Lake cauldron subsidence complex, British Columbia and Yukon Territory: GSC Bull., 227p.

LeBas, M.J., 1986, Chemical classification of volcanic rocks: Journal of Petrology, vol. 27, p. 745-750.

Lewis, A., 1982, Gold geochemistry: new ideas about the paragenesis of hydrothermal deposits have implications for finding undiscovered gold ore: Earth and Mining Journal, December, 1982, p. 56-60.

Lindgren, W., 1933, Mineral Deposits 4th ed., McGraw-Hill Book Co., 929p.

McDonald, B.W.R., and C.I. Godwin, 1986, Geology of Main Zone at Mt. Skukum, Wheaton River area, southern Yukon; in Yukon Geology, vol. 1 : Exploration and Geological Services Division, Yukon, Indian and Northern Affairs

Canada, p.6-10.

McDonald, B.W.R., E.B. Stewart, and C.I. Godwin, 1986, Exploration Geology of the Mt. Skukum epithermal gold deposit, southwestern Yukon; in Yukon Geology, vol. 1: Exploration and Geological Services Division, Yukon, Indian and Northern Affairs Canada, p.11-18.

McDonald, B.W.R., 1987, Geology and genesis of the Mount Skukum Tertiary epithermal gold-silver vein deposit, southwestern Yukon Territory (NTS 105D SW); Unpublished M.Sc. thesis, University of British Columbia, pp.177.

Meyer, C and J.J. Hemley, 1967, Wall rock alteration; in Barnes, H.L., (ed.), Geochemistry of Hydrothermal Ore Deposits, 1st ed.: Holt, Rinehart and Winston, p. 166-235.

Monger, J.W.H., and R.A. Price, 1979, Geodynamic evolution of the Canadian Cordillera -progress and problems: Canadian Journal of Earth Sciences, vol. 16, p. 770-791.

Morrison, G.W., C.I. Godwin, and R.L. Armstrong, 1979, Interpretation of isotopic ages and $^{87}Sr/^{86}Sr$ initial ratios for plutonic rocks in the Whitehorse map area, Yukon: Canadian Journal of Earth Sciences, vol. 16, p. 1988-1997.

Nash, J.T., 1972, Fluid inclusion studies of some gold deposits in Nevada: U.S. Geol. Surv., Professional Paper, 800-C, p. C15-C19.

O'Neil, J.R. and H.P. Taylor, 1967, The oxygen isotope and cation exchange chemistry of feldspars: American Mineralogist, vol. 52, p. 1414-1437.

O'Neil, J.R. and M.L. Silberman, 1974, Stable isotope relations in epithermal Au-Ag deposits: Ec. Geol., vol. 69, p. 902-909.

O'Neil, J.R. et al., 1973, Stable isotope and chemical relations during mineralization in the Bodie Mining District, Mono County, California: Ec. Geol., vol. 68, p.765-784.

Ohmoto, H. and R.O. Rye, 1979, Isotopes of sulfur and carbon; in H.L. Barnes, (ed.), Geochemistry of Hydrothermal Ore Deposits, 2nd ed.: Wiley, p. 509-567.

Potter, II, R.W., 1977, Pressure corrections for fluid inclusion homogenization temperatures based on the volumetric properties of the system NaCl-H_2O: U.S. Geol. Surv. J. Res., vol. 5, p. 603-607.

Potter, II, R.W., M.A. Clynne, and P.L. Brown, 1978, Freezing point depression of aqueous sodium chloride solutions: Economic Geology, vol. 73, p. 284-285.

Pride, M.J., 1986, Description of the Mount Skukum Volcanic Complex, Yukon Territory; in Yukon Geology, vol. 1: Exploration and Geological Services Division, Yukon, Indian and Northern Affairs, Canada.

Pride, M.J., 1985, Preliminary geological map of the Mount Skukum Volcanic Complex, 105D - 2, 3, 4, 5; Exploration and Geological Services Division, Yukon, Indian and Northern Affairs, Canada, Open File, 1:25,000 scale map.

Pride, M.J. and G.S. Clarke, 1985, An Eocene Rb-Sr isochron for rhyolite plugs, Skukum area, Yukon Territory: Can J. Earth Sci., vol. 22, p. 1747-1753.

Roedder, E., 1979, Fluid inclusions as samples of ore fluids; in H.L. Barnes, (ed.), Geochemistry of Hydrothermal Ore Deposits, 2nd ed.: Wiley, p. 684-737.

Roedder, E., 1984, Fluid inclusions; Reviews in Mineralogy, vol. 12: Mineralogical Society of America, 644p.

Roedder, E. and R.J. Bodnar, 1980, Geologic pressure determinations from fluid inclusion studies: Ann Rev. Earth and Planet. Sciences, vol. 8, p. 263-301.

Rose, A.W. and D.M. Burt, 1979, Hydrothermal alteration; in Barnes, H.L., (ed.), Geochemistry of Hydrothermal Ore Deposits, 2nd ed.: Wiley, p. 173-235.

Seward, T.M., 1973, Thio complexes of gold and the transport of gold in hydrothermal ore solutions: Economic Geology, vol. 37, p. 379-399.

Smith, M.J., 1982, Petrology and geology of high level rhyolite intrusives of the Skukum Area, 105D SW, Yukon Territory; in Yukon Exploration and Geology, 1981: Department of Indian and Northern Affairs, Whitehorse, p. 62-73.

Smith, M.J., 1983, The Skukum Volcanic Complex, 105D SW: geology and comparison to the Bennett Lake Cauldron Complex; in Yukon Exploration and Geology, 1982: Department of Indian and Northern Affairs, Whitehorse, p. 68-72.

Smith, R.L., R.A. Bailey, and C.S. Ross, 1961, Structural evolution of the Valleys Cauldera, New Mexico, and its bearing on the emplacement of ring dykes: U.S.G.S., Prof. Paper 424-D, p. D145-D149.

Smith-Pride, M.J., 1985, Interlayered sedimentary - volcanic sequence of the Mt. Skukum Volcanic Complex; in Yukon Exploration and Geology: Department of Indian and Northern Affairs, Whitehorse, p. 94-104.

Souther, J.G., 1966, North-central belt of the Cordillera of British Columbia; in Tectonic History and Mineral Deposits

of the western Cordillera: Can. Inst. Mining Met. Spec. Vol., no. 8, p. 171-184.

Souther, J.G., 1967, Acid volcanism and its relationship to the Cordillera of British Columbia, Canada: Bull. Volcanol., vol. 30, p. 171-176.

Souther, J.G., 1970, Volcanism and its relationship to recent crustal movements in the Canadian Cordillera: Can. J. Earth Sci., vol. 7, p. 553-568.

Spooner, E.T.C., 1981, Fluid inclusion studies of hydrothermal ore deposits; in Hollister, L.S., M.L. Crawford, (eds.), Short course in Fluid Inclusions: Applications to Petrology: Mineralogical Association of Canada, p. 209-240.

Taylor, H.P., 1973, O^{18}/O^{16} Evidence for meteoric - hydrothermal alteration and ore deposition in the Tonopah, Comstock Lode, and Goldfield Mining Districts, Nevada: Ec. Geol., vol. 68, no. 6, p. 747-764.

Taylor, H.P., 1974, The application of oxygen and hydrogen isotope studies to problems of hydrothermal alteration and ore deposition: Ec. Geol. vol. 69, p. 843-883.

Taylor, H.P., 1979, Oxygen and hydrogen isotope relationships in hydrothermal mineral deposits; in Barnes, H.L., (ed.), Geochemistry of Hydrothermal Ore Deposits: John Wiley & Sons.

Taylor, H.P., Jr., and S. Epstein, 1970, Oxygen and silicon isotope ratios of lunar rock 12013: Earth and Planetary Science Letters, vol. 9, p. 208-210.

Templeman-Kluit, D., 1981, Geology and mineral deposits of southern Yukon; in Yukon Geology and Exploration, 1979: Indian and Northern Affairs, Canada, p. 7-31.

Turner, S., 1986, Fluid inclusion, alteration and ore mineral studies of an epithermal vein system: Mount Kasi, Vanua Levu, Fiji; in Proc. of Symposium 5: Volcanism, Hydrothermal Systems and Related Mineralization: International Volcanological Congress, New Zealand, p. 87-94.

Wheeler, J.O., 1961, Whitehorse map-area, Yukon Territory, 105D: Geol. Surv. Can., Mem. 312, 156p.

White, D.E., 1981, Active geothermal systems and hydrothermal ore deposits; in Skinner, B.J., (ed.), Economic Geology, Seventy-Fifth Anniversary Volume: Ec. Geol. Publishing Co., p. 392-423

Winchester, J.A. and P.A. Floyd, 1977, Geochemical discrimination of different magma series and their differentiation products using immobile elements: Chemical Geology, vol. 20, Elsevier Sci. Publ. Co., p. 325-343.

APPENDIX A: GEOCHEMICAL DATA FOR IGNEOUS ROCKS AT MT. SKUKUM

Introduction

Major element contents of igneous rocks found in Main Cirque at Mt. Skukum (Table 2) were obtained from a suite of whole rock analyses on 16 samples. Samples include 10 specimens of porphyritic andesite, and 6 of rhyolite reflecting the relative abundances of these lithologies in Main Cirque. Samples taken from drill core are located in Appendix B.

Data

Data comprising a classical whole rock major element analysis and including zirconium are compiled in Table 2 for the purpose of allowing a broad geochemical classification of the two dominant igneous rock compositions found in Main Cirque. Samples were collected by the author during the 1984 and 1985 field seasons. All samples were analysed at X-ray Assay Laboratories Limited, Don Mills, Ontario using x-ray fluorescence techniques with results for major elements calculated as oxides in weight percent, and zirconium reported in parts per million.

Samples supplied to X-ray Assay Laboratories Ltd. by the author were taken from hand specimens averaging approximately 1 kg which were pulverized at The University of British Columbia and split to an average size of about 250 grams prior to dispatch. These were then roasted at 950°C by X-ray Assay Laboratories prior to analysis and L.O.I. was determined. Major elements and zirconium analyses were carried out on a 1.7 gram split of the original sample. This was fused with 5 grams of lithium tetraborate to form a 40 mm diameter disk. Fused disks were analysed on a Philips PW1600 simultaneous, multichannel spectrometer with calibration fixed using "preferred" values determined by Abbey (1979) on a collection of 40 international rock standards.

Conclusions

Absolute accuracy and precision for geochemical data cannot be assessed as independant standards and duplicates were not included in assay batches, however, values for accuracy and precision routinely obtained in these analyses by X-ray Assay Laboratories Limited are quoted as ±2 percent and ±4 percent respectively for all major elements (L. MacFarlane, pers. comm., 1987). These quoted values for accuracy and precision in routine analyses are confirmed as maximum values by an on-going survey of this lab conducted over the past 5 years by the Production Research Division of Exxon Corporation (A.E. Bence, verbal communication, 1987).

APPENDIX B: LOCATION OF DRILL CORE SAMPLES USED IN STUDY OF THE MT. SKUKUM DEPOSIT

Sample Number	Drill Hole Number	Sample Interval (m) From:	To:	Northing (UTM)	Easting (UTM)	Collar Elevation (m)	Dip	Azimuth (Degrees)
C005	82-10	80.45	80.47	4771.99	4267.24	1729.63	-45	104
C022	83-35	28.83	28.87	4743.04	4377.11	1731.24	-60	284
C040	83-35	107.53	107.57	4743.04	4377.11	1731.24	-60	284
C041	83-35	113.10	113.14	4743.04	4377.11	1731.24	-60	284
C042	83-35	116.39	116.43	4743.04	4377.11	1731.24	-60	284
C049	83-37	39.19	39.23	4751.00	4347.78	1733.08	-45	284
C072	82-25	23.53	23.57	4934.94	4439.19	1720.38	-45	104
C078	82-25	107.73	107.77	4934.94	4439.19	1720.38	-45	104
C095	83-68	83.00	83.06	4914.22	4514.91	1730.50	-45	284
C104	83-51	57.09	57.13	4570.18	4252.33	1734.55	-50	284
C172	83-63	52.07	52.11	4582.91	4297.92	1736.21	-61	284
C177	83-63	94.45	94.49	4582.91	4297.92	1736.21	-61	284
C278	84-83	33.04	33.25	4909.90	3721.67	1880.20	-70	104
C279	84-83	74.08	74.45	4909.90	3721.67	1880.20	-70	104
C280	84-83	96.33	96.56	4909.90	3721.67	1880.20	-70	104
C281	82-17	51.81	52.01	4898.10	3768.43	1890.43	-55	104
ASTN-10A	83-51	79.02	79.24	4570.18	4252.33	1734.55	-50	284
ASTN-13	83-63	57.61	57.91	4582.91	4297.92	1736.21	-61	284
ASTN-13A	83-63	58.08	58.42	4582.91	4297.92	1736.21	-61	284
ASTN-14	83-63	59.19	59.58	4582.91	4297.92	1736.21	-61	284

APPENDIX C: Potassium-argon data from whole rock analysis of andesite from the Mt. Skukum property, Main Cirque Zone

Sample Number	Location		Rock Description	%K (±)	40Ar* 2 --- 40Artotal	40Ar* 2 --- 10-5cm3 STP/g	Apparent Age3	Time4
	lat(°N)	long(°W)						
ASTN-13 DH83-63 57.61m	60.20	135.47	Fine grained andesite with pervasive propyllitic alteration.	2.71 ±0.01	0.674	0.5416	50.7±1.8	Tertiary
ASTN-14 DH83-63:	60.20	135.47	Fine grained, fresh andesite	2.18 ±0.04	0.938	0.4574	53.2±1.8	Tertiary

1. Argon analyses are by J. Harakal and potassium analyses are by K. Scott; all were done at the Geochronology Laboratory, The University of British Columbia. Potassium was determined in duplicate by atomic absorption using a Techtron AA4 spectrophotometer and Ar by isotope dilution using an AEI MS - 10 mass spectrometer and high purity 38Ar spike.
2. Ar* indicates radiogenic argon.
3. Constants used are from Steiger and Jäger (1977): K = 0.581 x 10-10 yr-1; K = 4.962 x 10-10yr-1; 40K/K = 1.167 x 10-4.
4. Time designation is from Harland et al. (1962).

APPENDIX D: CALIBRATION DATA FOR THE CHAIXMECA FLUID INCLUSION STAGE.

Introduction

Nine standards were used to calibrate the fluid inclusion stage, four over the temperature range -100° to +40°C and five over the temperature range +40° to +420°C. Only minor deviations between measured temperature and actual temperature were noted and estimates of the accuracy and precision of measurements using this equipment (p. 37) are similar to those encountered by Bloom (1983) using the same apparatus.

Calibration of Freezing Stage

The initial melting temperature (T(m)) of each standard was measured twice to obtain data in Table D.1 for the calibration curve in Figure D.1. Using the above formula a precision (1s) of within 0.6°C is expected for data in this temperature range. This indicates a 95% confidence that recorded T(m) is within 6.7°C of the actual T(m).

Table D.1 Freezing calibration curve data(-100 to +40C) or the Chaixmeca stage

Calibration Standard	T(m) Measurements	Ave.T(m)	Expected T(m)[1]
Acetone	-91.6	-91.4	-96.35
	-92.2		
Chloroform	-61.0	-60.6	-63.40
	-60.3		
Carbon Tetrachloride	-25.5	-25.6	-22.90
	-25.8		
Water	0.0	0.0	0.01
	0.0		

1. From Roedder (1984)

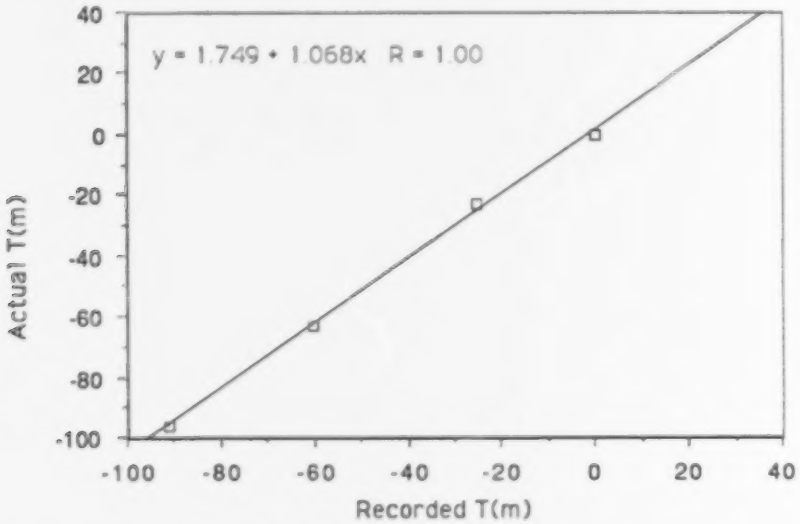

Figure D.1 Freezing calibration curve based on data in Table D. 1 for the Chaixmeca stage.

The above calibration curve and data demonstrate an accuracy, defined as twice the standard deviation of the difference between recorded T(m) and actual T(m), of ± 6.7°C for data in this temperature interval. Precision, defined as the measure of random error, was calculated using the following formula for each pair of measurements:

$$\text{Precision} = \sqrt{\frac{\Sigma(\text{difference}^2}{n-1}}$$

Using the above formula a precision (1s) of within 2.2°C is expected for data in this temperature range. This indicates a 95%confidence that recorded T(m)is within 6°of the actual T(m).

Calibration of Heating Stage:

The initial melting temperature (T(m)) of each standard was measured twice, and in one case three times, to obtain data in Table D..2 for the calibration curve in Figure D.2. Calibration curve and data demonstrate an accuracy, defined as twice the standard deviation of the difference between recorded T(m) and actual T(m), of ± 5.3°C for data in this temperature interval. Precision, defined as the measure of random error, was calculated using the following formula for each pair of measurements:

$$\text{Precision} = \sqrt{\frac{\Sigma(\text{difference})^2}{n-1}}$$

Using the above formula a precision (1s) of within 2.2°C is expected for data in this temperature range. This indicates a 95% confidence that recorded T(m) is within 5.3°C of the actual T(m).

Table D.2. *Heating calibration curve data (+40° to +420°C) for the Chaixmeca stage.*

Calibration Standard	T(m) Measurements	Ave.T(m)	Expected T(m)*
Napthalene	80.1 80.4	80.25	80.55
Merck 9735	135.5 135.7	135.6	135.0
Merck 9800	202.3 203.1	202.7	200.0
Sodium Nitrate	299.9 304.1 302.7	302.2	306.8
Sodium Acetate	323.4 324.3	323.8	324.0

*From Roedder (1984)

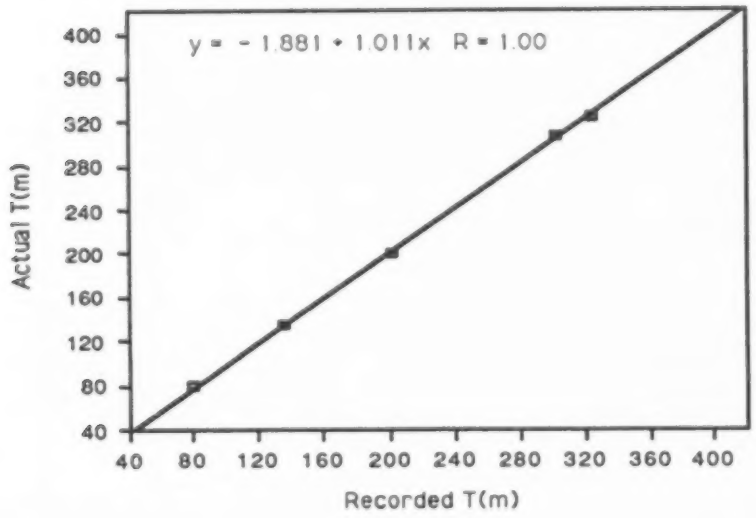

Figure D.2. *Heating calibration curve based on data in Table D.2.*

APPENDIX E: Homogenization and freezing data for fluid inclusions from quartz veins at Mt. Skukum, Yukon Territory.

Sample and Chip Number[1]	Sample Elevation (m)[1]	Inclusion Type (P,PS,S)2	Inclusion Size (μm)	Volume % Gas	Th(Ave.) (°C)	Eutectic Melting Temp.(°C)	Final Melting Temp.(°C)
C177-1	1653.6	P	14.0 x 22.6	10	327.0		
C177-1	1653.6	P	11.3 x 8.5	2	301.6		
C177-1	1653.6	P	19.8 x 8.5	10		-33.3	-0.9
C177-2	1653.6	P	8.5 x 5.1	5	305.3	-32.3	+7.2
C172-1	1690.7	P	19.8 x 5.1	5	255.9	-30.1	-1.1
C172-1	1690.7	P	19.8 x 14.1	10	354.2		
C172-2	1690.7	S	14.0 x 6.0	5	178.1	-23.7	+0.1
C172-2	1690.7	S	18.0 x 14.0	5	139.2		
C172-3	1690.7	S	11.3 x 8.5	2	186.7		
C172-3	1690.7	S	11.3 x 5.1	2	192.6		
C104-1	1690.8	P	14.0 x 8.5	20		-29.2	+0.1
C104-1	1690.8	P	14.0 x 8.5	10	325.3		
C104-1	1690.8	PS	17.0 x 14.0	5	263.6		
C104-1	1690.8	P	8.5 x 5.1	20	335.5		
C104-2	1690.8	P	14.0x11.0	10	297.0		
C104-3	1690.8	P	17.0 x 14.0	20	412.7	-34.2	-2.8
C104-4	1690.8	P	11.0 x 5.0	5	294.6		
C104-4	1690.8	PS	17.0 x 8.0	5	280.4		
C104-4	1690.8	P	14.0 x 5.1	20	340.6		
C104-4	1690.8	PS	14.0 x 5.1	5	241.9		
C104-5	1690.8	PS	8.5 x 8.5	5	274.8		
C104-5	1690.8	PS	11.3 x 5.1	5	266.7		
C104-5	1690.8	PS	11.3 x 11.3	10	236.1		
C104-5	1690.8	PS	11.3 x 8.5	5	235.4		
C104-5	1690.8	S	14.0 x 8.5	2	237.7		
C104-6	1690.8	P	28.3 x 8.5	10	313.9		
C104-6	1690.8	P	8.5 x 8.5	2	254.6		
C078-1	1644.2	S	10.0 x 5.0	2		-31.4	+0.1
C078-1	1644.2	P	22.6 x 8.5	20	300.0	-29.0	-0.1
C078-2	1644.2	PS	16.9 x 8.5	5	292.4		
C078-3	1644.2	P	8.5 x 4.2	1	323.2		
C078-3	1644.2	PS	17.0 x 8.5	10	310.4		
C078-3	1644.2	P	14.0 x 5.0	2	259.6		

APPENDIX E (continued)

C078-4	1644.2	PS	14.0 x 8.5	5		-30.2	-1.1
C078-4	1644.2	P	14.0 x 5.0	5		-30.5	+0.2
C078-4	1644.2	P	14.0 x 8.5	20	317.1		
C078-4	1644.2	P	8.5 x 3.0	5	318.2		
C078-4	1644.2	P	14.0 x 5.0	5	317.9		
C078-5	1644.2	PS	14.0 x 14.0	5	261.4	-32.3	+0.9
C078-6	1644.2	PS	8.5 x 14.0	10	289.2		
C041-1	1633.3	P	19.8 x 8.5	2		-31.1	-1.6
C041-2	1633.3	S	25.5 x 25.0	2	214.0		
C041-3	1633.3	S	19.8 x 14.0	2	172.1		
C041-4	1633.3	S	11.3 x 5.1	2	198.0		
C022-1	1706.3	P	11.3 x 5.1	2		-31.3	+1.4
C022-2	1706.3	P	14.0 x 8.5	20	321.6		
0244-1	1706.3	PS	7.1 x 5.7	1		-26.6	-3.8
0244-1	1706.3	P	5.1 x 2.8	20		-24.2	-2.8
0244-1	1706.3	P	7.1 x 5.7	10		-25.3	-4.6
0244-2	1706.3	P	7.1 x 7.1	20	338.5	-29.4	-3.7
0244-2	1706.3	P	5.7 x 4.7	1	337.4		
0244-3	1706.3	P	5.7 x 2.9	2		-31.7	-0.5
0244-4	1706.3	P	7.1 x 5.7	2			-0.3
0244-4	1706.3	P	5.7 x 5.7	20		-30.6	0.0
0244-4	1706.3	P	9.9 x 7.1	20	272.0		
0244-5	1706.3	P	7.1 x 5.6	5		-28.8	0.0
0244-5	1706.3	P	5.1 x 4.8	20		-33.1	0.0
0244-5	1706.3	P	8.5 x 7.1	2	274.2	-33.1	0.0
0244-5	1706.3	P	5.1 x 7.1	2	329.0		
0244-5	1706.3	S	8.5 x 5.1	10	252.7		
0244-5	1706.3	P	14.1 x 8.5	20	349.5		
0244-5	1706.3	P	5.1 x 2.0	1	306.2		
0244-5	1706.3	P	8.5 x 2.8	10	348.7		

1 Sample location details are in Appendix B. Elevations are calculated from data in Appendix B.
2 (P,PS,S) denote Primary, Pseudo-secondary and Secondary inclusions respectively.

APPENDIX F: OXYGEN ISOTOPE METHODS AND RESULTS

Mineral separation for quartz was achieved by coarsely crushing the sample, removal of carbonate by heating in concentrated HCl followed by hand picking. Calcite separation followed a similar procedure; however, samples were not treated with acid prior to hand-picking.

All samples were analyzed by K. Meulhenbachs at the University of Alberta. Results in TableF-1 are expressed in terms of $d^{18}O$ representing the per mil (‰) deviation of ^{18}O in the sample from that in the universal standard, SMOW (Standard Mean Ocean Water). All analyses were done on a gas source mass spectrometer. A precision of ±0.02 percent or better is routinely obtained using this technique (Field et al., 1985).

Table F-1. *Oxygen isotope data[1] From the Mt. Skukum deposit, south-central Yukon Territory.*

Sample Number	Sample Description	$d^{18}O^1$ (‰)
ASTN-15	Unaltered porphyritic andesite with relatively abundant magnetite and only slightly sericitized plagioclase phenocrysts. Whole rock analysis.	-6.8
ASTN-13A	Propylitized porphyritic andesite exhibiting bleached, chloritized appearance. Whole rock analysis.	-6.7
ASTN-10A	Propylitized porphyritic andesite exhibiting bleached, chloritized appearance. Whole rock analysis.	-7.2
C049-Qtz	Mineral separate of quartz from a 2m thick massive vein consisting of 60% calcite, 40% quartz, and 9 gms Au/tonne.	-3.5
C049-Cal	Mineral separate of calcite from a 2m thick massive vein consisting of 60% calcite, 40% quartz, and 9 gms Au/tonne.	-6.9
C005-Qtz	Mineral separate of quartz taken from a vein consisting of 70% fine grained quartz intergrown with 20% bladed calcite, 10% altered wall rock fragments, and 2.75 gms Au/tonne.	-4.3
C005-Cal	Mineral separate of calcite taken from a vein consisting of 70% fine grained quartz intergrown with 20% bladed calcite, 10% altered wall rock fragments, and 2.75 gms Au/tonne.	-6.8
C042	Quartz in a massive vein containing altered wallrock fragments in a matrix consisting of 90% quartz with minor calcite, sericite, and 0.07 gms Au/tonne.	-4.3
C040	Quartz in stockwork veins containing 90% quartz minor calcite and sericite, argillized wallrock fragments, and 0.07 gms Au per tonne.	-4.0
C072	Quartz in a stockwork of pre-ore chalcedonic veins in a highly argillized porphyritic andesite containing 0.07 gms Au/tonne.	-5.2
C095	Quartz in a stockwork of pre-ore chalcedonic veins in brecciated, propylitized andesitic lapilli tuff.	-6.8
M1[2]	Quartz	-4.71
M2[2]	Quartz	-4.3
M3[2]	Calcite	-8.6

[1] All analyses by K. Meuhlenbachs, University of Alberta. Error in analysis ± 0.0008 ‰ (Field et al., 1985).
[2] Samples obtained independently by Karlis Meuhlenbachs, University of Alberta.